CARBON NANOTUBE COMPOSITES – MECHANICAL, ELECTRICAL, AND OPTICAL PROPERTIES

Dissertation
zur
Erlangung des Doktorgrades (Dr. rer. nat.)
der
Mathematisch-Naturwissenschaftlichen Fakultät
der
Rheinischen Friedrich-Wilhelms-Universität Bonn

vorgelegt von
Maciej Olek
aus
Poznan (Polen)

Bonn 2006

Angefertigt mit Genehmigung der Mathematisch-Naturwissenschaftlichen Fakultät
der Rheinischen Friedrich-Wilhelms-Universität Bonn

1. Referent: Prof. Dr. Michael Giersig
2. Referent: Prof. Dr. Josef Hormes

Tag der Promotion: 08.02.2007

Diese Dissertation ist auf dem Hochschulschriftenserver der ULB Bonn
http://hss.ulb.uni-bonn.de/diss_online elektronisch publiziert

Erscheinungsjahr: 2007

To my wife Bernadeta and son Adam

The important thing in science is not so much to obtain new facts as to discover new ways of thinking about them.

Sir William Bragg

ABSTRACT

In the frame of this thesis novel concepts for the functionalization of nanotubes and fabrication of optimized, homogeneous MWNT/polymer heterostructures are presented. The effects of various dispersion states and morphologies of carbon nanotubes on mechanical, rheological, and electrical properties of the CNT-based nanocomposites were investigated. Additionally, a new approach for the fabrication of CNT/quantum-dots heterostructures for potential photoelectric and optical applications is shown.

The tensile strength and elastic modulus of polymeric systems are shown to be significantly improved (even by more than 1500 %) after introducing the MWNT-filler by using the layer-by-layer assembly technique. However, nanoindentation experiments reveal that the presence of MWNTs within the polymeric host material do not have any impact on the hardness of such composites. Furthermore, shear oscillatory tests show that the viscosity of MWNT/polymer composites increases together with the concentration of the nanotubes in polymer. The rheological percolation threshold is shown to be as low as 0.5 wt% of MWNTs.

Investigations of electrical properties of MWNT/polymer heterostructures show a significant increase of electrical conductivity with the increase of the MWNTs' content. The conductivity of the sample with only 8 wt% MWNTs load is as high as 10^{-2} S/cm which is four orders of magnitude higher than that of the neat polymer. The electrical percolation threshold is reached at 1.48 wt%.

Investigation of MWNT/quantum dots heterostructures reveal a complete quenching of the PL-bands, presumably through an electron transfer between QDs and MWNTs. The deposition of a silica shell (with thicknesses >20nm) around the CNTs preserves the fluorescence properties by insulating the QD from the surface of the CNT.

It is shown that carbon nanotubes as components of various nanocomposites have a significant effect on the mechanical, electrical, and optical properties of these hybrid materials. The results of this thesis indicate the potential of utilizing CNT-based nanocomposites towards mechanical, electrical, sensing, optical, and actuating applications.

CONTENTS

LIST OF SYMBOLS AND ABBREVIATIONS

3APTMS	3-aminopropyl trimethoxysilane
AFM	Atomic force microscope
CNT	Carbon nanotube
CVD	Chemical vapor deposition
E	Young's modulus
EDX	Energy dispersive X-ray analysis
EMI	Electromagnetic interference
EMT	Effective medium theory
E_r	Reduced modulus
G'	Storage modulus, elastic modulus
G''	Loss modulus
G^*	Complex modulus
GA	Glutaraldehyde
H	Hardness
LBL	Layer-by-layer
m_c	Rheological percolation threshold
MWNT	Multiwall carbon nanotube
MWNT@SiO_2	Silica-coated multiwall carbon nanotubes
MWNT-COOH	Oxidized multiwall carbon nanotube
MWNT-PAH	PAH-functionalized multiwall carbon nanotube
NC	Nanocrystal
NP	Nanoparticle
ODA	Octadecylamine
PAA	Polyacrylic acid
PAH	Poly(allylamine hydrochloride)
p_c	Electrical percolation threshold
PDDA	Poly(diallyldimethyl-ammonium chloride)
PEI	Polyethyleneimine
PMMA	Poly(methyl methacrylate)
PS	Polystyrene
PSS	Poly(styrenesulfonate)
QD	Quantum dot
Ra	Average roughness
SEM	Scanning electron microscope
SWNT	Singlewall carbon nanotube
TEM	Transmision electron micropscope
TEOS	Tetraethoxysilane
ε'	Real part of dielectric function
ε''	Imaginary part of dielectric function
ε^*	Complex permittivity
η^*	Complex viscosity
σ^*	Complex conductivity
σ_{DC}	Direct current conductivity
σ_T	Tensile strength
ω	Frequency

CHAPTER I

INTRODUCTION

One goal of today's technology is the miniaturization of the electronic, actuating, sensing, and optical devices and their components; hence, nanotechnology attracts much attention from the worlds of the science and industry. Nanotechnology offers new design, characterization, production, and application of systems, devices and materials at the nanometer scale. A nanocomposite is defined as a material of more than one solid phase, where at least one dimension falls into the nanometer scale. The fabrication of nanocomposites opens up an attractive route to obtain novel, optimized, and miniaturized compounds that can meet a broad range of applications. In this context, the exceptional properties of nanoparticles have made them a focus of widespread research in nanocomposite technology. Since composites consist of several different components, superior physical and chemical characteristics of novel materials can be achieved. Therefore, the development of nanoparticle modified composites is presently one of the most explored areas in materials science and engineering [1].

Nowadays polymers play a very important role in numerous fields of everyday life due to their advantages over conventional materials (e.g. wood, clay, metals) such as lightness, resistance to corrosion, ease of processing, and low cost production. Besides, polymers are easy to handle and have many degrees of freedom for controlling their properties. Further improvement of their performance, including composite fabrication, still remains under intensive investigation. The altering and enhancement of the polymer's properties can occur through doping with various nano-fillers such as metals, semiconductors, organic and inorganic particles and fibres, as well as carbon structures and ceramics [2-5]. Such additives are used in polymers for a variety of reasons, for example: improved processing, density control, optical effects, thermal conductivity, control of the thermal expansion, electrical properties that enable charge dissipation or electromagnetic interference shielding,

magnetic properties, flame resistance, and improved mechanical properties, such as hardness, elasticity, and tear resistance [6-8].

Unique properties of carbon nanotubes (CNT) such as extremely high strength, lightweight, elasticity, high thermal and air stability, high electric and thermal conductivity, and high aspect ratio offer crucial advantages over other nano-fillers. The potential utility of carbon nanotubes in a variety of technologically important applications such as molecular wires and electronics, sensors, high strength materials, and field emission has been well established. Recently, much attention has been paid to the use of carbon nanotubes in conjugated polymer nanocomposite materials to harness their exceptional properties [9,10]. CNT-based composites have attracted great interest due to an increasing technological demand for multifunctional materials with improved mechanical, electrical, and optical performance, complex shapes, and patterns manufactured in an easy way at low costs. However, several fundamental processing challenges must be overcome to enable applicable composites with carbon nanotubes. The main problems with CNTs are connected to their production, purification, processability, manipulation and solubility. Because of these difficulties, to date, the potential of using nanotubes as polymer composite has not been fully realized. There are only few nanotube-based commercial products on the market at present, which are in fact CNT/polymer composites with improved electrical conductivity [Hyperion Catalysis International]. This still requires intensive studies in order to compromise expectations with technological achievements in CNT composites. Since 1994, when Ajayan et al. [11] have firstly introduced multiwall carbon nanotubes (MWNTs) as filler materials in a polymer matrix, numerous projects have been focused on the fabrication, improvement, modeling, and characterization of such heterostructures [12-14].

The main objective of this study was to produce and investigate MWNT-based nanocomposites as candidates for next generation of high-strength, lightweight, and conductive plastics. However, the effective utilization of CNTs in composite applications strongly depends on the ability to disperse them homogeneously throughout the matrix[10,12,13]. The surface of CNTs has to be modified in order to overcome their poor solubility. In this context, several problems and issues concerning functionalizations and dispersion of MWNTs in solvents and polymers were addressed and discussed here. Various covalent and non-covalent approaches for efficient functionalization such as polymer wrapping, surfactant adsorption, oxidation, and silica coating are shown.

A uniform distribution of nanotubes within a polymer matrix and strong adhesion between structural components are necessary conditions for the effective improvement of the properties of the composites [13,15,16]. On this basis, we present in this work novel concepts for the fabrication of optimized, homogeneous CNT/polymer heterostructures, and show that the remarkable properties of carbon nanotubes can efficiently be transferred to the local matrix.

In order to fully understand the impact of carbon nanotubes on the performance of polymeric materials various characterization, tests have to be performed. Thus, the second part of the thesis is focused on the examination of the structural and physical properties of MWNT/polymer composites.
The effects of various dispersion states and morphologies of carbon nanotubes on mechanical, rheological, and electrical properties of the MWNT-based nanocomposites were investigated. Nanoindentation, tensile tests, and rheology were employed in order to evaluate the hardness, Young's modulus, tensile strength, and viscoelastic response of diverse heterostructures composed of the MWNTs and polymers, respectively.

Technological applications in many cases require reinforced polymers that are able to dissipate charge and reduce dangerous spark discharge, as well as to act as an electromagnetic interference shielding unit. In this context the use of metallic carbon nanotubes as fillers in dielectric hosts opens up possibilities for the fabrication of a new class of reinforced, lightweight, conductive materials. Electrical properties of CNT/polymer heterostructures were investigated in this study by means of dielectric spectroscopy.

The formation of CNT/nanoparticle heterostructures is both of fundamental and technological interest. Combining unique properties of CNTs and nanoparticles, a new class of nanocomposites can be made meeting a broad range of advanced applications [17-19]. The last part of this thesis shows a novel approach for the fabrication of nanocomposites composed of carbon nanotubes and semiconducting nanocrystals. The structural and optical properties of such heterostructures were investigated.

CHAPTER II

BASIC CONSIDERATION

2.1 Carbon nanotubes

The carbon nanotubes (CNT) were discovered in 1976 when Endo [20] synthesized vapour-grown carbon fibres, however at the time, it was not given any thought and focus. It was only after Iijima's work in 1991 [21] that global scientific attention was turned to these interesting carbon structures and intense studies on the properties [10,12,22], structure [23-25], and applications [10,13,26] of these unique materials have been carried out.

CNTs are considered to be a rolled-up graphene sheet that forms long concentric cylinders. Bonding in CNTs is essentially sp^2; the circular curvature causes σ bonds to be slightly out of plane, the π orbital is more delocalized outside the tube [13]. The properties of nanotubes depend on the structure, morphology, diameter, and length of the tubes. The structure of carbon nanotubes is described in terms of the tube chirality, which is defined by the chiral vector $\vec{C}_h$ and the chiral angle θ (Figure 2.1). The chiral vector indicates the way, in which graphene is rolled-up to form a nanotube. The chiral vector is described as [10]:

$$\vec{C}_h = n\vec{a}_1 + m\vec{a}_2 \qquad (2.1)$$

where the integers (*n*, *m*) indicate the number of steps along the zigzag carbon bonds of the hexagonal lattice, $\vec{a}_1$ and $\vec{a}_2$ are unit vectors (Figure 2.1). The chirality of the carbon nanotubes has a huge impact on their properties, especially electronic ones.

There are two main kinds of CNTs:

- Singlewall carbon nanotubes (SWNTs) are hollow single cylinders of a graphene sheet, which are defined by their diameter and their chirality [12,13]. The diameter of SWNTs varies from 0.5 to 5 nm. Depending on the chirality SWNTs may either be metallic or semiconducting.

- Multiwall carbon nanotubes (MWNTs) are a group of concentric SWNTs (Figure 2.2) often capped at both ends, with diameters in the range from several nanometers up to 200 nm [10,13]. These concentric nanotubes are held together by van der Waals bonding. MWNTs form complex systems with different wall numbers, structures, and properties and additional features such as: tips, internal closures within the central part of the tube, forming a so called "bamboo" structure (Figure 2.2), and even an angle Y-junction formation of MWNTs.

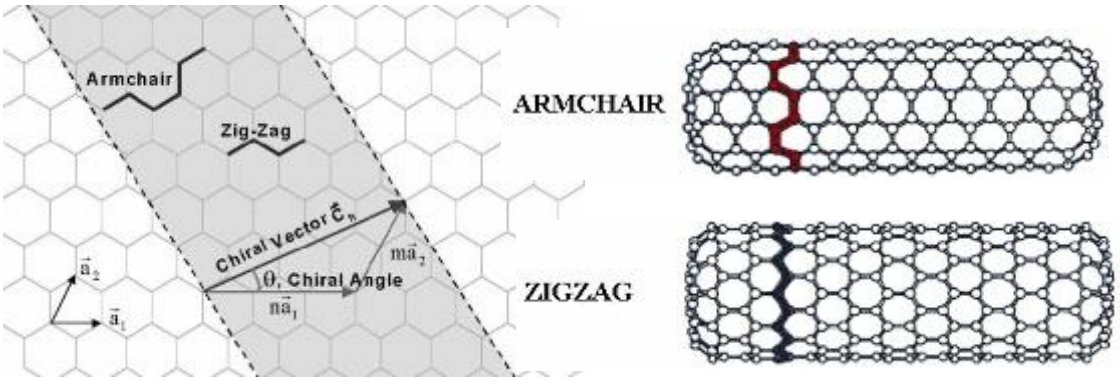

Figure 2.1 By rolling a graphene sheet in different directions typical nanotubes can be obtained: zigzag (n, 0), armchair (m, m), and chiral (n, m), where $n>m>0$ [10]. Integers (n, m) are the numbers of steps along which the zigzag carbon bonds of the hexagonal lattice, $\vec{a}_1$ and $\vec{a}_2$ are unit vectors, $\vec{C}_h$ is the chiral vector, and θ is the chiral angle (equation (2.1)).

Due to their properties CNTs have become very promising fillers for the fabrication of new advanced composite systems. It is commonly understood that carbon nanotubes cannot be utilized without any supporting medium, such as a matrix, to form structural components. Therefore, significant developments have been the subject of numerous studies in processing CNTs and CNT/polymer composite films or fibers [15,27-32]. The effective utilization of CNTs in composite applications depends strongly on the ability to disperse them homogeneously throughout the matrix. Chemical modifications have become an important issue due to the poor solubility of the CNTs in almost any solvent. Therefore, various functionalization strategies of the surface of the carbon nanotubes have been developed [10,16,33,34]. Chemical modification of CNTs ensures good dispersion of nanotubes in a medium, and enhances the interfacial bonding between filler and matrix, which is crucial to achieve a load transfer across the CNT/matrix interface. This is a necessary condition for the improvement of the mechanical properties of such composites and better stability of

the systems. Various studies include amorphous [35], semicrystalline [36], thermoplastic[26,37,38], water-soluble [39-41] and conjugated [29] polymers; resins [28,42]; ceramics [43,44], and metal matrices [45,46] as a supporting material for CNTs were shown. As a result of the presence of CNTs in composite, improvements of the properties of the matrix material such as: enhanced mechanical performance [27,30,39], high electrical conductivity [47-50], better thermal conductivity [51,52], and anisotropic optical properties [53,54], were shown.

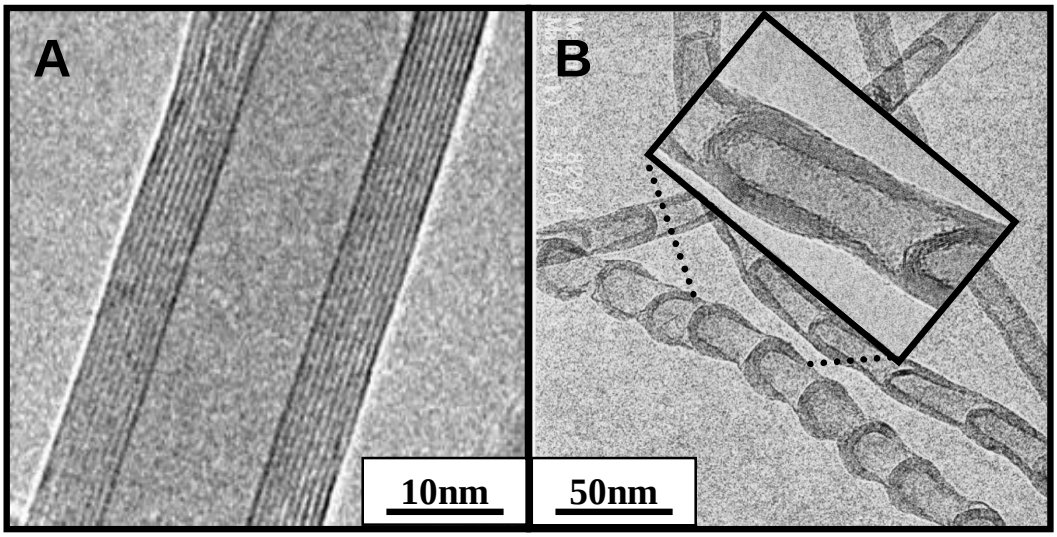

Figure 2.2 High resolution transmission electron microscope images of MWNTs used in this study: A) multiwall carbon nanotube (“hollow”) and B) “bamboo” type of MWNT (www.nanolab.com).

2.1.2 Manufacturing methods

At present carbon nanotubes are manufactured by different methods in laboratories and industry. The production of CNTs with a high order of purity, large amount, low costs, and uniformity are still one of the biggest issues in the carbon nanotube society. The most common techniques are (Table 2.1):

- Chemical vapor deposition (CVD): This technique involves the decomposition of hydrocarbon gases on the substrate in the presence of metal catalyst particles (Fe, Ni, Co). The synthesis of CNTs is often thermally or plasma-enhanced. MWNTs are mainly obtained by this method, with high purity but with limited control of the structure and diameter. Long nanotubes with diameters ranging from 0.6 - 4 nm

(SWNTs) and 10 - 200 nm (MWNTs) can be produced. The CVD technique is suitable for a large-scale industrial production of nanotubes. If plasma is generated by the application of a strong electric field during the growth process (plasma enhanced CVD), then the nanotube growth will follow the direction of the electric field [55] forming vertically aligned carbon nanotubes (e.g. perpendicular to the substrate).

- High pressure conversion of carbon monoxide (HiPCO): This method is considered as an improved CVD process which bases on the gas-phase growth of singlewall carbon nanotubes with carbon monoxide as a carbon source at high temperature and pressure. This technique is suitable for the production of large quantities of SWNTs with high purity [56].
- Arc discharge method: This bases on an electric arc discharge generated between two graphite electrodes under an inert gas atmosphere (argon, helium). This method requires very high temperatures (>5000 ^{o}C) and produces a mixture of different components (including fullerenes, amorphous carbon, and some graphite sheets) [57,58]. The carbon nanotubes need to be separated from the soot and the catalytic metals present in the crude product. Depending on the variation of the parameters (e.g. temperature, pressure, different gases and catalytic metals) employed in this technique, it is possible to selectively grow SWNTs or MWNTs. CNTs produced this way are normally tangled with poor control over the length and diameter. CNTs are short with diameters ranging from 1.2 - 1.4 nm (SWNTs) and 1 - 3 nm (MWNTs).
- Laser ablation: A graphite target is vaporized by laser irradiation under flowing inert gas atmosphere at high temperature [59,60]. Nanotubes produced in this way are very pure but the process is not effective for a large scale synthesis. Only bundles of individual SWNTs of 5 - 10 μm in length and 1 - 2 nm in diameter are being fabricated in this way.

All of these methods are still under development; there are numerous variations of these techniques operating under different conditions, with different set-ups, and process parameters. Every technique provides diverse advantages and disadvantages over the quality and kinds of synthesized CNTs. An overview of these techniques is given in Table 2.1. Nowadays, the main issue concerns the large-scale and low-cost production of nanotubes for industrial applications.

Table 2.1 An overview on the most common CNTs synthesis techniques and their advantages and disadvantages.

Method	***CVD***	***Arc Discharge***	***Laser Ablation***	***HiPCO***
Basics	Decomposition of hydrocarbon gases in the presence of metal catalyst particles	Electric arc discharge generated between two graphite electrodes under an innert atmosphere (argon, helium)	Graphite target is vaporized by laser irradiation under flowing innert atmosphere and high temperature	Gas-phase growth of singlewall carbon nanotubes with carbon monoxide as a carbon source at high temperature and pressure
SWNT	long, 0.6 - 4 nm diameter	short, 1.2 - 1.4 nm diameter	long, 1-2 nm diameter	~0.7 nm diameter, various lengths
MWNT	long, 10-200 nm diameter	short, 1-3 nm diameter	not applicable but possible	not applicable
Yield	up to 100 %	up to 90%	up to 65 %	up to 70 %
Advantages	high purity, large scale production, simple	easy, defect-free nanotubes, no catalyst	high purity, defect free SWNTs	large scale, high purity
Disadvantages	limited control over the structures, defects	short, tangled nanotubes, random structures	expensive, low scale production	defects

2.1.3 Properties of CNTs

Carbon nanotubes have gained in interest as nanoscale materials due to their exceptional, outstanding properties such as: extremely high Young's modulus and ultimate strength, high electric and thermal conductivity. Moreover, CNTs provide a remarkable model of a 1D system. More details on the properties of carbon nanotubes are presented below.

2.1.3.1 Mechanical properties

The structural properties of CNTs with strong σ bonds between the carbon atoms give nanotubes a very high Young's modulus and tensile strength. The strength of the carbon-carbon bonds in-plane, along the cylinder axis, retains the structure exceptionally strong resistance to any failure. CNTs also have very good elasto-mechanical properties. The two-dimensional (2D) arrangement of the carbon atoms in a graphene sheet permits a large out-of-plane distortion. Both experimental and theoretical investigations show extraordinary mechanical properties of individual MWNTs with Young's modulus being over 1 TPa and

a tensile strength of 10 - 200 GPa [61-63], which is several hundred times more than that of steel, while they are only one-sixth as heavy. The elastic response of a nanotube to deformation is also remarkable: CNTs can sustain up to 15 % tensile strain before fracture. Nanotubes are shown to be very flexible, with the reversible bending up to angles of 110º for both SWNT and MWNT [64]. Due to the extremely high strength of CNTs, they can bend without breaking. All of these properties open up broad possibilities for the use of CNTs as lightweight, highly elastic, and very strong composite fillers [30,43,47,56,65].

2.1.3.2 Electrical properties

Carbon nanotubes possess unique electrical properties. The diameter being in the nanometer range gives rise to quantum effects. The differences in the conducting properties are caused by the molecular structure. CNTs can either be conducting or semiconducting, depending on their chirality [62]. They are metallic if the integers of equation (2.1) are: $n=m$ (armchair structure) and $n-m=3i$ (where i is an integer). All other structures are predicted to be semiconducting [13]. The geometry of the nanotubes determines band structures and thus the energy band gap. The energy band gap of semiconducting CNTs highly depends on the nanotube diameter and is given by [66]:

$$E_{gap} = \frac{2\gamma_0 a_{C-C}}{d} \tag{2.2}$$

where γ_0 denotes the C-C tight binding overlap energy (2.45 eV), a_{C-C} the nearest neighbor C-C distance (~1.42 Å), and d is the diameter of a nanotube.

Multiwall carbon nanotubes are expected to behave like quantum wires due to the confinement effects on the tube circumferences. The conductance for carbon nanotubes is given by [10]:

$$G=G_0M=(2e^2/h)M \tag{2.3}$$

where $G_0=(2e^2/h)=(12.9k\Omega)^{-1}$ is the quantum unit of the conductance, e is electron charge, h is Planck's constant, M is an apparent number of conducting channels including electron-electron coupling and intertube coupling effects in addition to intrinsic channels.

In general, MWNTs are quite often found to be one-dimensional conductors with a high electrical conductivity (even $>10^3$ S/cm) [49]. The metallic properties of the MWNTs are due to their multiple-shell structure consisting of tubes with various electrical properties,

where additional electronic coupling between shells takes place. Moreover, MWNTs are predicted to have ballistic electron transport at room temperature (it refers to conduction where Ohm's law does not apply; the resistance is not dependent on the CNT's length) [67-69].

The electrical current that could be passed through a multiwall nanotube corresponds to a current density in excess of 10^7 A/cm^2. If nanotubes were classical resistors, the power dissipated by such a current would heat the nanotube so much that it would vaporize. The fact that this does not happen suggests that the electrons in nanotubes are strongly decoupled from the lattice [70].

2.1.3.3 Chemical properties

Functionalization of the carbon nanotubes (chemical or physical modification of the surface of CNTs, e.g. by the attachment of certain molecules or functional groups) is a very important issue in order to overcome their poor solubility in solvents (see 2.2.1). Functionalized CNTs are very attractive for chemical and biological applications because of their strong sensitivity to chemical or environmental interactions. This leads to a broad range of applications, e.g. as sensors. Covalent and non-covalent functionalization, doping, decoration with organic as well as inorganic species of the surface of CNTs lead to direct changes of the properties of carbon nanotubes (optical, electrical, and mechanical) [71-75].

2.1.3.4 Other properties

Besides the outstanding mechanical and electrical properties, CNTs exhibit interesting thermal and optical properties. Defect-free nanotubes, especially SWNTs, offer a direct band gap and a well defined band and sub-band structure, which is ideal for optical and optoelectronic applications. The experimental measurements of the optical absorption of a bundle of single-walled carbon nanotubes show that there are several groups of absorption peaks and each group is closely related to the nanotube geometry [22,71,76]. Typically, the optical absorption spectra of the SWNTs reveal peaks that correspond to the transition between the density of states (DOS), which strongly depends on the structure of nanotubes, e.g. chirality and the diameter.

CNTs are thermally stable up to 2800 °C in vacuum; their thermal conductivity in the axial direction is about twice as high as of present commercial synthetic diamond (6000 W/mK) but has very small values in the radial direction [77,78]. CNTs with high

aspect ratio and small tip radius of curvature are found to be excellent field emitters (electron emission). It was shown that relatively low voltages are needed for effective field emission with a high field amplification factor, this offers an advantage over other metallic emitters which need a high voltage for emission [79].

2.2 CNT-based composites

The outstanding properties of the carbon nanotubes make them promising filling material for the fabrication of new advanced composite systems for a broad range of applications. Efficient chemical functionalization of CNTs, homogeneous dispersions in solvents and supporting media, and good interconnectivity with matrix still remain very important issues that must be considered in order to achieve heterostructures with enhanced or even new properties. There are numerous methods and approaches for functionalization and further efficient dispersion of the carbon nanotubes in different media. More details on the chemical modification of CNTs, the fabrication of various CNT-based composites, and their possible applications are presented below.

2.2.1 Functionalization and dispersion of carbon nanotubes

CNTs in all their forms are difficult to disperse and dissolve in any organic and aqueous medium. Due to the strong attractive long-ranged van der Waals interaction, nanotubes tend to aggregate and form bundles or ropes, usually with highly entangled network structures. This attraction is fundamental for many body particles and well known for colloids dispersed in polymers [80]. When suspended in a polymer, an attractive force between fillers also arises due to the entropic effects [81]. Polymer chains in the region of the colloidal filler suffer an entropic penalty since roughly half of their configurations are precluded. Therefore, there is a depletion of the polymer in this region, resulting in an osmotic pressure forcing the filler particles to come together [10,16,72,82].

Homogenous dispersion of CNTs within a supporting medium is crucial for the fabrication of composites with improved properties, well defined and uniform structures. This issue stimulates intensive studies on the exfoliation of carbon nanotubes. Dispersion broadly falls into two main categories: mechanical/physical and chemical methods. The

mechanical techniques involve physically separating the tubes from each other. The chemical methods often use surfactant or chemical treatment of the tube surface. However, certain types of aggressive chemical treatment can lead to the key nanotube properties being compromised.

In general, the functionalization of CNTs requires chemical modifications of their surface supported by the mechanical agitation methods such as ultrasonication and shear mixing [23,37,69,83]. Several functionalization strategies have been reported recently. They are mainly based on the covalent ("grafting-to" and "grafting-from") [84-86], and non-covalent (polymer wrapping [33,87,88], π-π stacking interaction [89], adsorption of surfactants [34]) coupling of surfactants and functionalities to CNTs, and are described as follows:

- Covalent functionalization: Covalent methods refer to a treatment that involves bond breaking across the surface of the CNTs (e.g. by oxidation) which disrupts the delocalized π-electron systems and fracture of σ-bonds and hence leads to incorporation of other species across the CNTs' surface. Introducing defects to the CNT's shell significantly alters the optical, mechanical and electrical properties of the nanotubes and leads to an inferior performance of the composites [90]. The advantage is that this kind of modification may improve the efficiency of the bonding between nanotubes and the host material (cross-linking). Therefore, the interfacial stress transfer between the matrix and CNTs may be enhanced leading to better mechanical performance.
- Non-covalent functionalization: This modification of the carbon nanotubes is of great advantage because no disruption of the sp^2 graphene structure occurs and the CNT properties are preserved. Its disadvantage concerns weak forces between wrapped/coupled molecules that may lower the load transfer in the composite.

The chemical modification of the CNTs' surface improves solubility/separation of the nanotubes in a given solvent. A proper functionalization ensures homogenous and stable dispersion throughout the solvent and in the composite host material. Moreover, functionalities on the surface of CNTs may lead to enhanced interactions between filler and matrix due to the presence of the interfacial bonds between components.

2.2.2 CNT/ Polymer composites

Nowadays polymers play a very important role in numerous fields of everyday life due to their advantages over conventional materials (e.g. metals) such as lightness, resistance to corrosion, low-cost production, and ease of processing. Further improvement of their performance is still being intensely investigated. Altering and enhancement of the polymers' properties occur, for example, through doping with various fillers such as metals, semiconductors, organic and inorganic particles and fibers, as well as carbon structures and ceramics; thereby enabling polymers to be used as a structural unit [2-5].

Fillers are used in polymers for a variety of reasons: improved processing, density control, optical effects, thermal conductivity, control of thermal expansion, electrical properties, magnetic properties, flame resistance, and improved mechanical properties, such as hardness, elasticity, and tear resistance. Polymer composites can be used in many different forms in various areas ranging from structural units in the construction industry to the composites of the aerospace applications [10,13].

The extraordinary properties of carbon nanotubes make them very promising and favorable as fillers for fabrication of a new class of polymeric heterostructures. Polymer matrices have been widely exploited as a medium for CNTs. Research projects are focused on the development of CNT-based polymer materials that utilize the carbon nanotubes characteristics and properties, such as [26]:

- The high strength and stiffness of the CNTs are used for developing superior polymer composites for structural applications which are lighter, stronger, and tougher than any polymer-based material [25,47,65,83,91]. The exemplary results of the mechanical properties of CNT/polymer composites are summarized in Table 2.2.
- Effort is being made to exploit the electrical conductivity of the CNTs to develop new materials e.g. electromagnetic interference (EMI) shielding, conductive polymers, or antistatic coatings [92-95].
- The efficient thermal conduction of the CNT improves the high temperature characteristics of the polymer matrix, by dissipating the heat through the CNTs that prevents the degradation of the surrounding polymer [96].

- The alignment of CNTs in composites provides enhanced anisotropic characteristics of materials due to the anisotropic properties of 1D structure of the CNTs. The alignment of CNTs improves also the mechanical properties of composites [97,98].

Table 2.2 Mechanical properties of various CNT/polymer composites evaluated from tensile tests. E_p, σ_{Tp}, E_c, σ_{Tc} indicate elastic modulus and tensile strength of the polymer and composite, respectively. PMMA - poly(methyl methacrylate) PS - polystyrene, HDPE - high density polyethylene, PP - polypropylene, PVA - polyvinyl alcohol, PA6 - polyamide 6, PA12 - polyamide 12, PBO - Poly(p-phenylene benzobisoxazole), PEI polyethyleneimine.

CNT type	***Polymer***	***Preparation method***	E_p ***[GPa]***	σ_{Tp} ***[MPa]***	E_c ***[GPa]***	σ_{Tc} ***[MPa]***	***CNT content***	E_c/E_p	σ_{Tc}/σ_{Tp}	***Ref.***
MWNT	PS	solution processing	1.19	12.8	1.69	16	1 wt%	1.42	1.25	[99]
MWNT	PS	solution processing	1.53	19.5	3.4	30.6	5 wt%	2.22	1.57	[48]
MWNT	HDPE	solution processing	0.98	20	1.35	25	1 wt%	1.38	1.25	[100]
MWNT	PVA	solution processing	1.9	81	7.4	348	0.6 vol%	3.9	4.29	[101]
MWNT	PMMA	melt processed	2.7	64	3.7	80	10 wt%	1.37	1.25	[102]
MWNT	PA6	melt processed	2.6	-	4.2	-	12 wt%	1.61	-	[103]
MWNT	Nylon	melt processed	0.4	28	1.24	58	2 wt%	3.13	2.07	[104]
MWNT	PA12	melt processed fibers	0.8	-	1.6	-	10 wt%	2	-	[105]
MWNT	Polyimide triple A PI	thermoset resin/hardener	2.84	115	3.9	95	14.3 wt%	1.37	0.83	[106]
MWNT	Epon 828/T-403	thermoset resin/hardener	2.15	64.6	2.16	63.9	1 wt%	1.01	0.99	[107]
MWNT	Nylon 610	in situ polymerization	0.9	35.9	2.4	51.4	1.5 wt%	2.66	1.46	[108]
SWNT	PVA	solution processing	2.4	74	4.3	107	0.8 wt%	1.81	1.45	[109]
SWNT	PP	melt processed	0.85	30.8	0.93	33.7	0.75 wt%	1.09	1.09	[110]
SWNT	PP	melt processed fibers	6.3	709	9.8	1032	1 wt%	1.55	1.45	[111]
SWNT	PA6	in situ polymerization	0.44	40.9	1.2	75.1	1.5 wt%	2.73	1.83	[112]
SWNT	PBO	in situ polymerization	138	2600	167	4200	10 wt%	1.21	1.61	[25]
SWNT	PEI	LBL assembly	-	9	-	220	~50 wt%	-	24.4	[113]

There are several important requirements for an effective improvement of CNT-based composites' properties, such as: a large aspect ratio of a filler, good exfoliation and dispersion of nanotubes, and good nanotube-nanotube and nanotube-polymer interfacial bonding. Numerous studies have shown already, that an effective performance of the carbon nanotubes in composites for a variety of applications strongly depends on the ability to disperse the CNTs homogenously throughout the matrix [24,100,114]. Good interfacial bonding and interactions between nanotubes and polymers are also necessary conditions for improving mechanical properties of the composites. Due to the nanoscale size of the CNTs the active CNT/matrix interface is significantly higher than that of other conventional fillers.

Various approaches for the fabrication of CNT/polymer composites were shown including different functionalization and dispersion methods of nanotubes [26]. The most important are:

- Solution processing of composites: The most common method based on the mixing of the CNTs and a polymer in a suitable solvent before evaporating the solvent to form a composite film. The dispersion of components in a solvent, mixing, and evaporation are often supported by mechanical agitation (e.g. ultrasonication, magnetic stirring, shear mixing) [26,48,99].
- Melt processing of bulk composites: This method concerns polymers that are insoluble in any solvent, like thermoplastic polymers [26,37,38]. It involves the melting of the polymers to form viscous liquids to which the CNTs can be added and mixed.
- Melt processing of composite fibers: CNTs are added to the melts of the polymers. The formation of CNT/polymer fibers from their melts occurs through e.g. the melt-spinning process [115].
- Composites based on thermosets: A thermoset polymer is one that does not melt when heated such as epoxy resins. The composite is formed from a monomer (usually liquid) and CNTs, the mixture which is cured with crosslinking/catalyzing agents [51,73].
- Layer-by-layer assembly (LBL): CNTs and polyelectrolytes are used to form a highly homogeneous composite, with a good dispersion, good interpenetration, and a high concentration of CNTs. This method involves alternating adsorptions of a

monolayer of components which are attracted to each other by electrostatic interactions resulting in a uniform growth of the films [113].

- In-situ polymerization: The polymer macromolecules are directly grafted onto the walls of carbon nanotubes. This technique is often used for insoluble and thermally unstable polymers which cannot be melt processed. Polymerization occurs directly on the surface of CNTs [10,13].

In general, all of these different techniques give various results in terms of the efficiency of the nanotubes' dispersion, interfacial interaction between components, properties of the composites, and possible applications.

2.2.3 CNT/nanocrystals nanocomposites

The formation of CNT/nanoparticle heterostructures is of both fundamental and technological interest. Combining the unique properties of CNTs and nanoparticles (NPs) a new class of the nanocomposites can be made meeting a broad range of advanced applications [17-19].

Recently, it was shown, that the physical properties of CNTs can be significantly affected, not only by the chemical surface modifications, but also by the attachment of inorganic, organic, and biological objects [116-119]. The decoration of the surface of the CNT with a variety of elements creates new ways for the invention of novel one-dimensional (1D) hybrid materials. Different strategies were presented for the decoration of CNTs with various compounds including metals Ag, Pd, Pt, Si, Fe, Au, Ni, Co [120-122] and semiconductor nanocrystals (NCs) [90,123-132]. Enhanced or even new properties of these CNT heterostructures were reported; this opens up new potential for applications including electronic and optic devices [90,119,127], sensors [133,134], and solar cells [119,135].

Colloidal semiconductor nanocrystals are of great interest due to the size-dependent photoluminescence tunable across the visible spectrum [136-139]. The band gap of these materials increases with decreasing particle size, the electronic structure exhibits typical quantum confinement effects. It is possible to manipulate nature, and thus the optical properties of the quantum dots (QDs) by surface modification such as: attachment of various organic capping groups or covering the nanoparticles with inorganic semiconductor shells, where the band gap of the core lies energetically within the band gap of the shell material.

These core-shell NCs have been shown to be in general highly resistant to chemical degradation or photo-oxidation [140]. Due to these remarkable properties of semiconducting nanocrystals various studies have focused on the fabrication of the CNTs/quantum dots' complexes. Different semiconductor nanoparticles were attached to the surface of carbon nanotubes utilizing various methods: CdSe [141,142], CdSe-ZnS [90,129], CdS [130] have been covalently bound to the surface of CNTs; CdTe [119] and CdSe-ZnS [143] have been attached by electrostatic attraction; ZnO and ZnS [128,144] have been used as a template for direct thermal growth of nanocrystals; an in-situ chemical-solution synthesis of crystalline CdTe [125], CdSe [124], ZnS [126,132], and CdS [131]on CNTs also was shown.

2.2.4 Potential applications of CNTs and their composites

Carbon nanotubes are being wildly considered for the use as energy storage materials (fuel cells), advanced aerospace composites, co-axial cable, field emitting devices, transistors, EMI shielding in electronic devices, nanoprobes and sensors, composite materials, to name a few. The potential applications of carbon nanotubes and their composites are listed below:

- Field emitters: Carbon nanotubes have been shown to have excellent emission characteristics: emission has been observed at fields lower than 1 V/μm, and high current densities of over 1 A/cm^2 have been obtained [79,145].
- Energy storage: The advantages of considering CNTs to store energy are their cylindrical and hollow geometry, nanometer scale diameter, and perfect surface specificity. Energy carriers such as hydrogen can be stored in an adsorbed form on CNTs, which are capable of absorbing and releasing large quantities of this element easily and reliably [146].
- Sensors: Strong dependence of the properties of CNTs on surface modification, mechanical deformation, doping, coating, etc. make them a very attractive material for chemical, biological, and physical sensors. Small changes in the environment of the CNT can cause drastic changes to its electrical properties [147-150].
- High strength composites: The outstanding properties of CNTs have enabled the development of composite systems with improved mechanical performance [27,30,99,113].

- Conducting polymer composites: A high aspect ratio of CNTs allows for lower percolation than other fillers [47,151,152].
- Heat dissipation coatings: Extraordinary thermal properties make CNTs a promising filler for heat dissipating materials [35,96].
- EMI shielding materials: CNTs act as an absorber/scatterer of radar and microwave radiation [23,153].
- Aligned CNT systems for data storage, optical transmitters, detector sensory systems etc. [15,35,53].

2.3 Theoretical background

Different theoretical models have been used to explain experimental results and to predict new applications of composite materials. Besides others, the effective medium theory (EMT) and the modeling of the electrical and rheological percolation threshold are of the focus of the work presented here.

The EMT is essential for the evaluation of the electromagnetic properties of composites composed of an insulating matrix and conducting inclusions e.g. carbon nanotubes. The effective dielectric constant of such composites can be determined this way. The analysis of the propagation of electromagnetic waves in different media can be performed.

Systems composed of two materials, in particular, polymeric matrix and its filler may experience the percolation transition, which refers to the critical concentration of the filler at which the rheological or electrical properties of the composite are significantly changed. In this study, rheological and electrical percolation thresholds of CNT-based nanocomposites are described and further experimentally characterized. More details on EMT and rheological and electrical percolation threshold are given below.

2.3.1 Effective medium theory

The effective medium theory can be used to calculate the effective properties of composites with located symmetric inclusions. EMT can be applied to a wide variety of problems in the general area of condensed matter. It is used to analyze the propagation of electromagnetic waves in heterogeneous media. In the case of the composite systems consist-

ing of a random distribution of fillers, the properties of the composite can be evaluated from equations describing the dielectric response [154].

Composites containing conducting fibers are advantageous over conventional powder or particle-filled composites, because they allow for high values of dielectric constant at low concentration of the filler to be obtained [155]. This opens up promising applications of fiber-filled systems as antistatic materials, electromagnetic shields, and radar absorbers [156]. The EMT considers a model that describes dielectric properties of composites with a concentration of the filling fibers below or near the electrical percolation threshold. In the vicinity of the percolation threshold the complex dielectric constant may reach high values at low frequencies [50,157].

The Maxwell-Garnett (MG) and the Bruggeman effective medium theories are the most widely used methods for calculating the dielectric properties of the composites [154,158,159]. In the MG method, the complex dielectric function $\varepsilon^*(\omega)=\varepsilon'(\omega)-i\varepsilon''(\omega)$ of the bulk material can be evaluated from the expression for the effective (e.g. measured) dielectric function ε_{eff} which is related to the dielectric function of the polymer ε_d and the dielectric function of a spherical filler ε_m:

$$\varepsilon_{eff} = \varepsilon_d \frac{2\varepsilon_d(1-f)+\varepsilon_m(1+2f)}{\varepsilon_d(2+f)+\varepsilon_m(1-f)} \tag{2.4}$$

where f is a volume fraction of the filler in the composite given by $f=(4\pi/3)na^3$, which defines the volume or filling fraction of the spheres (with radius a and density n) . This model is generally used in the case of particles of a randomly distributed filler in the continuous medium and sufficiently far from each other to avoid direct interactions. The MG approach for fiber-like fillers (however with a low aspect ratio) was found to be a good approximation for large distances between fibers, where the interaction between them can be neglected [156]. The Bruggeman model is generally calculated for the composite composed of two kinds of spherical particles (1 and 2) being randomly distributed in the sample:

$$f\frac{\varepsilon_1-\varepsilon_{eff}}{\varepsilon_1+2\varepsilon_{eff}}+(1-f)\frac{\varepsilon_2-\varepsilon_{eff}}{\varepsilon_2+2\varepsilon_{eff}}=0 \tag{2.5}$$

Since the MG and Bruggeman models describe the dielectric function of the materials composed of particles in a continuous medium and particle-particle mixture, respectively, new theoretical approaches were necessary for the evaluation of the properties of the composites with carbon nanotubes as fillers, where longitudinal conductive inclusions with

high aspect ratio are considered. Therefore, more theoretical studies based on the MG and Bruggeman models have been carried out recently to calculate the dielectric function of the composite consisting of stick-like fillers with a high aspect ratio that represents the metallic nanotubes in a polymer medium.

Lagarkov et al. [160] presented the calculation of the permittivity spectra of a composite material comprising of conducting elongated stick-like inclusions with large aspect ratios (where the length and the radius of conductive filler can be defined) dispersed inside a dielectric matrix. Grimes at al. showed results on the complex permittivity of multiwall carbon nanotubes/polystyrene composite [161,162]. The experimental data were fitted to the theoretical predictions of EMT of Lagarkov et al. The results of experimental and calculated spectra correspond relatively well to each other.

Alvarez et al. studied the nature of the electric field screening of the metallic single-wall carbon nanotubes ropes [158]. Different factors contributing to the longitudinal dielectric response of the system were considered such as: intratube and intertube Coulomb interaction, the presence of a glassy graphite environment and the influence of a weak relaxation effects produced by impurities or defects.

Garcia-Vidal et al. presented an effective medium approach to analyze the optical properties of aligned CNTs in composites [156]. It considers electromagnetic interactions between fillers as a function of the volume fraction. This type of model was used to analyze spectroscopic properties of nanostructured materials. The numerical results were consistent with experimental data obtained.

Kempa et al. demonstrated theoretically and experimentally that the dielectric function of the composites can be significantly enhanced through a careful choice of the insulated metallic nanostructures, like silica coated multiwall carbon nanotubes [163]. Carbon nanotubes were found to markedly improve the dielectric properties of the polymer matrix at low loading level. The experimental results conformed to the theoretical dielectric function of composites based on elongated carbon nanotubes incorporated in a polymeric matrix. For the composites with a broad range distribution of filler length, the dielectric constant is given by:

$$\varepsilon(\omega) \approx \varepsilon_m + \int_0^x \frac{f(x)\omega_p^2}{x - \omega^2 - i\gamma\omega} dx \qquad (2.6)$$

where ε_m is matrix dielectric constant, plasma frequency of the metal $\omega_p = \sqrt{4\pi ne^2/m}$, n and m are electron density and mass, respectively; γ the damping constant, $f(x)$ distribution function of the nanotube lengths (with a different resonant frequency for a given length). Assuming that the distribution is uniform, e.g. $f(x)=p/(x_{max}-x_{min})$ equation (2.6) is given by:

$$\varepsilon(\omega) = \frac{p}{(x_{MAX} - x_{MIN})} \ln\left(\frac{x_{MAX} - \omega^2 - i\omega\gamma}{x_{MIN} - \omega^2 - i\omega\gamma}\right) \tag{2.7}$$

where x_{max} and x_{min} are the maximum and minimum values of lengths x in the size distribution, p is a filler concentration.

Various studies have shown that the complex permittivity of the CNT/polymer systems reaches high values in the vicinity of the percolation threshold. Even small weight percentage additions of the nanotubes to the polymer were found to increase the magnitude of the permittivity spectra [50,160,161,163-166].

2.3.2 Percolation theory

The percolation theory may be used to describe the structure and properties' transitions in the filled polymers. The structure and properties changes of such composites can usually be referred to the concentration of the filler at which the interconnected clusters of the filling material reach a well defined threshold. For concentrations above this threshold it can be seen to be an infinite cluster (formed by filler) that connects two sides of an arbitrarily large sample. This work is focused on the percolation theory in terms of transition of the rheological and electrical properties of the CNT/polymer composites.

Systems composed of an insulating material and a conductive filler experience an insulator-conductor transition at the electrical percolation threshold. The electrical percolation threshold is the minimal volume fraction of fillers so that a continuing conductive network exists in the composite. Above this volume fraction, the electrical resistivity of the composite is relatively low. Below the electrical percolation threshold, the compound essentially behaves as an insulator. There are different models and theories that define an insulator-conductor transition and a corresponding percolation threshold of the conductive filler concentration with regard to the DC and AC conductivity [165,167,168].

The liquid-solid transition of melt polymer composites is described by the rheological percolation threshold. The viscoeleastic properties significantly change while increasing the concentrations of the filler within the host material.

It has been shown, that the rheological percolation threshold may significantly differ from the electrical one; as a result many studies were focused on these phenomena. Fundamentally, polymer chain immobility and the distance between neighboring nanotubes determine the rheological and electrical percolation threshold, respectively [168-172].

The rheological and electrical percolation thresholds of CNT-based polymeric composites and differences between them are described below.

2.3.2.1 Electrical percolation threshold of CNT/polymer composites

The compositions of different materials have, in the past, been of great significance and attract a great deal of interest in the physics. Various properties can be attained by the formation of hybrid systems. The presence of conductive fillers like CNTs within an insulating matrix material alters the electric properties of the composite [49,94]. The composite becomes conductive above a critical value – percolation threshold that defines the insulator-conductor transition. The electrical percolation threshold depends on many factors including the size and shape of the filler, matrix properties, preparation method, filler properties, dispersion of the filler within matrix, interaction between compounds etc. A high aspect ratio and a good dispersion of CNTs in a matrix enable percolation at a very low weight fraction of nanotubes.

While the effective medium theory refers to the composites' dielectric properties below or in the vicinity of the electrical percolation threshold, where the system remains insulating; the electrical percolation theories concern systems with filler concentrations above the electrical percolation threshold. In the classical electrical percolation theory, the relationship between the composite direct current (DC) conductivity σ_{DC} and the concentration (p) above the percolation threshold (p_c) can be described by a scaling law [94,165,167]:

$$\sigma_{DC} \propto \sigma_0 (p - p_C)^t \quad \text{for } p > p_c \tag{2.8}$$

where σ_0 is a constant parameter and t the critical exponent that is dependent on the dimension of the lattice. According to the percolation theory, a theoretical value of $t \cong 2.0$ for a percolation network in three dimensions was estimated [165,167]. Value of the critical

exponent *t* obtained by fitting a power law relation to the experimental data was shown to lay in the range of 1.1 - 3.1 [49,94,165,167].

In the percolation theory σ_0 should approach the conductivity of the filler (CNTs) by itself. However, there is the contact resistance between CNTs or their clusters in the system, which decreases the effective conductivity of the CNTs. Moreover, in CNT/polymer composites, conducting nanotubes are separated by insulating polymers that act as a potential barrier, so that it is likely that the electrical conductivity is limited by hopping and/or tunneling of the charge carriers between conductive nanotubes. However, the tunneling and hopping is temperature-dependent. This behavior is described by the fluctuation induced tunneling model which takes into the account tunneling through potential barriers due to the local temperatures fluctuations [94,167]:

$$\sigma_{DC} \propto \sigma_0 \exp[-T_1/(T+T_0)] \tag{2.9}$$

where T_1 represents the energy required for an electron to cross the insulator gap between conductive clusters and T_0 is the temperature above which the thermal activated conduction over the barrier begins to occur.

The dielectric properties of the composites are also characterized by means of the dynamic dielectric spectroscopy. For the frequency dependent AC conductivity σ^* and the real part of the permittivity ε' power law equations are given by [165]:

$$\sigma^*(\omega) \propto \omega^s \tag{2.10}$$

$$\varepsilon'(\omega) \propto \omega^{-u} \tag{2.11}$$

where *s* and *u* denote scaling exponents (in range of 0 - 1), which in vicinity of the percolation threshold are related to each other: $s + u = 1$.

The relation between the frequency dependent AC complex conductivity σ^* of a composite system and the filler concentration above the percolation threshold is given by power law equation:

$$\sigma(\omega) \propto \sigma_0 (p - p_C)^t \tag{2.12}$$

where *p* is the concentration of conducting filler for $p > p_c$, σ_0 is a constant parameter, *t* is critical exponent. This relation is valid for low frequency AC conductivity ($\omega \rightarrow 0$) at which σ_{AC} approaches the DC conductivity value. Below critical frequency σ_{AC} becomes frequency independent which refers to σ_{DC}.

In this study frequency dependent dielectric spectroscopy was used in order to characterize electrical properties of the CNT/polymer composites. The experimental data were fitted to the power law equations presented above (equations (2.10), (2.11), and (2.12)). From the fitting curves the electrical percolation threshold and critical exponents were obtained.

Numerous studies were conducted on the evaluation of the electrical percolation threshold of CNT/polymer systems. Depending on the functionalization, exfoliation and dispersion of CNTs, composite processing, properties of components etc., different values of p_c were obtained ranging from 0.005 up to 4 wt% [49-51,151,152,165,167,173,174] (Table 4.4).

2.3.2.2 Rheological percolation threshold of CNT/polymer composites

Transition from viscoeleastic properties exhibiting liquid-like characteristics to pseudo-solid-like behavior can be expressed by the rheological percolation threshold. To determine the rheological percolation threshold of CNTs/polymer composites, the relations between rheological quantities and the concentration of the filler in a medium are drawn into two modified power law equations [92,169,171,172]:

$$\eta \propto (m - m_c)^a \tag{2.13}$$

$$G' \propto (m - m_c)^t \tag{2.14}$$

where, η is the complex viscosity, G' the elastic (storage) modulus, m CNTs' loading, m_c the rheological percolation threshold, a and t are the critical exponents, that are dependent on the oscillatory shear frequency. The percolation theory predicts $a=t\cong 2$ in three dimensions; however as it is explained in the next paragraph, the rheological percolation threshold does not relate to the geometrical percolation threshold (where the physical contact between particles is assumed). Thus, this fitting parameter may significantly vary from the expected theoretical value.

In percolated systems one can observe a drastic change of the storage modulus and viscosity at a fixed shear frequency for a given concentration of the filler. This indicates that the CNT/polymer composite reaches a rheological percolation threshold at which the nanotubes block the motion of the polymer molecules.

The rheological percolation threshold has also been shown to be temperature dependent, which is in contrast to the assumption that the liquid-solid transition originates only

from the network formation of the filler [169]. This reveals, that rheology reflects a combined network of the polymer chains and nanotubes, not only the interconnection between CNTs. The entangled nanotube-polymer network dominates the rheological properties of the composites [92].

The experimental data from the rheological investigation of the CNT/polymer composites obtained in this study has been fitted to the power law equations (2.13) and (2.14). The rheological percolation threshold and critical exponents have been calculated.

2.3.2.3 Differences between rheological and electrical percolation thresholds

There are essential differences between electrical and rheological percolation thresholds, which are basically related to the nanotube-nanotube distances and polymer-nanotube interactions. It is assumed that for the nanocomposite to reach the electrical percolation threshold and therefore be electrically conductive, direct connection and overlapping of the CNTs is not necessary – nanotubes do not need to physically touch each other. Nanotubes can just be close enough to allow for a hopping/tunneling electron effect; these mechanisms require the CNT-CNT distance to be less than 5 nm [172]. However, CNTs are often functionalized with different surfactants, polymers, and bio-species; in composite system CNTs are also coated with a layer of an insulating polymer. All of this reduces the quality and quantity of electrical contacts between the nanotubes, and also diminishes the tunneling effect; but it does not affect the rheological percolation. It must be noted that in the batch of synthesized carbon nanotubes, there are always CNTs with various electrical properties including semiconductors and nanotubes with surface defects (e.g. caused by functionalization). Such CNTs do not contribute significantly to the electrical conductivity. As a result, a higher volume fraction of the CNTs' filler is needed to achieve electrical percolation threshold in comparison to the rheological percolation [92,170,172]. The rheological percolation refers to the system of interconnected polymer chains and carbon nanotubes. Therefore the distance between nanotubes must be smaller than the average radius of gyration of polymer chains. The average radius of gyration of polymer chains in the melt state is estimated to be more than 10 nm [172]. To form the rheological percolating system, nanotubes can be linked by random coils of polymer chains, which consequently impede the polymer chains' mobility. Thus, the CNT-CNT distance required for the rheological percolation threshold is longer than that for the electrical percolation threshold (Figure 2.3). Therefore, a lower volume fraction of nanotubes can restrict polymer motion

in contrast to the higher volume fraction, which is required to form a conductive network throughout the matrix [168,169].

In general, the values of the rheological and electrical percolation thresholds of CNT-based nanocomposites are sensitive to:

- the electrical and mechanical properties of CNTs,
- polymer type (radius of gyration, molecular weight, properties),
- interfacial properties between matrix and filler,
- aspect ratio of CNTs,
- homogenous dispersion of CNTs within polymer matrix,
- efficient exfoliation of bundles of nanotubes (functionalization),
- filler orientation (it reduces tube-tube interactions).

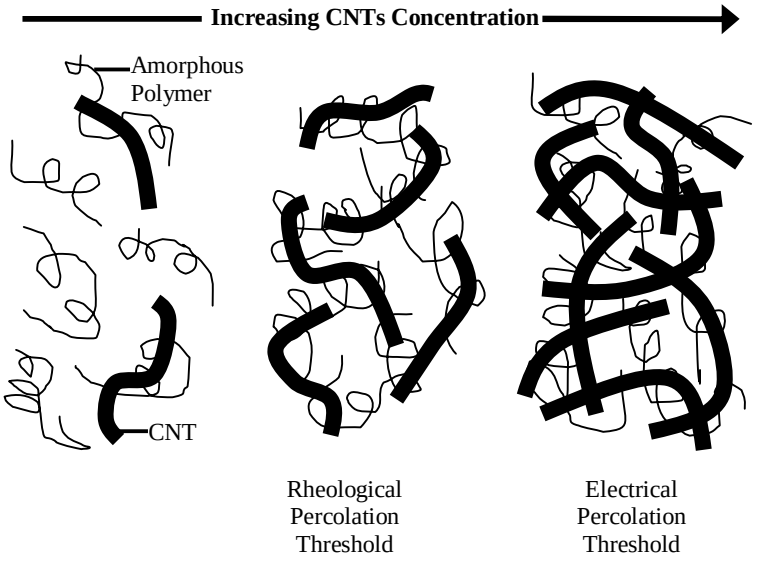

Figure 2.3 Schematic of CNTs/polymer nanocomposite with isotropic orientation of nanotubes. At low concentration of CNTs (left), the rheological and electrical properties of the composite are comparable to those of the host matrix. Rheological percolation threshold takes place when the distance between nanotubes is comparable to the average radius of gyration of the polymer (center). Electrical percolation threshold (right) is observed when nanotubes are sufficiently close to each other to form a percolating conductive path [172].

CHAPTER III

SAMPLE PREPARATION AND INVESTIGATION METHODS

3.1 Materials and samples

Multiwall carbon nanotubes were obtained from NanoLab Inc., synthesized by chemical-vapor deposition in a tube furnace with flowing acetylene gas as the carbon source. Alumina nanoparticles, coated with iron catalyst, were used as seeds for the CNT growth. Multiwall carbon nanotubes with "hollow" and "bamboo" morphologies (Figure 2.2) with a diameter in the range of 15 - 45 nm, lengths between 1 – 20 μm, and purities of 95 %, were used in this study. The chemicals that have been used in the functionalization processes and composite fabrications are described in the text below.

3.1.1 Functionalization and dispersion of MWNTs

Various methods of functionalization of multiwall carbon nanotubes were used in order to achieve a good level of exfoliation of the bundles and agglomerations of CNTs. Since chemical modification of CNTs is crucial for obtaining uniform dispersions and a high stability of nanotubes in organic or aqueous solvents, both covalent and non-covalent functionalizations of the surface of MWNTs were introduced.

3.1.1.1 Adsorption of surfactant

Nanosperse AQ (NaAQ) aqueous dispersant obtained from NanoLab Inc. was utilized as an agent for the functionalization of carbon nanotubes (www.nano-lab.com). NaAQ is a

specially formulated surfactant for creating dispersions of multiwall carbon nanotubes in aqueous solvents (MWNT-NaAQ).

NaAQ was used to disperse the MWNTs in pure water (Milli-Q, resistivity 18.2 MΩ); typically: 0.01 g MWNTs and 0.02 g NaAQ in 20 ml of water. The mixture was treated for 0.5 – 3 h in an ultrasonic bath (200 W). To eliminate non-dispersed agglomerations of MWNTs, the sample was centrifuged three times (1157g, 20 min.) and the supernatant was taken. To remove excess surfactant from the solution, the samples were again centrifuged at 4629g for 2 h; the sediment was then taken and re-dispersed in 20 ml of water by treatment in an ultrasonic bath (200 W, 60 min.). The process was repeated three times. Such non-covalent functionalization results in the presence of a negative charge on the surface of carbon nanotubes, which makes the suspensions stable for months [175].

3.1.1.2 Polymer wrapping

MWNTs were non-covalently functionalized by a polymer wrapping method with poly(allylamine hydrochloride) (PAH) [176,177]. PAH is a positively charged polyelectrolyte (PE) (Figure 3.1).

CNTs (50 mg) were dispersed in a 0.5 wt% PAH (Sigma-Aldrich, Mw=70 000) salt solution (0.5 M NaCl, 500 ml) and sonicated for 5 - 10 h. Excess polymer was removed by centrifugation (18514g, 90 min.) and the sediment was washed with water (40 ml added to 50 ml plastic tubes); this process was repeated five times. A final residual black solid was re-dispersed in water (500 ml) by ultrasonication (200 W, 120 min.), forming a stable, homogenous suspension of nanotubes. The polymer chain is non-covalently adsorbed around carbon nanotubes due to van der Waals interactions, mechanical wrapping and anchoring. The charged amine functionalities on the MWNTs surface ensure good separation and stability due to the electrostatic interactions (repulsions) in aqueous solution.

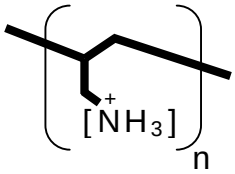

Figure 3.1 Schematic presentation of poly(allylamine hydrochloride)

PAH-modified CNTs (MWNT-PAH) were further coated with another oppositely charged polyelectrolyte (polyanion) such as: poly(styrenesulfonate) sodium salt (PSS,

Sigma-Aldrich, Mw=70 000) or polyacrylic acid (PAA, Sigma-Aldrich, Mw=450 000). Subsequently, different polycations (e.g. PAH, Poly(diallydimethyl-ammonium chloride) (PDDA, Sigma-Aldrich, Mw=100 000), or polyethyleneimine (PEI, Sigma-Aldrich, Mw=70 000)) were deposited again, forming a multi-layered structure of polymers on the surface of the CNTs.

In addition, it was possible to transfer PAH modified carbon nanotubes to organic solvents. First, a 100 ml aqueous suspension of CNTs was precipitated by centrifugation (18514g, 90 min.) and re-dispersed in 100 ml of ethanol (EtOH) three times. In the final centrifugation step (18514g, 90 min.), the sediment of PAH functionalized carbon nanotubes was transferred into an organic solvent (e.g. chloroform, hexane) and re-dispersed by a short treatment in an ultrasonic bath (200 W, 30 min.). Due to the branched nature of PAH, the presence of this polymer on the surface of CNTs allows the preparation of homogenous and stable dispersions. CNT-PAH suspensions in chloroform remain stable for weeks.

The same protocol was employed for the wrapping of CNTs with PDDA (Sigma-Aldrich, Mw=100 000) and PSS (Sigma-Aldrich, Mw=70 000) polyelectrolytes (MWNT-PDDA, MWNT-PSS). The key advantage of this method is that the bonding symmetry of CNTs can be preserved and no defects are introduced to the structure.

3.1.1.3 Oxidation with acids

Carbon nanotubes (100 mg) were oxidized with a mixture of sulfuric and nitric acids (1:3 v/v, 200 ml), (H_2SO_4: Sigma-Aldrich, >95 %; HNO_3: Sigma-Aldrich, >70 %). MWNTs were suspended in this solution followed by sonication (ultrasonic bath, 200 W) for 4 h, and left aside for 20 h. Excess concentrated acid was removed by centrifugation (18514g, 60 min.), and the resulting black solid sediment was washed thoroughly with pure water (40 ml of water added to 50 ml plastic tubes); this process was repeated five times. Finally, the nanotubes were re-dispersed in 500 ml of water by a short treatment in ultrasonic bath (200 W, 30 min.). Carboxylic, keto, aldehyde, and alcoholic groups are formed this way on the sides and caps of the carbon nanotubes. Oxidation disrupts the π bonding symmetry of the sp^2 hybridize carbon atoms and therefore leads to numerous side defects along the entire length of CNTs. Oxidized CNTs (carboxylic groups are dominant, therefore the CNT-COOH abbreviation is used to refer to oxidized nanotubes) remain stable in aqueous solvent for months [175].

3.1.1.4 Modification of oxidized side-walls

The oxidized CNTs can be further modified by covalent functionalization with various chemical groups. In this study, oxidized MWNTs (200 mg) were stirred in 100 ml of thionyl chloride ($SOCl_2$, Sigma-Aldrich, >99 %) at 70 °C for 24 h in order to convert surface-bound carboxylic acid groups into acyl chloride groups. After centrifugation (18514g, 60 min.), the remaining solid was rinsed with 100 ml of anhydrous tetrahydrofuran (THF, Carl-Roth, >99.9 %) and dried under vacuum at room temperature. A mixture of the resulting MWNTs and 3 g of octadecylamine (ODA, Sigma-Aldrich, >99 %) was then stirred under N_2 atmosphere at 80 °C (above melting point of ODA) for 96 h. After cooling to room temperature, the excess of ODA was removed by intensive washings with 100 ml of ethanol by subsequent centrifugation (six times, 18514g, 60 min.) and re-dispersion. A dry black solid of such functionalized MWNTs (MWNT-ODA) was dispersed in 200 ml of chloroform by sonication in an ultrasonic bath (200 W, 120 min.), resulting in a stable suspension [176]. This functionalization is shown schematically in Figure 3.2.

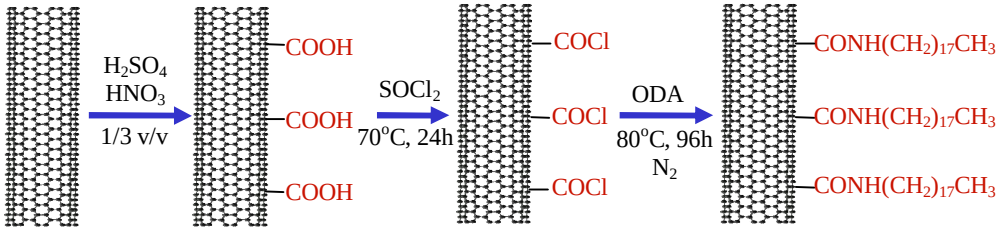

Figure 3.2 Schematic of covalent functionalization of the oxidized CNTs with ODA.

3.1.1.5 Silica coating of MWNTs

The surface of multiwall carbon nanotubes was modified by uniform coating with silicon dioxide shell. The coating steps were as follows: A MWNT-PAH water dispersion (see 3.1.1.2) was transferred to a silica sol (mixture of tetraethoxysilane (TEOS, Sigma-Aldrich), H_2O, and EtOH with mass ratio 2:1:4) in a 5:1 volume ratio (400 ml : 80 ml). The mixture was sonicated (2 h, 200 W) and then left aside overnight at room temperature. After 12 h, the mixture was centrifuged (18514g, 30 min.), the supernatant removed and the carbon nanotubes washed with 450 ml of ethanol and centrifuged again. The sediment was re-dispersed in a solution of ammonia in ethanol (4.2 vol.% ammonia (28 wt% aque-

ous solution) in ethanol, 450 ml of EtOH). Immediately after this, 5 ml of TEOS solution (10 vol.% in ethanol) was added under stirring. The reaction mixture was stirred for another 8 h and sonicated (200 W) from time to time (every 20 - 30 min.). Finally, the CNTs were washed with 400 ml of ethanol and again re-dispersed in an ultrasonic bath (200 W, 15 min.) [176,177].

Silica coated MWNTs (MWNT@SiO_2) form stable suspensions in EtOH and water. In order to modify the surface properties of the silica shell, an ethanolic solution of silica coated CNTs was mixed and stirred with 3-aminopropyl trimethoxysilane (3APTMS, Sigma-Aldrich, 97 %) or phenyltrimethoxysilane (PhTMS, Sigma-Aldrich, 97 %) (typically, to 20 ml of MWNT@SiO_2 solution 0.1 ml of 3AMPTMS or PhTMS). The unreacted components were removed by rinsing in 20 ml of chloroform.

3.1.2 Composite preparation

Functionalized carbon nanotubes were incorporated into polymers utilizing different approaches including layer-by-layer assembly and solution processing. Since various experimental setups used in this study require different samples (in size and shape, assembled on different substrates or free-standing films, solution dispersions or solid materials), the CNTs/polymer composites were suitably processed and prepared to meet all necessary experimental conditions and requirements of applied investigation methods. A general description of the preparation techniques that have been used in this study is presented below and summarized in Table 3.1.

3.1.2.1 Layer-by-layer assembly

The LBL composites were formed on solid substrates by sequential deposition of oppositely charged polyelectrolytes and functionalized MWNTs [175,178]. Adsorptions of the materials on glass slides or silicon wafer substrates were carried out at room temperature in open beakers containing aqueous dispersions of components. Substrates were cleaned in EtOH, supported by ultrasonic bath (200 W, 30 min.). The samples were prepared either manually by cyclic immersion in polyelectrolytes and MWNTs solutions or by automated processing using an automatic dipping machine (Dipping Robot DR3, Kirstein GmbH, Germany). After every layer deposition, samples were rinsed thoroughly with water. In a typical experiment, a deposition time of 10 min. was used for the polyelectrolytes,

20 - 30 min. for carbon nanotubes and 3 min. for rinsing in water. 25 ml beakers were used with 20 ml of solutions.

Table 3.1 Summary of the different composites prepared in this study and corresponding experimental methods employed to characterize their properties. TT – tensile test, NI – nanoindentation, RH – rheometry, DS – dielectric spectroscopy, MC – structural characterization with atomic force or electron microscopes, OS – optical spectroscopy, EL – ellipsometry.

Sample	Description	Characterization Methods						
		TT	NI	RH	DS	MC	OS	EL
LBL assembly:								
MWNT-PAH/PSS	film on silicon wafer		X			X	X	
MWNT-COOH/PAH	film on silicon wafer		X			X	X	
MWNT-NaAQ/PEI	free-standing film	X				X	X	X
MWNT-COOH/PEI	free-standing film	X				X	X	X
PEI/PAA	free-standing film	X				X	X	X
PEI/PSS	film on silicon wafer		X			X		
PSS/PAH	film on silicon wafer		X			X		
Solution processed composites:								
MWNT/PMMA	spin-coated on silicon wafer		X			X		
MWNT@SiO_2/PMMA	spin-coated on silicon wafer		X			X		
MWNT@SiO_2/PMMA-f	free-standing film				X			
MWNT-COOH/PEI	viscous fluid			X				
MWNT-COOH/PDDA	pressed disc-shaped pellets				X	X		

In this work diverse morphologies and combinations of polyelectrolytes and modified multiwall carbon nanotubes were used. Typically, composites were fabricated with the following structures: $[(PE^+/MWNT^-)_5(PE^+/PE^-)]_n$ and $[(PE^-/MWNT^+)_5(PE^-/PE^+)]_n$, where PE^+ and PE^- are polycations and polyanions, respectively; $MWNT^+$ and $MWNT^-$ are functionalized nanotubes with negative and positive functionalities on the surface, respectively; *n* is an integer that indicates a number of cycles. Different structures containing 100 bi-layers and more ($n \geq 20$) were fabricated (the term bi-layer does not imply real structural properties of the produced films, but refers to the CNT/PE layers) [175].

LBL composites were additionally cross-linked in order to introduce bonds between and within polyelectrolyte chains and CNTs. The composites were cross-linked in two ways: by heating and chemical reactions. After deposition of every five cycles $(PE/MWNT)_5$, the films were heated up to 120 °C for 30 min. The films were also cross-linked chemically with glutaraldehyde (GA, $OCHCH_2CH_2CH_2CHO$, Sigma-Aldrich) 0.5 wt% solution in H_2O for 2 h. After this treatment the film was rinsed three times in pure water in order to remove un-reacted glutaraldehyde.

In order to obtain free-standing films, the LBL composites were peeled off from the substrate by chemical delamination. The samples were immersed into 1 % aqueous hydrofluoric acid (HF, Sigma-Aldrich, 48 wt%) for 1 - 2 min., and then washed in acetone and pure water; this resulted in a separation of the multilayer composites from glass. Dry free-standing films remained stable and could be cut to a desired size or shape.

LBL CNT/polymer composites were investigated in terms of their mechanical properties. Additionally, the polymer compositions were fabricated and used as reference samples. Different procedures and structures were engaged to prepare suitable samples for a given experimental setup (Table 3.1):

MWNT-PAH/PSS: The sequence of $[(PSS/MWNT\text{-}PAH)_5(PSS/PAH)]_n$ was employed to produce this LBL composite. Solutions were prepared as follows: 0.5 wt% PSS (Mw=70 000) and PAH (Mw=70 000) salt solutions (0.5 M NaCl) were at pH=6.5; MWNT-PAH water solutions were at pH=6.5. Samples were deposited on silicon wafers (1 x 2 cm^2). Typically, 200 - 300 deposition cycles were used, resulting in thicknesses of the samples greater than 3 μm.

MWNT-COOH/PAH: The compositions of $[(PAH/MWNT\text{-}COOH)_5(PAH/PSS)]_n$ were fabricated on the silicon wafer substrate (1 x 2 cm^2). 0.5 wt% PSS (Mw=70 000) and PAH (Mw=70 000) salt solutions (0.5 M NaCl) were at pH=6.5; MWNT-COOH water solution

was at pH=6.5. Thicknesses of the samples greater than 3 μm were obtained after 250 - 300 deposition cycles.

MWNT-NaAQ/PEI: LBL composites have been prepared on glass substrates (2.5 x 5 cm^2) with a layer sequence of $[(PEI/MWNT\text{-}NaAQ)_5(PEI/PAA)]_n$. The 1 wt% PEI (Mw=70 000) solution was at pH=8.5; 1 wt% PAA (Mw=450 000) solution was at pH=6; and MWNT-NaAQ solution was at pH=6.5. After the deposition of around 100 - 150 numbers of bi-layers (*n*=20-30), the films were peeled off from the substrate in order to achieve free-standing composites. Two different morphologies of the multiwall carbon nanotubes were used: "hollow" and "bamboo" (Figure 2.2). The final thicknesses of free-standing films were estimated to be in the range of 1.5 - 2 μm.

MWNT-COOH/PEI: LBL assembly of polyelectrolytes and oxidized multiwall carbon nanotubes with the sequence of $[(PEI/MWNT\text{-}COOH)_5(PEI/PAA)]_n$ were produced on glass substrates (2.5 x 5 cm^2). 1 wt% PEI (Mw=70 000) solution was at pH=8.5; 1 wt% PAA (Mw=450 000) solution was at pH=6; and MWNT-COOH solution was at pH=6.5. After deposition of 100 - 150 bi-layers of PAH/MWNT-COOH, the composites were delaminated from the substrate following the previously described procedure. Composites with thicknesses of 1.5 – 2 μm were obtained this way.

PEI/PAA: LBL assembly of PEI and PAA polyelectrolytes. 1 wt% PEI (Mw=70 000) solutions were at pH=8.5; 1 wt% PAA (Mw=450 000) solution was at pH=6. Films of $[PEI/PAA]_n$ with 150 - 200 bi-layers were produced on the glass substrate (2.5 x 5 cm^2). The composite was peeled off from the substrate in order to achieve a free standing film.

PEI/PSS and PSS/PAH: Layer-by-Layer compositions of polymers $[PEI/PSS]_n$ and $[PSS/PAH]_n$, respectively. 0.5 wt% PEI (Mw=70 000) salt solution (0.5 M NaCl) was at pH=8.5; 0.5 wt% PSS (Mw=70 000) and PAH (Mw=70 000) salt solutions (0.5 M NaCl) were at pH=6.5. Films were prepared on silicon wafers (1 x 2 cm^2) with thicknesses greater than 3 μm.

3.1.2.2 Solution processing

Carbon nanotube dispersions were mixed together with the polymers in suitable solvents. To form a composite, the solvents were then evaporated from the mixture. The formation of a homogeneous mixture was supported by intensive ultrasonic agitation and mixing. Following MWNT-based composites were obtained utilizing this method (Table 3.1):

MWNT/PMMA: An appropriate amount of poly(methyl methacrylate) (PMMA, Carl-Roth, Mw=320 000) was added to well dispersed MWNT-ODA in chloroform in order to

achieve a desired weight concentration of CNT with respect to PMMA. The final mixture was then thoroughly mixed and sonicated (200 W) until a stable, black-colored chloroform solution of MWNT/PMMA composite was formed. The MWNT/PMMA samples were prepared with 1, 2, 3, 4 and 5 wt% of MWNT.

MWNT@SiO_2/PMMA: To a chloroform solution of the MWNT@SiO_2 poly(methyl methacrylate) (PMMA, Carl-Roth, Mw=320 000) was added. This mixture was further homogenized in an ultrasonic bath (200 W) and mixed until a uniform blend was obtained. Different MWNT@SiO_2/PMMA composites were prepared with 1, 2, 3, 4 and 5 wt% of CNTs in a polymer matrix.

Chloroform dispersions of both MWNT/PMMA and MWNT@SiO_2/PMMA composites were spin-coated on silicon wafers. The thickness of the films was controlled by altering the concentration of composites in the solution, or by the speed of spinning. In general, thin films with a thickness greater than 3 μm were formed at speeds ranging from 1200 - 2500 rpm in 25 s, followed by drying in an oven (100 °C, 3 min.). Furthermore, the samples were left in an oven at 70 °C for a few days (7 – 9 days) to ensure a full solvent evaporation [176].

MWNT@SiO_2/PMMA-f: A 1 wt% sample of MWNT@SiO_2/PMMA was cast into a petri dish that was wrapped with aluminum foil. The sample was then dried (oven, 70 °C, 3 days) and the composite with a thickness of around 1 mm was peeled off from the aluminum foil, resulting in a uniform free-standing film.

MWNT-COOH/PEI: Composites composed of MWNT-COOH and high molecular weight liquid cationic polyethylenimine ($H(NHCH_2CH_2)_nNH_2$, PEI, Sigma-Aldrich, Mw=25 000, water-free) were fabricated. An aqueous dispersion of nanotubes was mixed with a suitable amount of the PEI (in order to achieve the desired concentration of nanotubes with respect to polymer). The samples were mixed and ultrasonicated (200 W, 60 min.) until uniform and stable dispersions were obtained. The solvent was removed from the composite by subsequent evaporation in low pressure atmosphere (10 mbar), at room temperature. After removal of the residual water from the sample, a viscous black fluid was formed. In general, MWNT-COOH/PEI composites with concentrations ranging from 0.5 to 8 wt% were produced.

MWNT-COOH/PDDA: Oxidized carbon nanotubes were dispersed in water and an appropriate amount of PDDA (Sigma-Aldrich, Mw=350 000) was added in order to achieve the desired weight concentrations of the MWNTs in the polymer matrix. The composites were thoroughly mixed mechanically and sonicated (200 W) until uniform and stable dis-

persions were obtained. The samples were then left for two weeks in an oven at 100 °C in order to efficiently evaporate water from the composite. Dry samples were grinded using an agate mortar and pestle, the powder product was again left in the oven for two days at 100 °C. The composites were then formed to disc-shaped pellets with diameter of 10 mm utilizing the SPECAC hot-press system at room temperature and a pressure of 2 kPa. Composite tablets with different nanotube concentrations ranging from 0.5 to 10 wt% were fabricated.

3.1.2.3 CNT/NPs heterostructures

Semiconductor nanocrystals (NCs) were covalently attached to the functionalized MWNTs and MWNT@SiO_2 [179]. In a typical experiment, 15 µL of 8 µM solution of QDs was added to 2 ml dispersion of PAH functionalized MWNTs. The reaction mixture was briefly sonicated (200 W, 10 min.) and then stirred for 15 min. [177]. Excess particles were removed by subsequent centrifugation (1157g, 15 min) and re-dispersion of sediment in 5 ml of chloroform. Due to the presence of the amine functionalities on the surface of CNTs, various colloidal nanoparticles have been attached covalently to MWNTs. An analogous approach was used for the connection of QDs to silica coated multiwall carbon nanotubes. The quantum dots were covalently attached to the amine groups of 3APTMS functionalized silica coated MWNTs (see 3.1.1.5). As a result, the uniform coating of QDs on an electrically insulated (SiO_2) surface of MWNTs took place [177].

The monodisperse CdSe cores used in this study were synthesized by Joel van Embden [180]. The over-coating of these cores with both CdS and ZnS was undertaken using an adaptation of the SILAR technique (successive ion layer adsorption and reaction).

3.2 Experimental techniques

The structural, mechanical, electrical, and optical properties of the MWNT-based composites were characterized utilizing various experimental techniques including tensile tests, nanoindentation, rheology, dielectric spectroscopy, electron/atomic microscopes, optical spectroscopy, and ellipsometry. The general description of the experimental setups used in this study, as well as conditions and parameters of each experiment are the purpose of the following section.

3.2.1 Tensile tests

The mechanical properties of MWNT composites were measured using a servo-controlled electromechanical testing device (100R Test Resources, Shakopee, MN, USA). In this test the sample is pulled until fracture. The load is applied in the axial direction (in-plane) of the samples. The composites with size of 2.0 x 4.0 cm^2 were stretched at a constant load speed of 0.2 mm/min until the specimen cracked. Load F and strain ε were recorded by a computer connected to the control unit of the tensile apparatus. From the stress-strain curve the tensile strength of the samples was estimated and the elastic modulus calculated. At least three independent samples of particular composite were investigated.

3.2.2 Nanoindentation

Nanoindentation experiments were carried out using an atomic force microscope (AFM) (NanoScope IV Digital Instruments) with a conjugated TriboScope Nanomechanical Test Instrument from Hysitron Inc. In this test, hardness and elastic modulus were calculated. A typical indentation test was conducted with diamond conical or Berkovich indenters, using a triangular load profile with an indentation force ranging from 25 to 1500 μN and a loading/unloading rate of 40 μN/s. In general, indents with a contact depth ranging from 80 to 500 nm were performed. To minimize the effect of the material's creep at the maximum load a hold time of 20 s was introduced. Prior to the indentation, a tip was used for surface scanning to find reasonably smooth areas of the tested materials. The indentation depth was maintained to be less than 15 % of the film's thickness in order to avoid or at least minimize substrate contributions to the measured nanomechanical properties. The average roughness (Ra) of the samples was estimated to be in the range of $2 - 25$ nm, which is low enough to avoid major influence of the roughness on the evaluation of the hardness H and the effective elastic modulus E_r. At least five indents were performed for each maximum applied load throughout the whole area of the sample. The results obtained under the same maximum load were averaged; mean and standard deviations of the measured quantities for all samples were calculated [176].

The tip calibration procedure has to be employed to determine the geometry of the indenter tip. For this purpose a series of indentations at different contact depths were performed in a sample with a known elastic modulus. In this study, the tip calibration was car-

ried out on poly(methyl methacrylate) with well defined mechanical properties (elastic modulus of 3.6 GPa) [176,181].

3.2.3 Rheometry

Rheological measurements were carried out in an oscillatory shear mode utilizing the RheoStress RS600 rheometer (Haake) with a temperature controller (Phoenix RS600). The cone and plate geometry (Ti, 35 mm diameter, 2° cone angle) was used with a 0.105 mm gap. All experiments were performed at a constant temperature of 25 °C. Dynamic oscillatory experiments were carried out under controlled stress (CS) and controlled strain (CD) modes. In CD experiments, a frequency sweep was performed at constant strain, in CS tests constant stress was used. Frequency sweeps between 0.1 - 100 Hz were performed at low strain (0.1 - 2 %) or stress (10 - 500 Pa), which were shown to be in the linear elastic range of the tested samples. To verify the linear viscoelastic regime for every sample, dynamic strain sweeps were performed at a constant frequency. In a linear viscoelastic region the elastic (storage) G' and loss G'' moduli were independent of the strain amplitude γ_0. The results were reproducible after every frequency sweep, indicating that there is no chain degradation. Samples were left for 15 min. prior to the measurements in order to reach the temperature equilibrium. The complex viscosity η^*, storage modulus G', and loss modulus G'' were calculated and recorded as a function of the oscillation frequency.

3.2.4 Dielectric spectroscopy

AC dielectric spectroscopy was performed with a dielectric spectrometer BDS-80 (Novocontrol) equipped with a Hewlett Packard 4291B probe head operating in the frequency range of 10^6 to $1.8 \cdot 10^9$ Hz. Samples with a diameter of 10 mm and thicknesses ranging from 1 - 4 mm were placed in the holder between two parallel gold-plated electrodes (10 mm in diameter). All experiments were carried out at a constant temperature of 25 °C – the sample holder was placed in a cryostat that enables the control of the temperatures with an accuracy of 0.1 °C. Prior to each test, a 30 min. time interval was applied in order to achieve temperature equilibrium. Novocontrol WinDETA software was used for the evaluation of the electrical properties of the samples. Complex permittivity and conductivity were calculated and plotted as a function of the frequency.

3.2.5 Structural characterization (TEM, SEM, AFM)

Structural properties of multiwall carbon nanotubes, their heterostructures, and composites were characterized by means of atomic force and electron microscopes.

Atomic force microscope (AFM) investigations were performed, in air, by using a Nanoscope IV system (Veeco/Digital Instruments, Santa Barbara, California, USA), operating in the tapping mode.

Scanning electron microscope (SEM) images were taken with a LEO Supra 55, operating at an acceleration voltage of up to 20 kV (spatial resolution: 1.7 nm at 1 kV, 1nm at 15 kV).

High-resolution transmission electron microscopy (HRTEM) was carried out on a Leo 922A with an acceleration voltage of 200 kV and lattice imaging with 2.9 Å point or 1.9 Å line resolutions. An attached Oxford X-ray system of TEM was used for Energy Dispersive X-ray Analysis (EDX) with 136 eV energy resolution.

3.2.6 Ellipsometry

Ellipsometry measurements were taken using an M-44 ellipsometer (J.A. Woollam Co, Lincoln, NE, USA) set up in a rotating analyzer configuration with a detector array of 44 wavelengths between 428 - 726 nm. The measurements were performed using light of an Xe arc lamp (with systems of optical and electronic filters). The incident angle onto the sample is kept fixed at 75°. The WVASE program supplied by J.A. Woollam Co was employed to determine the thickness of the films with a resolution of a few angstrom. Calibration was performed on the standard silicon wafer with a well defined layer of silicon dioxide. Ellipsometry was used to determine the thickness of the particular layers of the LBL structures.

3.2.7 ζ-potential

Electrophoretic mobility of functionalized multiwall carbon nanotubes were measured using a Malvern Zetasizer 4 operating with a 633 nm He-Ne laser. The mobility μ is converted into a ζ-potential using the Smoluchowski relation [182]:

$$\zeta = \frac{\mu\eta}{\varepsilon} \tag{3.1}$$

where η and ε are the viscosity and the dielectric constant of the solvent, respectively. ζ-potential measurements are taken on MWNTs dispersions after further dilution. A standard 1x1 cm^2 cuvette was used in these measurements. ζ-potentials of functionalized MWNTs with PDDA, PAH, COOH, NaAQ, and PSS were determined.

3.2.8 Optical spectroscopy

UV-vis absorption measurements in the range of 300 - 800 nm were carried out with a Varian Cary 5000 spectrometer. Dispersions of MNWT/NP heterostructures were investigated in a quartz cuvette. Also, the progress of LBL composite assembled on glass substrates was monitored by UV-vis spectrometry. UV-vis readings were taken after every 5 bilayers of MWNT/PE. The dependence of the adsorption increment on the number of layers was observed at 550 nm.

Photoluminescence (PL) measurements were carried out by a Horiba Jobin Yvon FluoroMax-3 spectrometer. PL spectra of solutions of quantum dots and their heterostructures with carbon nanotubes were obtained at a suitable excitation wavelength (with energies above the absorption edge of particular particles). Samples were placed in quartz cuvettes (1 cm width).

CHAPTER IV

RESULTS AND DISCUSSION

4.1 Structural properties of the samples

Prior to the experimental determination of the mechanical, electrical, and optical properties of MWNT-based composites, the structure and morphology of samples have been characterized by means of atomic force and electron microscopy. Additionally, UV-vis spectroscopy, ellipsometry, and ζ-potential measurements have been employed in order to achieve a better understanding and control over the fabrication of the composites.

4.1.1 Silica coated MWNTs

The novel method for silica coating of carbon nanotubes presented in this study results in the formation of a uniform and thick layer of SiO_2 on every individual MWNT. A schematic presentation of silica coating is given in Figure 4.1. The key advantage of this technique is its efficiency and simplicity. TEM investigations confirm that every single nanotube in a sample is homogenously coated with a layer of silicon dioxide (Figures 4.2 and 4.3). The method allows coatings in a broad thickness range of SiO_2 between 20 nm and over 100 nm. This can be easily controlled by subsequent addition of TEOS solution to the CNT@SiO_2 (see 3.1.1.5). SEM characterizations also confirm that every single nanotube has a silica shell (Figure 4.4). The picture demonstrates many MWNT@SiO_2 with an average diameter of 100 nm (pristine non-coated MWNTs are 5 - 35 nm in diameter). Finally, energy dispersive X-ray analysis (EDX) proves that the obtained heterostructures are composed of carbon, silicon, and oxygen (Figure 4.5). EDX mapping images are selectively contrasted with the characteristic X-ray radiation emitted by carbon (C), oxygen (O), and silicon (Si), respectively.

The functionalization of silica coated nanotubes with 3AMPTMS or PhTMS occurs through a silanization reaction on the surface of silicon dioxide and results in stable dispersions of MWNT@SiO_2 in hydrophobic organic solutions (e.g. chloroform).

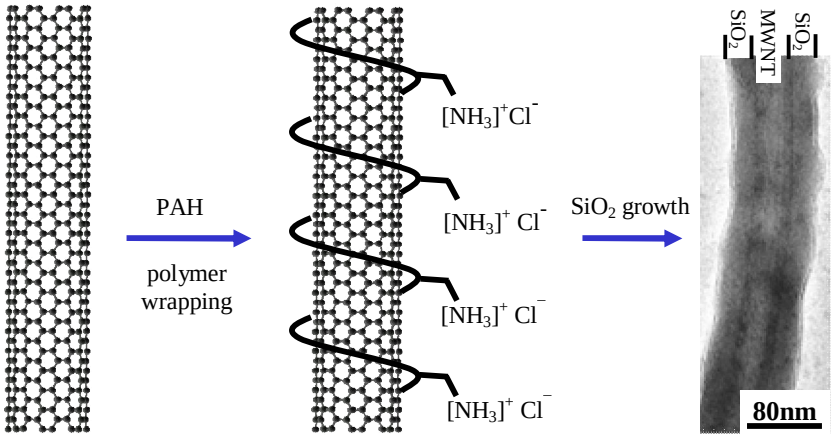

Figure 4.1 Schematic presentation of silica coating of multiwall carbon nanotubes. The TEM image on the right hand side presents a MWNT coated with silicon dioxide (the image is over-contrasted in order to expose the core-shell structure).

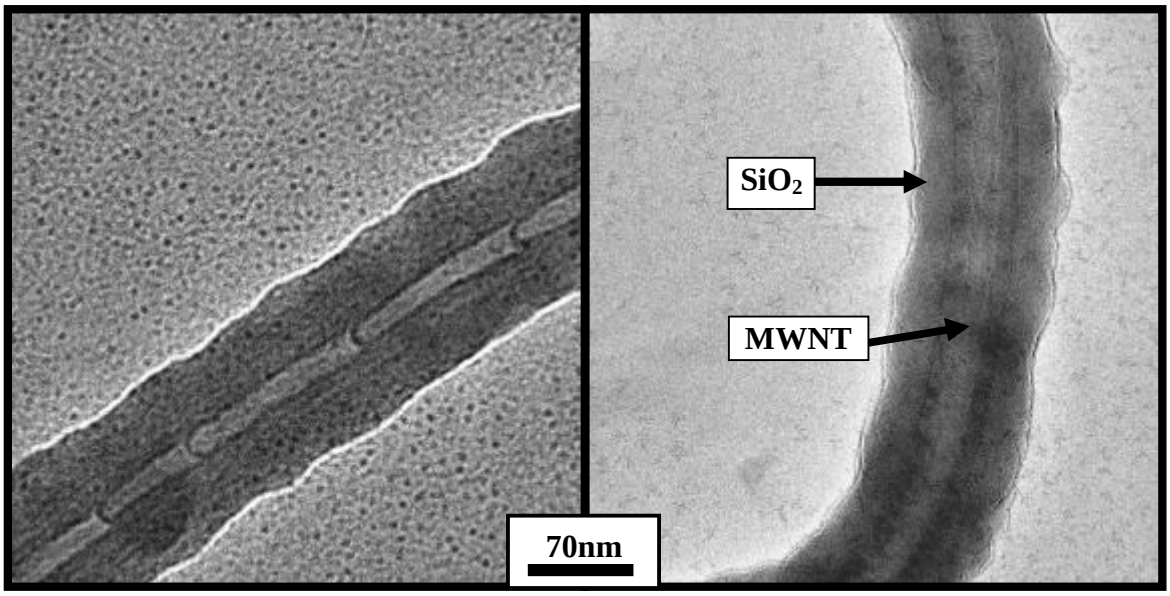

Figure 4.2 TEM images of the silica coated MWNT ("bamboo"). Right image is over-contrasted in order to expose the core-shell (MWNT-SiO_2) structure.

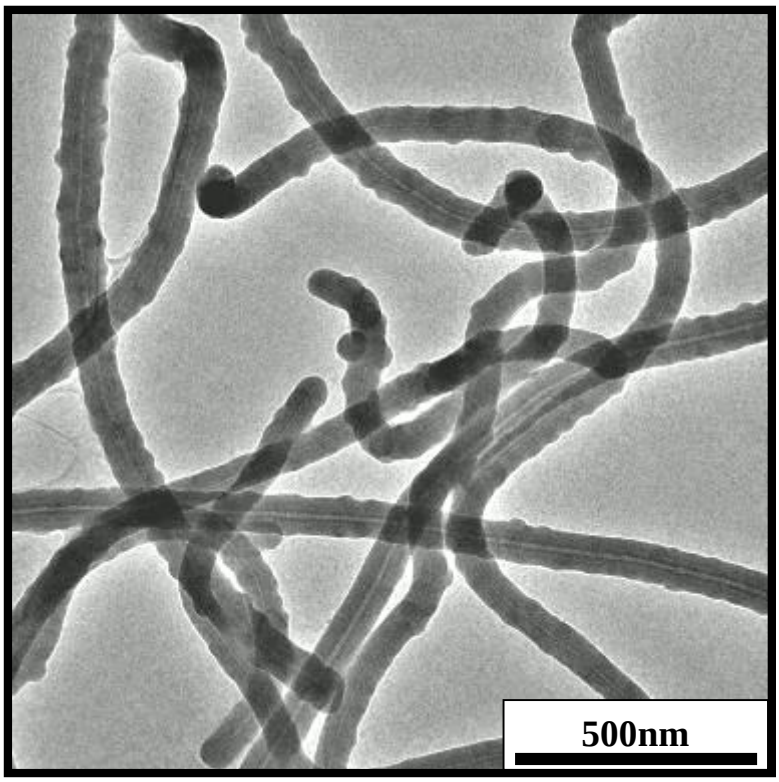

Figure 4.3 TEM image of several MWNT@SiO_2. The uniform coverage of each individual MWNT with silica shell can be seen.

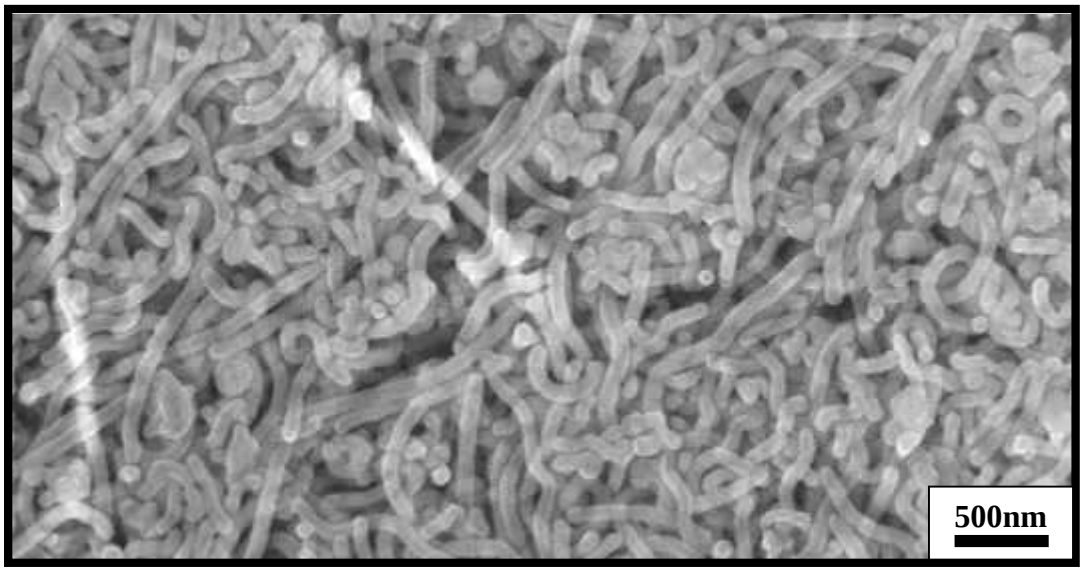

Figure 4.4 SEM image of silica coated MWNTs deposited on a substrate. It can be seen that every carbon nanotube in a sample has a silica shell.

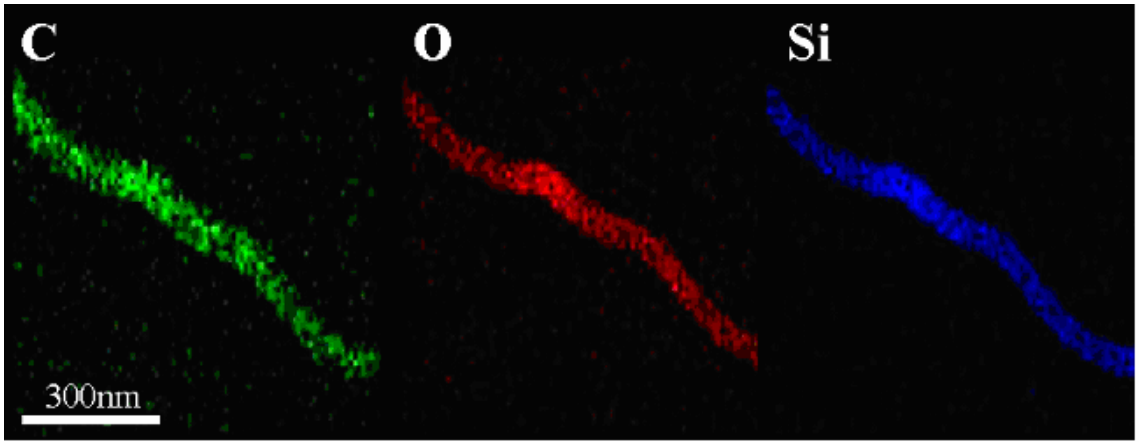

Figure 4.5 EDX mapping of one MWNT@SiO_2. The EDX images are contrasted with carbon (C), oxygen (O), and silicon (Si), respectively.

4.1.2 LBL structures

The LBL assemblies with carbon nanotubes were obtained according to the method described in chapter (3.1.2.1). In order to perform the cyclic adsorption of the oppositely charged components, a proper selection of the polyelectrolytes and modified nanotubes is necessary. The charge of functionalized MWNTs was determined utilizing ζ-potential measurements. The values of ζ-potentials at pH=6.5 (pH that was established for all MWNTs aqueous solutions) for particular functionalized CNTs were: MWNT-COOH: -52 mV, MWNT-PAH: +45 mV, MWNT-PDDA: +42 mV, MWNT-PSS: -38 mV, and MWNT-NaAQ: -49 mV. The results confirm efficient surface modification of the CNTs with polyelectrolytes (by polymer wrapping) and indicate the charge of functionalized nanotubes.

The surface charge and linear charge density of the weak polyelectrolytes (e.g. PAA, PEI, PAH) depend strongly on the pH of the solution; therefore, the pH of the polymer dispersions was adjusted with 0.1 M HCl or 0.1 M NaOH according to the references [113,183]. Strong polyelectrolytes (e.g. PSS, PDDA) dissociate completely, independently on a wide range of pH. The addition of NaCl into the aqueous dispersions of the PEs changes the ionic strength and leads to the coiling and entangling of chains (e.g. due to charge screening) that may result in a high interpenetration of the assembled multilayers

[184]. In this context 0.5 M NaCl solutions were used for the preparation of all polyelectrolyte dispersions in this study.

Chemical cross-linking of LBL assemblies with GA results in covalent links (formation of imines) between amino groups of carbon nanotubes and polyelectrolytes. Modification of the LBL films by heating leads to the formation of amide bonds between functionalities of polyelectrolytes and nanotubes (between amine and carboxylic groups) enhancing the interfacial interactions between these components [175,178].

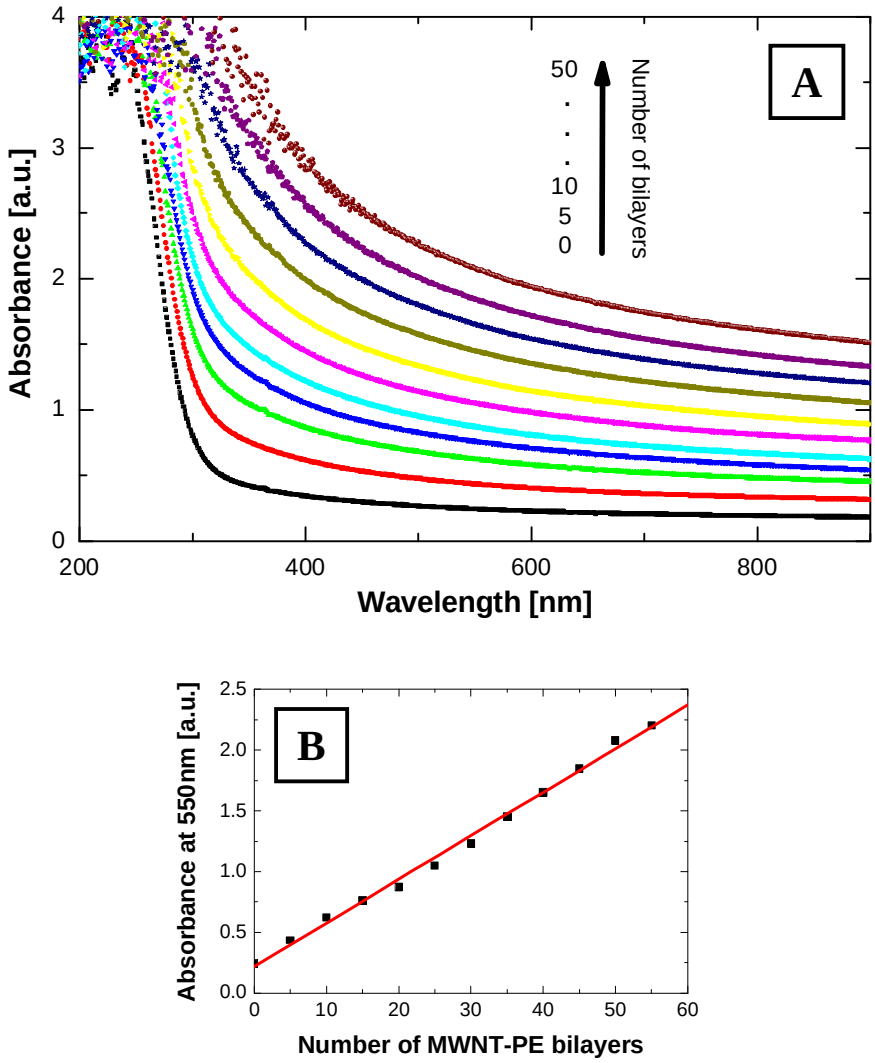

Figure 4.6 UV-vis absorbance spectra of the MWNT-NaAQ/PEI LBL composite. The spectra were taken for a total number of MWNT/PE bi-layers as indicated in the graph (A). (B) shows the dependence of the absorbance at 550 nm of growing films on a number of absorbed MWNT layers.

The growth of MWNT/PE multilayer films was examined using UV-vis absorption spectroscopy. Figure 4.6 (A) shows typical spectra of the LBL composites after every five deposition cycles $(MWNT/PE)_5$. The absorption edge of the glass substrate is at 280 nm. The spectra of MWNT/polymer composites are featureless in the employed wavelength region; a modest monotonic increase of absorption occurs with decreasing wavelength, which is characteristic behavior related to the MWNTs in the UV-vis-NIR region [185]. Figure 4.6 (B) shows the dependence of the absorption (at wavelength of 550 nm) on the number of LBL cycles. The linear increase confirms a reproducible growth of MWNT layers from cycle to cycle, as every assembling step results in the deposition of essentially the same amount of nanotubes in the composite. This trend was also confirmed by ellipsometric measurements of multilayer films prepared on silicon wafers. The results again show a linear growth of composites with basically similar thicknesses of every MWNT/PEI bi-layer. Specifically, for films made of MWNT-COOH/PEI, the average thickness of each bi-layer was measured to be d=13±2 nm; for MWNT-NaAQ/PEI films, d=14±2 nm.

AFM studies on the LBL assemblies of PE and CNTs deposited on silicon wafers reveal the presence of well-dispersed and exfoliated carbon nanotubes. Figure 4.7 (A) shows randomly orientated carbon nanotubes, uniformly covering the entire surface of the sample. Subsequent treatments of films with PE and MWNT layers makes the films rougher, with interweaved CNTs covered with the polymer (Figure 4.7 (B)). As a consequence, a porous film, containing voids between layers and bundles of nanotubes was formed. The image after three assembling steps (Figure 4.7 (B)) confirms the film growth due to the adsorption of the carbon nanotubes in every deposition cycle. The carbon nanotubes appeared to be interweaved with each other and with the polyelectrolyte chains, forming a reasonably homogeneous structure. These observations are supported by SEM investigation. Figure 4.8 shows the top-layer of MWNTs after 100 deposition cycles. The picture displays a large amount of nanotubes covering the entire film. The individual carbon nanotubes are interpenetrated, and homogenously dispersed within the polyelectrolyte, without any sign of phase segregation. Nanotubes are uniformly distributed across the matrix; there is no clear indication of the preferred orientation of nanotubes or island formation. It is evident that, as the number of the absorption cycles was increased, an increased layering of the film was observed.

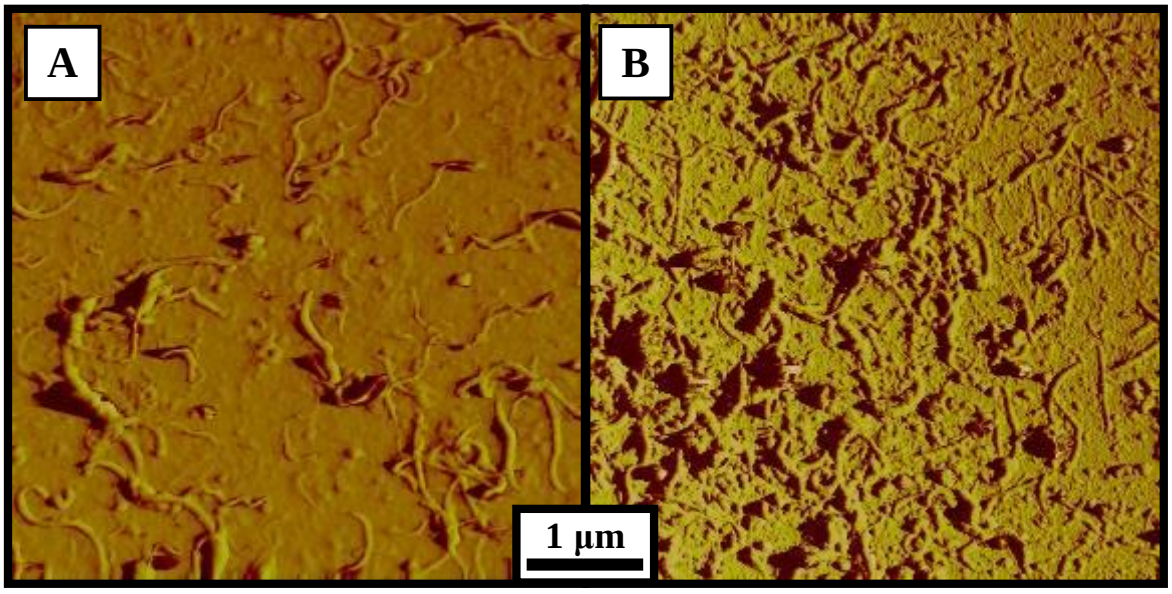

Figure 4.7 Tapping mode AFM images of the LBL of a MWNT-NaAQ/PEI composite prepared on a silicon wafer after various numbers of deposition cycles. One bi-layer of MWNT-NaAQ/PEI (A) and three bi-layers of MWNT-NaAQ/PEI (B).

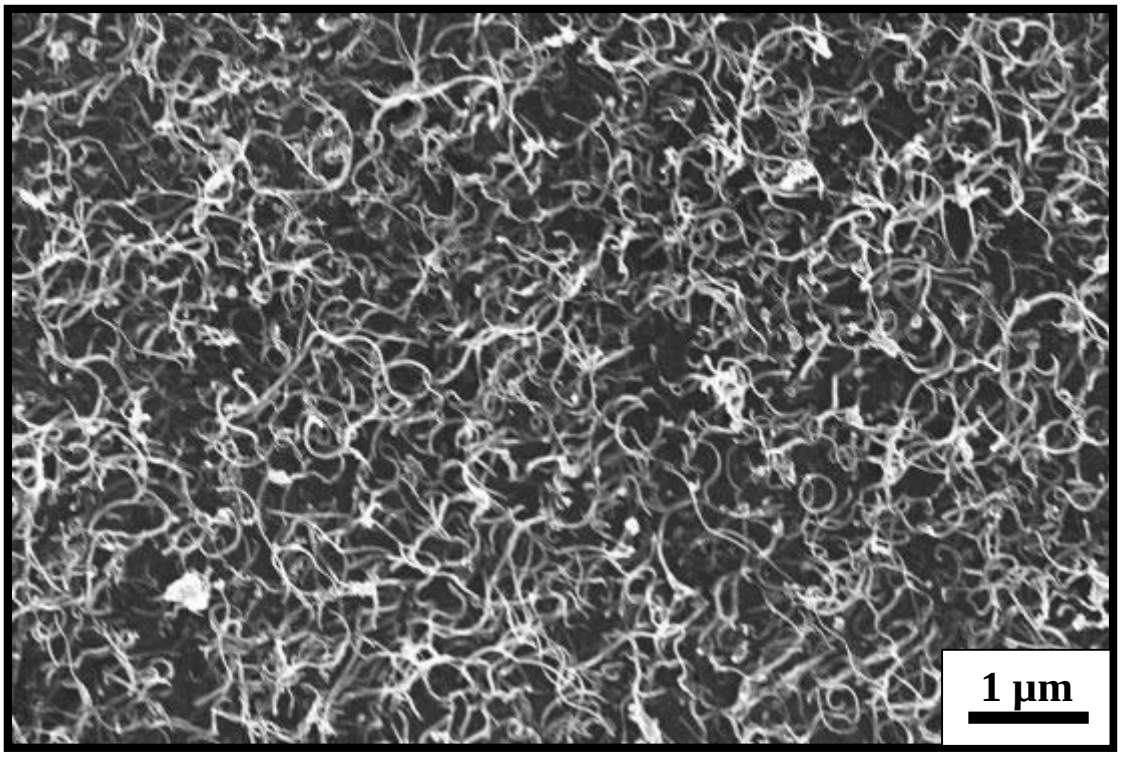

Figure 4.8 SEM image of a MWNT-PAH/PSS composite after 100 deposition cycles.

Tensile tests were carried out on free-standing LBL composites. Therefore, films were peeled off from the substrate (see 3.1.2.1). As a result compact, black films were achieved. Figure 4.9 shows an LBL composite deposited on a glass substrate (A) and a free-standing composite film after delamination from the substrate (B).

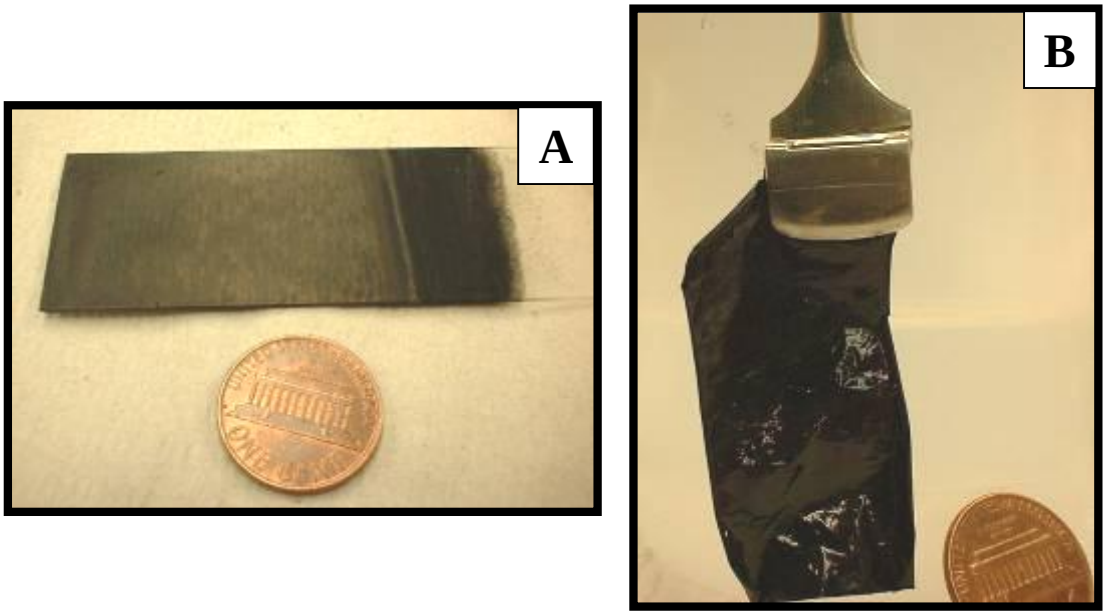

Figure 4.9 Digital camera pictures of MWNT-COOH/PEI composite fabricated on a glass substrate (A), and its free-standing film after delamination (B).

TEM examinations show the morphology of the multilayer assemblies in cross section. The composites are compact and fairly homogenous throughout the whole sample (Figure 4.10). There are some darker inclusions and also a small amount of air pockets, which basically can be attributed to the deformations created during the preparation of the cross-sectional sample of the LBL film. The inset in Figure 4.10 shows a magnified part of the film. Individual multiwall carbon nanotubes can be seen clearly. The MWNTs are mainly oriented parallel to the substrate, which reflects the layered structure of the films. The sides of the free-standing film are different in roughness. As expected, the one that was attached to the substrate is smoother.

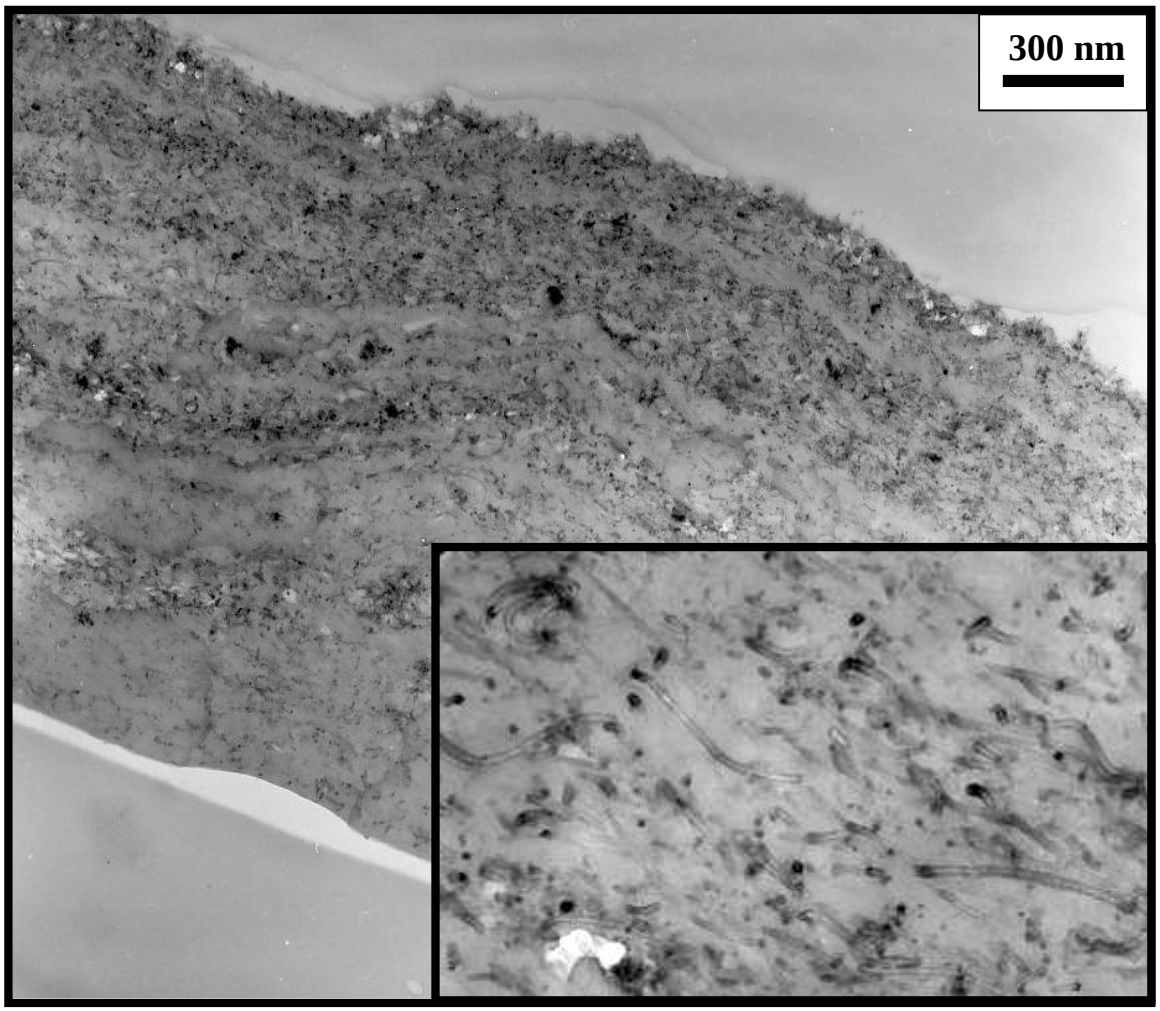

Figure 4.10 TEM image of cross section of the free-standing MWNT-COOH/PEI composite. The inset represents a five times magnified part of the film.

4.1.3 Solution processed composites

Solution mixed composites of MWNTs and polymers (PMMA, PDDA and PEI) (see 3.1.2.2) were found to be relatively homogeneous without any obvious phase segregation of the components. The mixtures were black and uniform in color, stable for weeks, indicating efficient dispersions of CNTs in polymeric matrices. The solution mixtures of the compounds remain stable until complete evaporation of the solvents. Only composites of MWNT@SiO_2/PMMA at 5 wt% of nanotubes revealed some phase segregation while

evaporating the solvent from the mixture. This is due to the moderate solubility of silica coated CNTs in chloroform; at higher concentrations particles tend to aggregate during the evaporation process.

In order to confirm the homogeneity of the composites, samples were investigated by means of SEM. Various CNT-polymer mixtures were spin coated on the silicon wafers and subsequently dried in an oven. The SEM investigation confirmed good exfoliation and a homogeneous distribution of multiwall carbon nanotubes within a polymer matrix.

Figures 4.11 and 4.12 show exemplary images of 3 wt% of CNT@SiO_2 in PMMA and 3 wt % of MWNT-ODA in PMMA, respectively. Individual carbon nanotubes are inter-woven with each other, forming the interconnected network within the host material. In general, nanotubes are fairly uniformly dispersed across the matrix. There are no obvious indications of any phase segregation between the CNTs and the polymer. It is confirmed that functionalization methods employed in this study result in good exfoliation of bundles of both, MWNTs and MWNT@SiO_2.

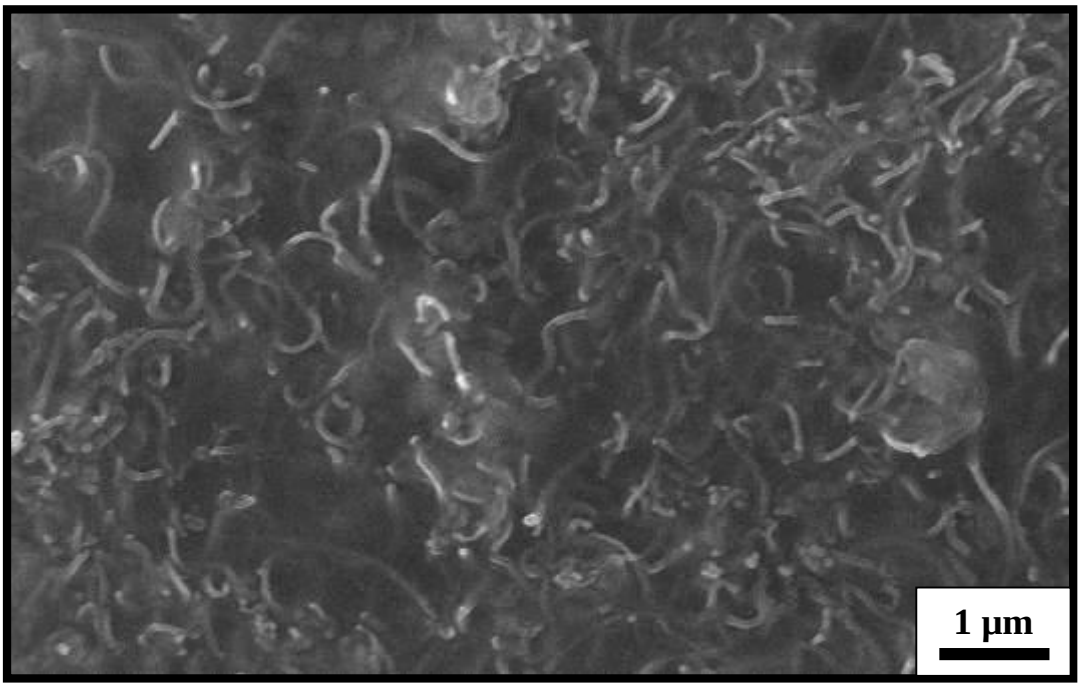

Figure 4.11 SEM image of the silica coated carbon nanotubes in PMMA (3 wt%) deposited on a silicon wafer, showing relatively uniform distribution of the filler throughout the polymer.

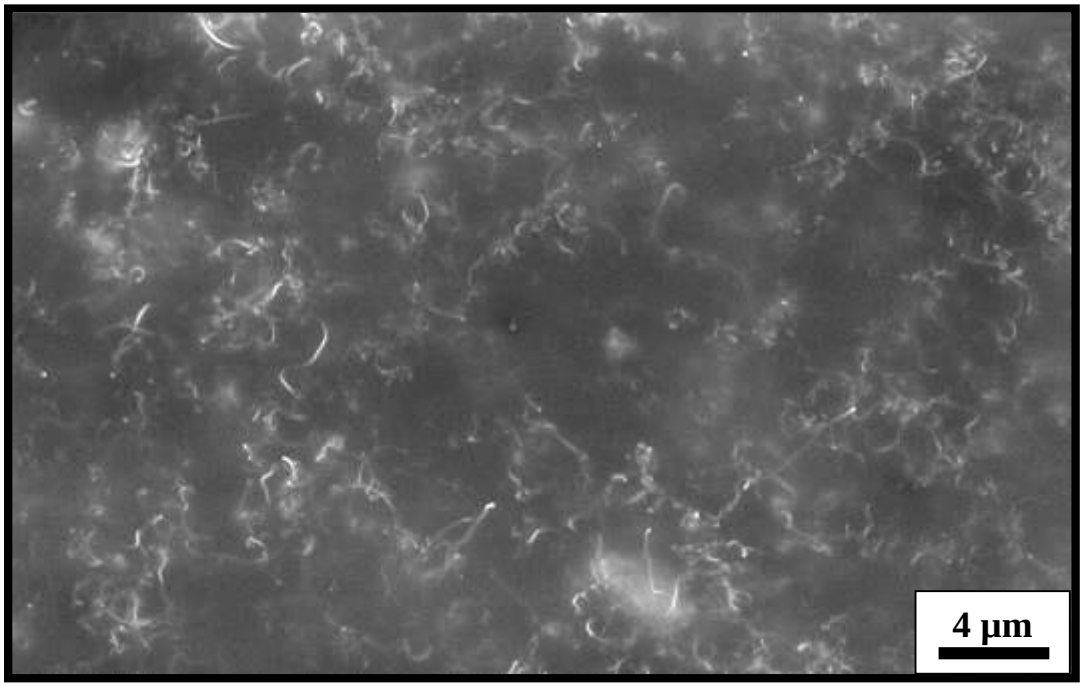

Figure 4.12 SEM image of MWNT-ODA incorporated into the PMMA (3 wt%) matrix by the solution mixing technique and deposited on silicon wafer. A relatively good dispersion of nanotubes can be observed without any obvious phase segregation.

4.1.4 CNT/NPs

The novel and versatile technique for the attachment of nanocrystals to CNTs is introduced in this study (see 3.1.2.3). A schematic presentation of the functionalization of carbon nanotubes and the coupling of nanocrystals to the amine functionalities is shown in Figure 4.13. Different nanocrystals were covalently bonded to PAH-modified MWNTs in a uniform and controllable manner, independent of their size, charge, or surface properties (e.g. hydrophilic or hydrophobic). The direct evidence for the conjugation of NCs to functionalized carbon nanotubes was given by the transmission electron microscopy.

Figure 4.14 shows TEM images of diverse nanoparticles conjugated to the surface of MWNTs. CNTs are homogeneously coated with nanocrystals and no obvious clustering of the attached species was observed. The density of the nanoparticles can easily be controlled by changing the concentrations of the mixed dispersions of nanotubes and nanocrystals. The coupling of NCs to CNTs may be performed either in hydrophilic (e.g.

aqueous) or hydrophobic (organic) solvents. This is of major advantage, since both aqueous syntheses and organometallic approaches for the fabrication of different nanoparticles offer various benefits.

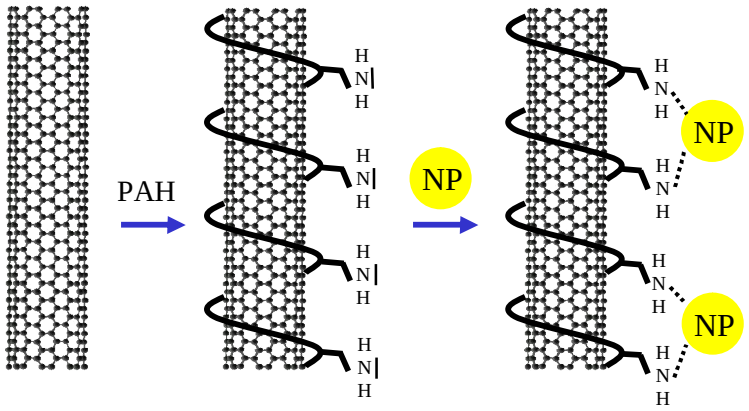

Figure 4.13 Schematic presentation of the functionalization of MWNTs with PAH and the coupling of nanoparticles to the amine group functionalities.

Figure 4.15 presents heterostructures of MWNTs and MWNT@SiO_2 decorated with diverse semiconducting nanoparticles: ZnO, CdSe, and CdSe-CdS. Again, TEM pictures provide evidence for the formation of the homogeneous hybrid systems composed of nanotubes and particles. Individual quantum dots are uniformly coupled to the surface of functionalized MWNTs and MWNT@SiO_2.

Figure 4.16 displays several CNTs decorated with CdSe-ZnS core-shell semiconducting nanocrystals. This image clearly indicates that every individual nanotube within the sample is decorated with nanoparticles.

The technique presented here offers a lot of advantages. In a simple way different NCs can be homogenously bonded to the carbon nanotubes, therefore heterostructures of various compositions and morphologies can be achieved [179]. The formation of the CNT/NCs composites may take place in many commonly used solvents, since the PAH-functionalized MWNTs are stable in aqueous and some organic solvents like chloroform, toluene, and hexane.

.

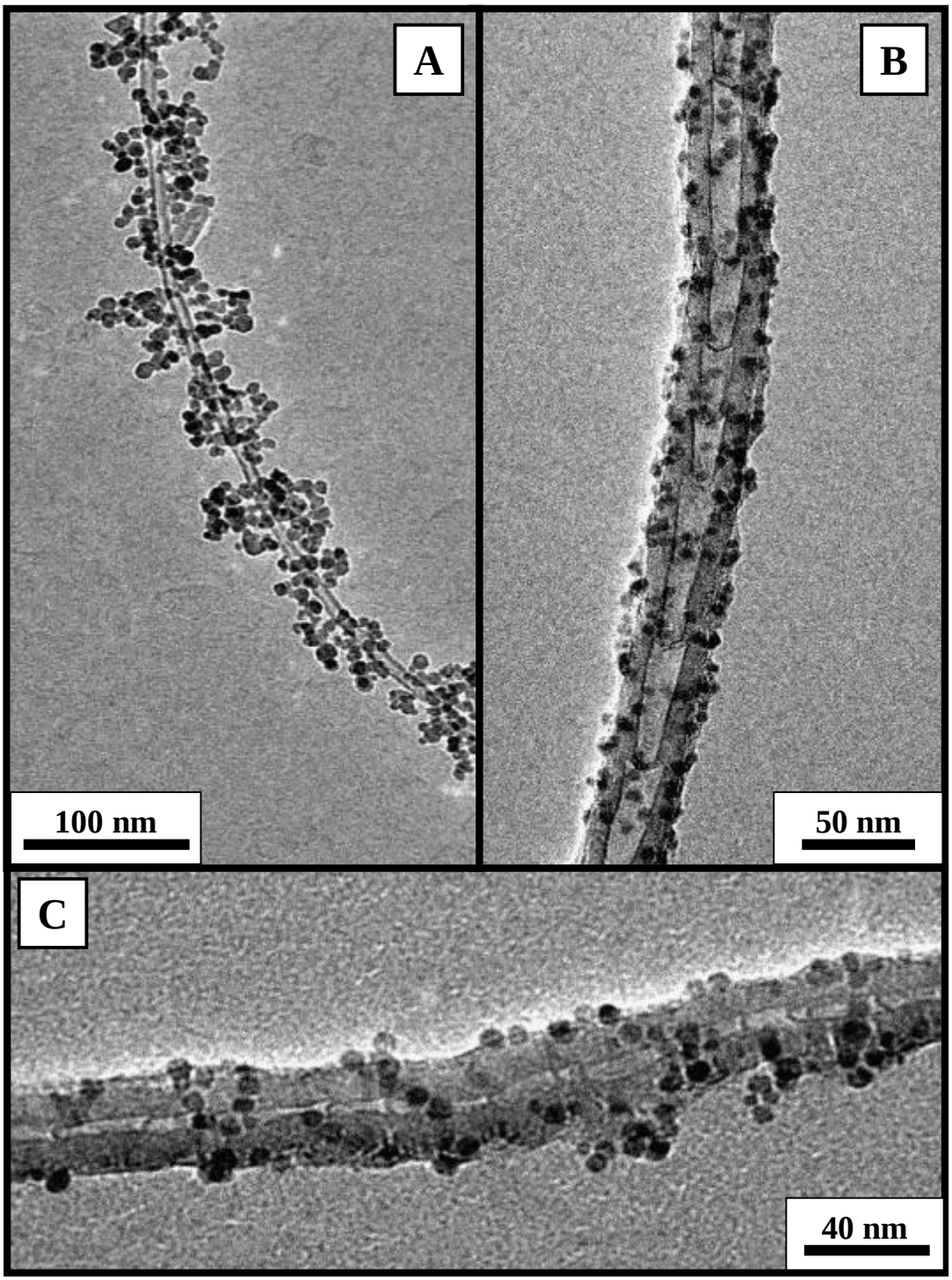

Figure 4.14 TEM images of the MWNTs decorated with: Fe_2O_3 – reaction performed in H_2O (A), Au in water (B), and FePt in toluene (C).

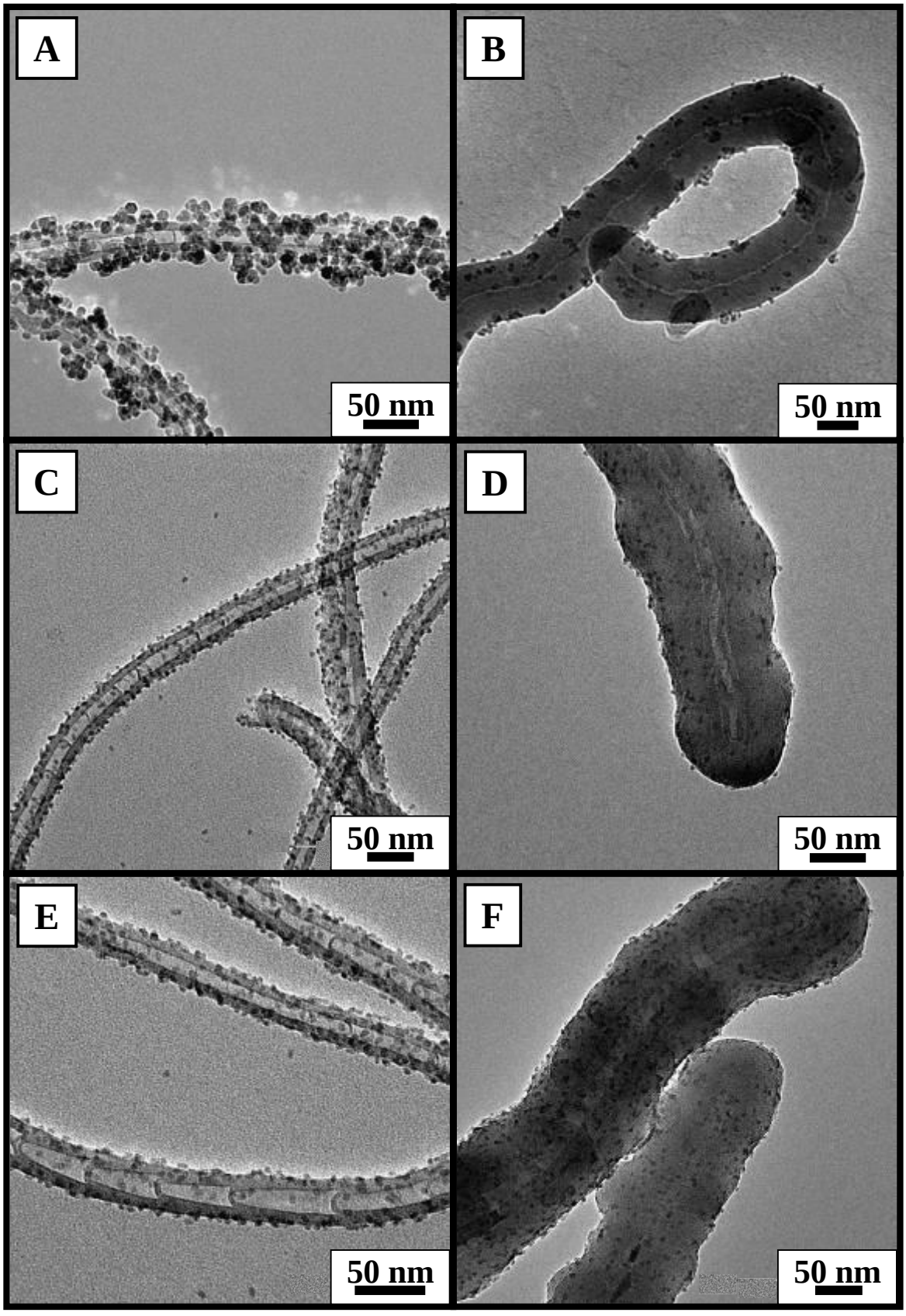

Figure 4.15 TEM images of the MWNT and MWNT@SiO_2 coated with: ZnO reaction performed in EtOH (A) and (B); CdSe in chloroform (C) and (D); CdSe-CdS core-shell QDs in chloroform (E) and (F).

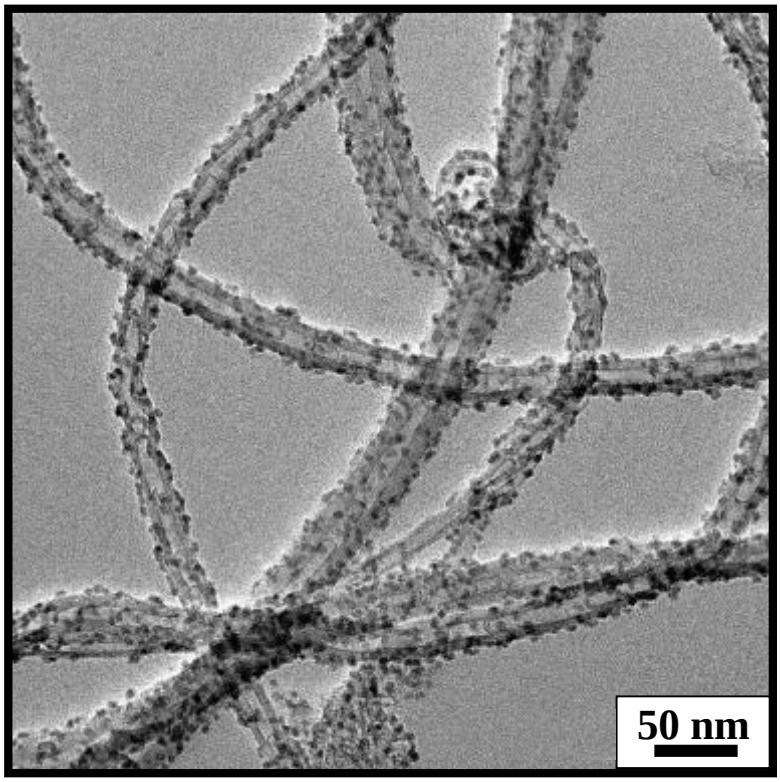

Figure 4.16 TEM image of the multiwall carbon nanotubes decorated with CdSe-ZnS core-shell semiconducting nanocrystals.

The step-by-step process presented here gives the flexibility to tailor the QDs prior to conjugation. This is advantageous over the other reported methods for the formation of CNT/QDs heterostructures. In example, the *in-situ* chemical synthesis of QDs directly on the surface of carbon nanotubes, usually leads to the formation of inhomogeneous crystalline structures with large poly-dispersity in shape and size [123,132,186]. Furthermore, the utilization of oxidized CNTs (which is commonly used by different groups) leads to non-uniform coverage of the surface as particles tend to be attached at the ends of carbon nanotubes and defect sides, where the concentration of carboxylic groups is the largest [90,141,142]. The TEM images of Figures 4.14 and 4.16 confirm that the QD nanoparticles are homogeneous in size and shape, with coatings along the entire lengths of the MWNTs. Notably, there are scarcely any unbound QDs with a few of the QDs making hetero-junctions between individual carbon nanotubes. Besides, different procedures for the formation of CNT/QDs nanocomposites involve complex reactions and functionalizations, making these strategies more complicated and time consuming [90,129,142,187]. The

new strategy introduced here allows for straight coupling of QDs to CNTs in a simple and quick way.

4.2 Tensile strength of LBL composites

Due to their exceptional mechanical properties multiwall carbon nanotubes have been employed as reinforcing fillers for high-strength polymeric composites. In this context, various polymers have been used as matrix materials, and different preparation techniques were employed. In general, the tensile moduli and ultimate strengths of CNT-based composites are reported to increase compared to neat polymer, however below the level of expectation (Table 2.2). The assessment of the data accumulated in numerous studies on carbon nanotube composites revealed that effective reinforcement of these materials strongly depends on several factors such as: a high aspect ratio of the CNTs, good dispersion of the nanotubes in a matrix, good interfacial bonding, interactions and mechanical anchoring between CNTs and polymer molecules. These fairly simple design guidelines for carbon nanotube composites may permit substantial advances in the composites' mechanical properties [31,91,188,189].

The layer-by-layer deposition technique reduces the phase segregation and makes composites highly homogeneous (see 4.1.2), with particles and polymers well dispersed and interpenetrated [190-192]. Recently, it was demonstrated that it can be very successfully applied to the preparation of single wall nanotube (SWNT) composites [113,114]. The LBL assembly technique allows the fabrication of heterostructures with high nanotube contents, even up to 50 wt% [113], which is substantially higher than in any typical nanotube composite (Table 2.2). Even when the concentration of nanotubes in LBL systems is high, the uniform distribution of the filler in the polymer matrix is retained. This is a simple way to produce fundamentally and practically interesting multilayer structures with unique mechanical properties and precise control over film composition and thickness. More importantly, this technique offers a possibility of multifunctional composites in which the strength will be only one of the factors determining its applications.

There are two main motivations for using MWNTs instead of SWNTs in the fabrication of reinforced composites: (1) MWNTs are more resistant to chemical modification and mechanical agitation than SWNTs due to their multiwalled structure. In many cases, even extensive surface modification of MWNTs does not significantly harm the aromatic bonds

inside the multiwall "onion" structure which may preserve their mechanical properties; (2) MWNTs are substantially less expensive than SWNTs, which can accelerate the practical utilization of these composites. 1 g of a high purity sample of SWNTs costs 200 - 1000 $, while 1 g of MWNTs may be purchased for 1.5 $ (October 2006). The synthesis of MWNTs is simple and cheap, which allows the fabrication of large quantities at a low cost. Nowadays, the amount of 250 kg of MWNTs can be purchased, while it is still difficult to buy 1 kg of SWNTs due to the synthesis difficulties [193].

While the LBL assembly technique offers vast advantages, it became very attractive to utilize this method for fabricating the multilayered structures composed of multiwall carbon nanotubes and polyelectrolytes and investigate their mechanical properties. In this study the tensile tests were performed on LBL assemblies of MWNT-NaAQ/PEI, MWNT-COOH/PEI, and PEI/PAA. MWNT-NaAQ/PEI films were prepared using two different types of multiwall carbon nanotubes: "bamboo" and "hollow" (Figure 2.2). CNT/polymer composites prepared in a solution mixing process have not been investigated in this work, since numerous studies have already been focused on the characterization of tensile properties of such composites (Table 2.2). The main goal of this work is to present novel composites with significantly improved mechanical performance; elastic modulus and tensile strength of various composites have been determined.

The elastic modulus E and tensile strength σ_T were evaluated from the recorded stress-strain curves. The Young's modulus was obtained by analysis of the elastic part of the stress-strain curve and calculated from [194]:

$$E = \frac{\sigma}{\varepsilon} = \frac{F / A_0}{\Delta l / l_0} \tag{4.1}$$

where σ and ε indicate stress and strain in the elastic region of the stress-strain curve, respectively. F is the force applied to the sample, A_0 is the original cross-sectional area, Δl is the length change of the specimen, while l_0 is the original length of the sample. The ultimate tensile strength was calculated using the equation:

$$\sigma_T = \frac{F_{MAX}}{A} \tag{4.2}$$

where F_{MAX} is the maximum load prior to break and A is the cross-section area of the sample.

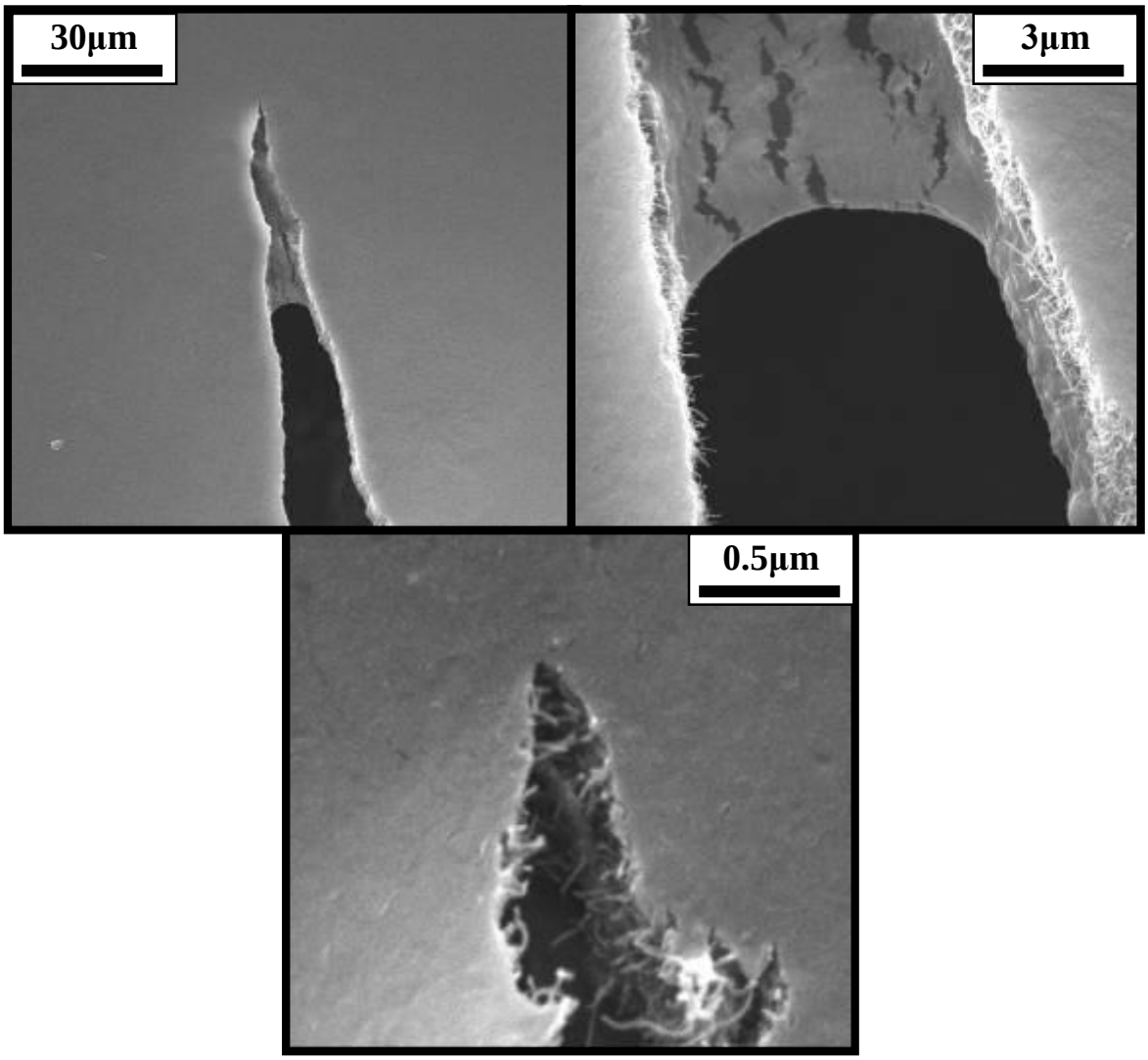

Figure 4.17 SEM images of the rapture region of a MWNT-NaAQ/PEI free-standing film after the stretching test.

In order to understand the mechanisms of the tensile fracture of LBL composites made from MWNTs, SEM studies of ruptured areas of the free-standing films were carried out. Figure 4.17 shows SEM pictures of such a rupture region with individual nanotubes or their bundles pulled out or still bridging the break region, mostly aligned perpendicularly to the break face. Recent structural studies [48,113] of the rupture regions showed that carbon nanotubes can even break under a stretching force due to the structural defects which make them drastically weaker. There are many reasons for fractional defects existing on the nanotubes walls such as impurity, chemical oxidation, and synthesis imperfections [99,195]. While oxidized carbon nanotubes were used in many studies, non-

covalently functionalized MWNTs are of main interest in this work. SEM examinations of rupture areas show that many MWNTs have rather been just pulled out of the matrix, indicating that the used dispersant does not reduce the strength of MWNTs. In comparison, oxidized MWNTs ("hollow") were also used to produce the LBL films; as expected a drastic decrease of the tensile strength was observed. It is worthy noting that the images of pulled-out MWNT strands also suggest a solution to the efficient reinforcement problem (Figure 4.17). The interfacial stress transfer remains the key issue for the efficient enhancement of the mechanical performance of the composites. The external load applied to the composite should be transferred to the nanotubes; therefore, only strong interconnections between CNTs and polymers may lead to the great mechanical improvement of heterostructures. This is the clue to fully utilize the outstanding mechanical performance of CNTs in a composite system.

The stress-strain curves of investigated films are given in Figure 4.18. Plots show a clear fracture point in the elastic part of the stress-strain curve, without any plateau area that would indicate a plastic deformation. Two distinct elastic regions can be resolved in every graph and have been marked in Figure 4.18 (A). These regions are related to the complex behaviour of the composite under external stress applied to the sample. Initially (region I) randomly orientated and curvy MWNTs tend to align along the stretching direction under the load. Consequently, the composite becomes more compact and MWNTs become more interwoven and knotted. Region II reflects the tensile properties of compact and packed composite with aligned and taut nanotubes; the slope becomes much steeper than in region I, resulting in a higher value of the elastic modulus.

The tensile modulus (obtained from region II), ultimate strength, and elongation up to the breaking point are: 5.5 ± 0.8 GPa, 160 ± 35 MPa, 0.03 - 0.07 % for the "bamboo"; and 2.7 ± 0.7 GPa, 110 ± 30 MPa, 0.03 - 0.06 %, for the "hollow" nanotubes, respectively. Young's modulus and tensile strength of the PEI/PAA composite were estimated to be: 0.26 ± 0.03 GPa and 8.5 ± 3.0 MPa, respectively [113]. These results show that the presence of carbon nanotubes is crucial for achieving improved mechanical properties of polymer-based multilayer stacks. The tensile strength of the neat polymers increased roughly from 8.5 to 160 MPa (around 20 times); the elastic modulus increased from 0.26 GPa to 4.0 GPa (16 times), when "bamboo" MWNTs were incorporated into the host material.

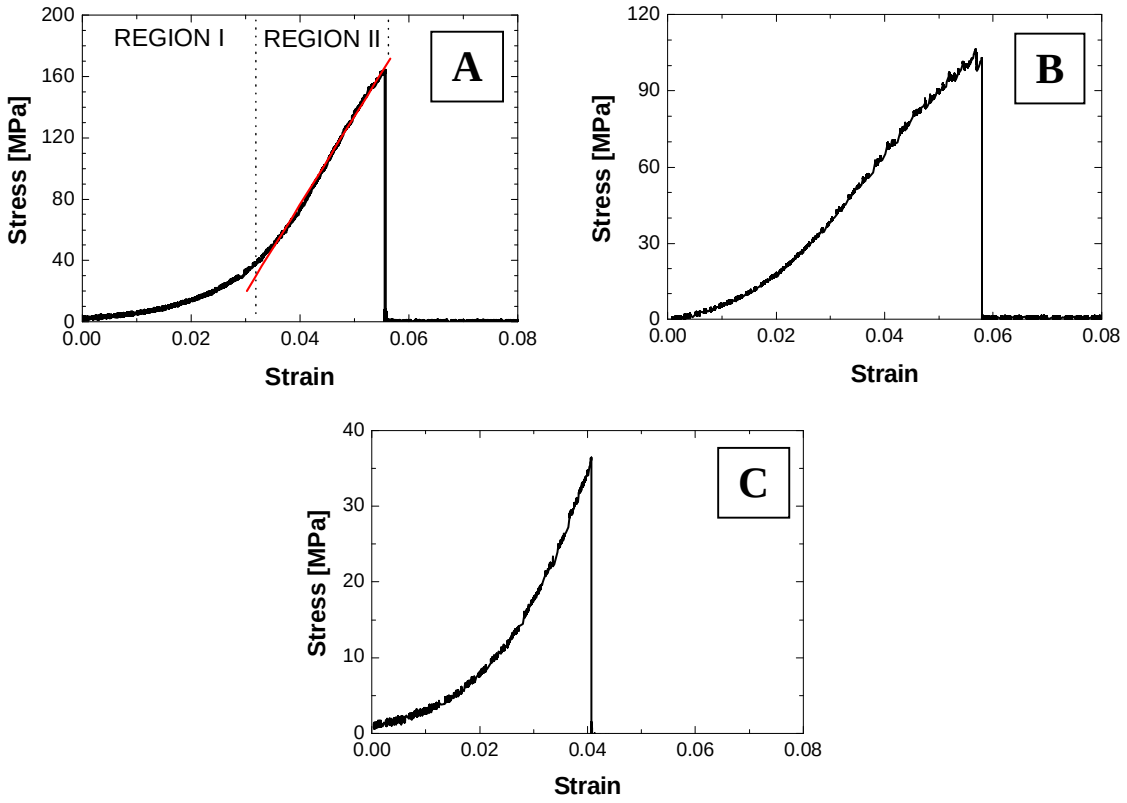

Figure 4.18 Exemplary stress-strain curves of LBL assemblies: (A) MWNT-NaAQ/PEI with "bamboo" nanotubes; (B) MWNT-NaAQ/PEI with "hollow" nanotubes; (C) MWNT-COOH/PEI ("hollow")

The mechanical properties of the LBL structures with MWNTs have been found to exceed the tensile strength of some MWNT composites made by mixing, extruding, or polymerization (Table 2.2). The absolute increase of the elastic modulus and tensile strength of those composites has been shown to change by a factor in the range of 1.09 – 4.29 (E_c/E_p and σ_{Tc}/σ_{Tp}), indicating relatively modest reinforcement of the polymeric systems with CNTs. Only LBL assemblies demonstrate a great increase of the ultimate strength from 9 to 160 MPa (around 20 times stronger polymeric system after CNT addition).

These results indicate the remarkable effect of carbon nanotubes on the tensile properties of LBL composites. The LBL technique can be efficiently applied for the fabrication of strong, homogeneous composites with carbon nanotubes as filler. This is achieved by strong interfacial bonding between MWNTs and polyelectrolytes, mediated by electrostatic attraction, van der Waals adhesion, mechanical interlocking, and chemical bonding. The multilayer films with "bamboo" MWNT are substantially mechanically stronger than com-

posites with “hollow” nanotubes. The “bamboo” morphology provides structural anchors, which enhance the mechanical bonds between MWNTs and the polymer. “Hollow” nanotubes have smooth walls, which reduce the friction forces with the matrix; these nanotubes can be pulled out of the matrix more easily, resulting in the reduction of the film strength.

As mentioned above, LBL multilayer films with oxidized “hollow” MWNTs have also been investigated. The stretching results show, as expected, a drastic decrease in the strength of the composites (Figure 4.18 (C)). Young’s modulus, tensile strength, and elongation at break are: 1.1 ± 0.3 GPa, 40 ± 15 MPa, and 0.03 – 0.05 %, respectively. This confirms that composites with oxidized nanotubes are far weaker than films with non-covalently functionalized MWNTs. Oxidation and any further covalent functionalization of carbon nanotubes apparently reduces the mechanical performance of nanotubes due to the disruption of the aromatic bonds of the CNTs. Oxidation also cuts carbon nanotubes, thus reducing the mechanical bonds between shorter nanotubes.

On the basis of the investigated structural and mechanical properties of LBL MWNT/polymer films, one can see that the tensile strength increase is much greater than that of nanotube composites made by solution mixing, melt-mixing, and the *in-situ* polymerization of monomers in the presence of nanotubes (Table 2.2). Additionally, it has been shown that the morphology of MWNTs can also result in a big difference of their mechanical performance. The replacement of standard, “hollow” MWNTs with “bamboo”-type MWNTs results in a significant improvement of composites’ ultimate strength. The “knots” on the “bamboo”–like MWNTs stem afford a tighter matrix connectivity with the polymer, thus reducing the pull-out of the nanotubes from the polymer.

4.3 Nanoindentation experiments

On the basis of the mechanical performance of the CNT-based composites obtained in tensile tests, it has become interesting to study the properties of various polymeric heterostructures with MWNT fillers by means of nanoindentation. The nanoindentation technique has been proven as a useful tool for the determination of the mechanical properties of thin films, coatings, and composites, including polymers [181,196-200]. Depth-sensing indentation allows a displacement of the indenter to be measured as a function of an ap-

plied, controlled load. The resulting load vs. displacement curves, together with the indenter geometry, are used to evaluate the elastic modulus and hardness of tested samples.

Nanoindentation experiments have been carried out on different MWNT- and MWNT@SiO_2-based polymer composites with different morphologies, polymers and nanotubes compositions, and fabricated utilizing diverse processes (Table 3.1) [201]. The obtained values of hardness H and elastic modulus E_r have been plotted as a function of the contact depth.

4.3.1 Data analysis and discussion on instrument calibration

The hardness and elastic modulus of the composites were evaluated from the recorded unloading slope of the depth-displacement curve, based on the method of Oliver and Pharr [202]. A general relation between the penetration depth h and the load P is given by:

$$P=D\,(h - h_f)^m \tag{4.3}$$

where D contains all the geometric constants, sample elastic modulus, Poisson's ratio, the indenter elastic modulus, and the indenter Poisson's ratio, h_f is the final unloading depth, and m is the power law exponent that is related to the geometry of the indenter (e.g. for flat-ended cylindrical punch m=1, cone m=2, paraboloid of revolution m=1.5, approximation of paraboloid of revolution is taken when considering Berkovich tip [202]). Hardness and reduced modulus are defined as:

$$H = \frac{F_{\max}}{A_C} \tag{4.4}$$

$$E_r = \frac{1}{2}\sqrt{\frac{\pi}{A_C}} \times S \tag{4.5}$$

where H is the local hardness, A_c is the contact area between indenter and sample, S is the contact stiffness, defined as a slope of the unloading curve fitted to the power law equation (4.3), E_r is the reduced Young's modulus (effective elastic modulus) that combines the properties of the indenter and the tested sample, and is given by:

$$\frac{1}{E_r} = \frac{(1-\nu_S{}^2)}{E_s} + \frac{(1-\nu_i{}^2)}{E_i} \tag{4.6}$$

where v_i and v_s are the Poisson's ratios for the indenter and the sample, respectively, and E_i and E_s are the respective elastic moduli. Since we used a diamond tip with high elastic modulus E_i=1170 GPa and low Poisson's ratio v_i=0.07, the second term in equation (4.6) can be neglected. The Poisson's ratio of most polymers lies in the range of 0.25 – 0.45, therefore, the elastic modulus of the structures investigated here is numerically equal to the 80 – 95 % of the calculated reduced (effective) modulus from the indentation experiments (equation (4.6)). Since the accurate values of Poisson's ratio of polymers and their compositions with CNTs are not known, the values of reduced modulus have been used in this study to quantitatively describe the mechanical properties of the samples. In this work the term "reduced modulus" is alternately used with the terms: "elastic modulus" or "Young's modulus" – meaning the same quantity of E_r obtained in the nanoindentation test and calculated from equation (4.5).

Since the contact area is a function of the contact depth, a tip calibration procedure has to be employed to determine the geometry of the indenter tip. For this purpose a series of indentations at different contact depths were made in a sample with a known elastic modulus. The dependence of the contact area as a function of contact depth was plotted afterwards, and the area function was found using the following polynomial expression:

$$A_C = C_O h_C^2 + C_1 h_C + C_2 h_c^{\frac{1}{2}} + C_3 h_C^{\frac{1}{4}} + C_3 h_C^{\frac{1}{8}} + \ldots \qquad (4.7)$$

where C_n (n=0,1,2…) are the fitting coefficients, and h_c is the contact depth, being determined from:

$$h_c = h_{\max} - \varepsilon \frac{F_{MAX}}{S} \qquad (4.8)$$

where h_{max} is the maximum displacement at maximum load, ε is a function of the particular tip geometry (e.g. for flat-ended cylindrical punch ε=1, cone ε=2(π-2)/π, paraboloid of revolution ε=0.75, the approximation of a paraboloid of revolution is taken when considering the Berkovich tip [202]).

The tip calibration was carried out on PMMA with well defined mechanical properties (see 3.2.2), instead of the commonly used hard standard materials like fused quartz. Klapperich et al. called into question the validity of using hard standard materials for tip calibrations, when soft materials are investigated [198]. Briscoe et al. remarked that a calibra-

tion against a hard surface may produce an error and does not represent the contact situation with softer surfaces [200]. Moreover, contact depths obtained in this study were in the range of several hundred nanometers. This range cannot be obtained from a calibration performed on hard materials. The geometries of the used tips (Berkovich and conical) were estimated in the calibration procedure. The contact area as a function of contact depth was estimated from equation (4.7). Prior to each experiment, a series of depth-dependent indents in a standard sample were carried out, to ensure that the tips' shape did not change. No significant changes in the calibrated tip area had been noticed.

The diamond tips have been used to perform *in-situ* visualization of the samples'surface before the indent in order to find reasonably smooth areas. The imprints after indent were also imaged using the same diamond tip. Figure 4.19 shows typical imprints after indentation performed in PMMA using a conical (A) and a Berkovich (B) tip.

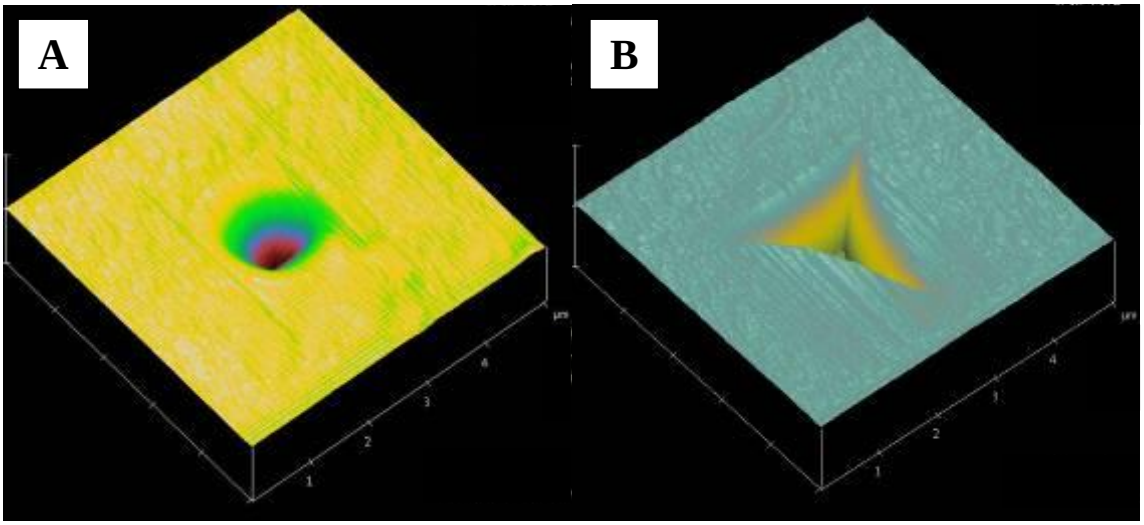

Figure 4.19 Typical imprints after indentation experiments using conical (A) and Berkovich (B) diamond tips. Images were obtained using the same indent tips. These images were performed on PMMA sample, with a maximum applied load of 400 μN.

There are many factors that have a great influence on the recorded data-points, and consequently calculated physical quantities in the nanoindentation test. The nanoindentation results are affected by: machine compliance, roughness of the sample, calibration procedure, time-dependent behavior of the specimen (thermal drift, creep), sample inhomogeneity, and contact area changes [203]. Therefore, the computed values of H and E_r are error-laden and may not reflect the absolute values. However, since all experiments were

conducted under the same experimental conditions, the relative comparison of results of different samples can be performed. Mechanical responses to the deformation of various composites have been evaluated in this work.

4.3.2 Nanoindentation of polymeric films

Prior to the experiments performed on CNT-based composites, a series of indents were carried out on polymeric materials such as PMMA and PS. This was necessary in order to adapt the finest experimental conditions including area tip calibration, hold time, and load/unload rate. The results from nanoindentation tests on the polymers were consistent for PMMA and PS in terms of the general behavior of the H and E_r as a function of contact depth, hold time, and load/unload rate. Due to this consistency and for reasons of clarity, only data from studies on PMMA is presented here. Nanoindentation on PMMA revealed a high reproducibility of results and a small data deviation.

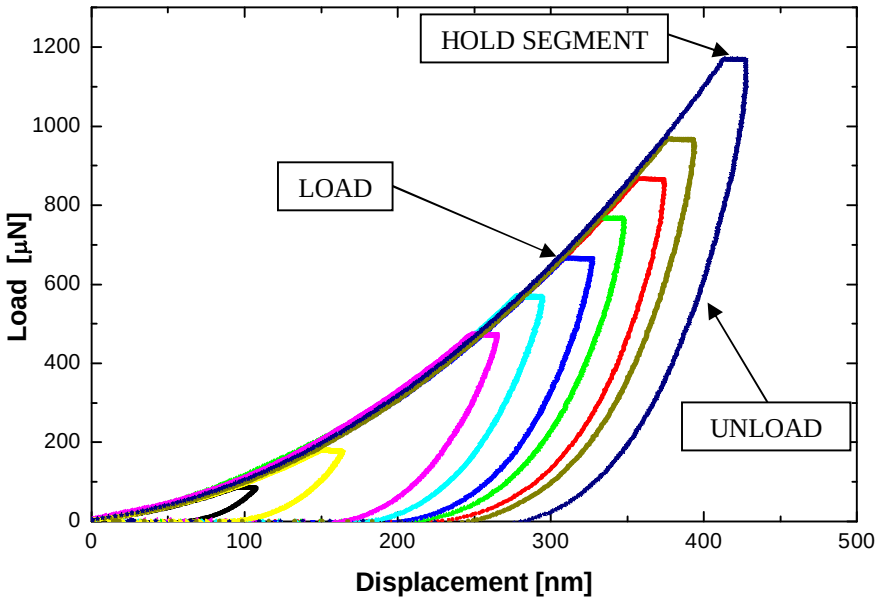

Figure 4.20 Load-displacement curves of several indents performed in PMMA at different applied loads (ranging from 100 to 1300 µN). The graphs depict the typical load, hold, and unload segments of the nanoindentation experiments.

Typical load-displacement curves of the indents are shown in Figure 4.20. The image represents data obtained for a PMMA sample at different applied maximum loads ranging

from 100 to 1200 µN. The absence of steps and discontinuities on the curves indicates that neither cracks nor fractures occurred during the indentation [204]. The hold time segment at the peak load is used to minimize the creep effect, that might influence the shape of the unload curve, and as a result, would affect the calculated values of the Young's modulus and hardness [205].

Reduced modulus and hardness as a function of the indentation contact depth for PMMA are shown in Figures 4.21 (A) and (B), respectively. The data represent nanomechanical properties of PMMA obtained from different indenter tip geometries (Berkovich and conical), with a load/unload rate equal to 40 µN and 20 s hold time. Several indents were performed under the same maximum force and the collected data was then averaged. The error bars in the graphs represent the standard deviation of calculated mean values of the hardness and elastic modulus. The indents were performed at a maximum load ranging from 100 to 1500 µN, resulting in contact depths ranging from 50 to 500 nm.

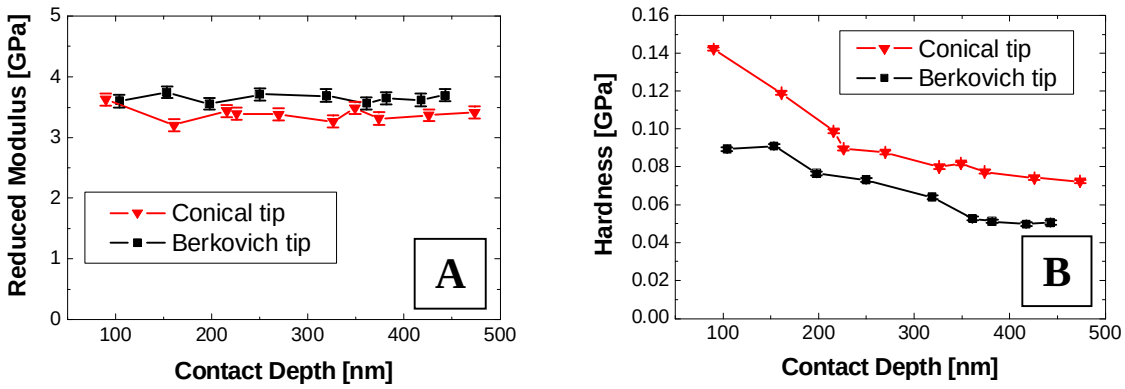

Figure 4.21 Reduced modulus (A) and hardness (B) as a function of the contact depth. Indents were performed in PMMA using both, Berkovich and conical tips at load/unload rate of 40 µN/s and 20 s hold time.

Figure 4.21 (A) reveals that the elastic modulus is relatively constant and that there is no clear relationship between E_r and the contact depth of the indentation. This behavior corresponds to previously reported results by Klapperich et al. [198]. Figure 4.21 (B) shows, in the initial stage, the decreasing trend of the hardness with increasing contact depth for both indenter tips. For contact depths greater than 350 nm, the curves smoothly come into the plateau region. This relationship between H and the contact depth is inconsistent with the study on different polymers (including PMMA) of Klapperich et al., who

showed that the hardness increased with increasing contact depth. The surface roughness, time dependent plastic deformation (e.g. creep) and nano-structural differences in the morphology of the PMMA films may give rise to such disagreement in the depth-dependent behavior of the hardness. It is possible that at particular depths, diverse samples may relax differently or exhibit dissimilar chain slip, resulting in different values and behaviors of H and even E_r.

Both, Berkovich and conical tips are commonly used to investigate soft materials such as polymers [203]. As shown in Figure 4.21, the hardness and Young's modulus display a similar trend for conical and Berkovich tips. All of the tests on the polymers were performed utilizing those two indenter geometries. It was found that results were fairly consistent, and only modest differences in values were recorded. In this context, for reasons of clarity the following plots present data from the tests carried out using the Berkovich tip only.

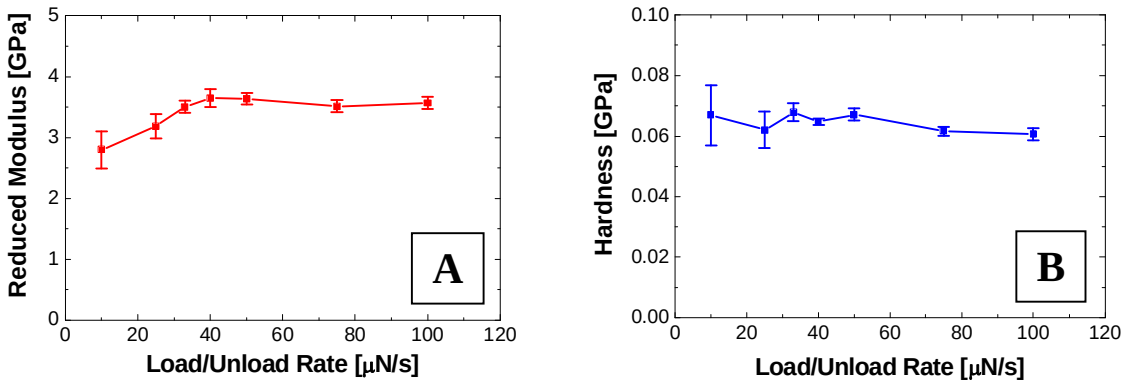

Figure 4.22 Reduced modulus (A) and hardness (B) as a function of the load/unload rate. Indents were made using a Berkovich tip in PMMA with a maximum load of 500 μN and 20 s hold time.

The nanomechanical response of the PMMA was also tested under different load/unload rates varying in the range from 5 to 100 μN/s. All indents were conducted at a maximum load equal to 500 μN, with 20 s hold time. Again, several indentations were performed and data for the same peak load were averaged and the deviation of H and E_r calculated. Figure 4.22 illustrates the behavior of the reduced modulus (A) and hardness (B) as a function of load/unload rate. The hardness is not significantly affected by the load/unload rate. On the other hand the E_r initially increases with increasing load/unload rate. At rates greater than 30 μN/s, the elastic modulus does not show any dependency on the indentation

velocity. These investigations show that at low load/unload rates, the mechanical response may slightly differ from that obtained for higher rates. Such behavior can be explained by plastic deformation of the material. Under low load/unload rates the indenter‘s volume may be accommodated by plastic flow of the material that piles up around the tip, so plastic deformation is more prominent in this case.

As mentioned before, in all experiments the hold time of 20 s at maximum load was employed, which reduces the creep effect. As a consequence, the material has sufficient time to minimize the mechanical disequilibrium (the delayed response of the material to the applied stress or strain) before the unloading step begins [198,200]. The creep effect especially relates to visco-elastic materials like polymers, with time-dependent properties. The time-dependent creep within the specimen occurs under indentation load and manifests itself as a change (increase) of the indentation depth under a constant load (Figure 4.20 shows the changes of the displacement at constant maximum load). The creep has a great influence on the load/unload slope [205]. The level of this influence depends not only on the hold time but also on the displacement rate. If the load rate is large, the creep is higher than for indentation with a lower load rate, because viscoelastic material can not keep up with the “fast” indenter, giving a rise to the material’s flow during the indentation test.

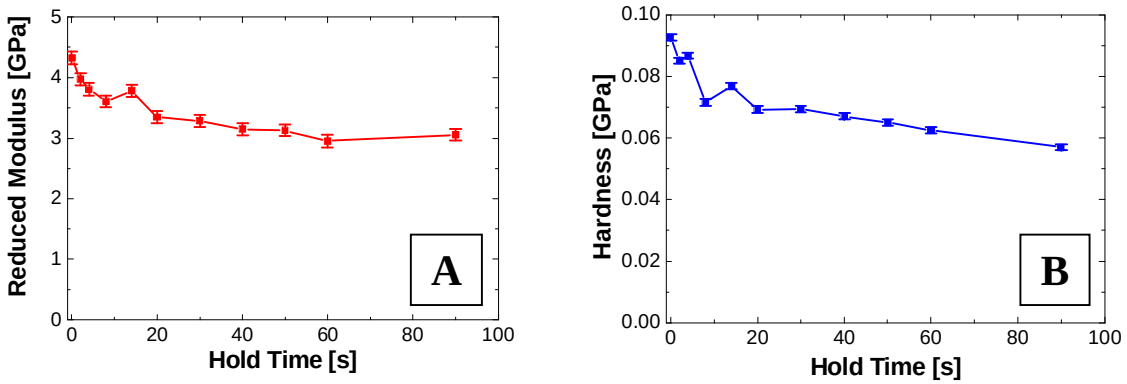

Figure 4.23 Reduced modulus (A) and hardness (B) as a function of hold time. Indents were performed using a Berkovich tip in PMMA with a peak load of 500 μN, at 40 μN/s load/unload rate.

A significant influence of the hold period on the calculated values of H and E_r was observed. Indents with peak loads of 500 μN at 40 μN/s load/unload rate were carried out for different hold time periods. Figure 4.23 illustrates decreasing values of the hardness and

reduced modulus while increasing the hold time, until a plateau is reached at around 18 - 20 s (some modest decrease in hardness still exist). On this basis a hold time of 20 s can be used to diminish the creep effect in nanoindentation tests of the polymeric materials.

To standardize the experimental conditions for all specimens in this study, the hold time and the load/unload rate of indentations were set to 20 s and 40 μN/s, respectively.

4.3.3 Nanoindentation of CNT-based composites

Figures 4.24 and 4.25 show the nanomechanical properties of MWNT/PMMA composites. The tests were performed under fixed experimental conditions (see 4.3.2), using a Berkovich tip. The homogeneity of our samples is confirmed by the relatively small standard deviation of data points. The reduced modulus and hardness are shown as a function of the contact depth for different MWNT content. The nanoindentation studies reveal that the properties of the MNWT composites are comparable to those of thin films of PMMA. Moreover, H and E_r as a function of contact depth, exhibit exactly the same behavior as was shown for neat PMMA. The hardness shows a decreasing trend with increasing contact depth. There are no significant changes in H values with increasing concentration of carbon nanotubes in the polymer. E_r of thin films presents independent behavior on indentation contact depth with values close to that obtained for neat PMMA.

Li et al. [204], Dutta et al. [206], and Penumadu et al. [207], investigated CNT-based composites with different morphologies and content of nanotubes (up to 5 wt%). They reported a modest but quantifiable increase of the hardness and elastic modulus while increasing the content of nanotubes, which is in contrast to our observations. The differences, in contrast to this study, can arise from the different matrix materials and preparation procedures used in their studies. In reports of Ref. [204,206,207] singlewall carbon nanotubes were introduced into epoxy resins. The presence of nanotubes can influence the polymerization process of the epoxy resulting in different molecular weights and cross-linking of matrix. On this basis, the mechanical response of the investigated samples can be mainly affected by the structural changes of the host material. It has been shown that comparisons of the elastic modulus and hardness are more appropriate for samples with a similar chemistry, molecular weight, and processing history [198,203,208]. In this context, the results of Ref. [204,206,207] can be error-laden due to the differences in the structure of particular composites with various CNT concentrations. Therefore, in this study, to avoid such uncertainty, MWNTs were incorporated into the PMMA with a well

defined molecular weight; additionally, every sample was prepared using the same procedure.

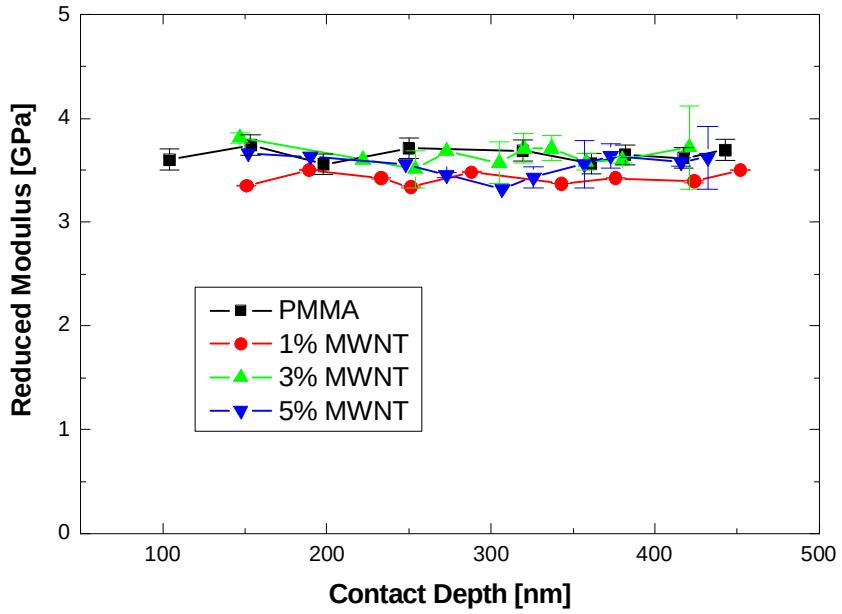

Figure 4.24 Reduced modulus of MWNT/PMMA composites with different CNT concentrations, as a function of the contact depth. A Berkovich tip was used at a load/unload rate of 40 µN/s and 20 s hold time.

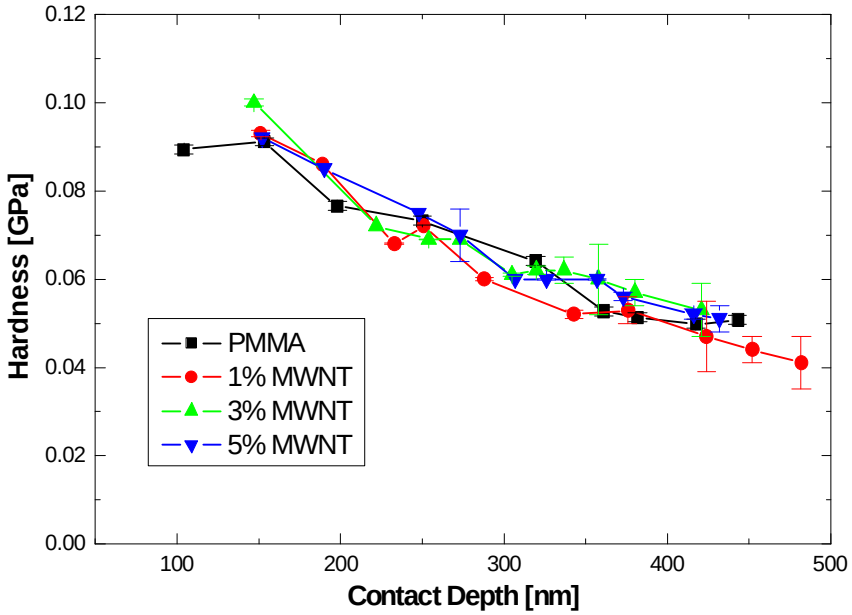

Figure 4.25 Hardness of MWNT/PMMA composites with different CNT concentrations, as a function of the contact depth. A Berkovich tip was used at a load/unload rate of 40 µN/s and 20 s hold time.

Figures 4.26 and 4.27 show data from nanoindentation experiments conducted on various LBL structures under the same fixed conditions. Reduced modulus and hardness as a function of the contact depth are presented.

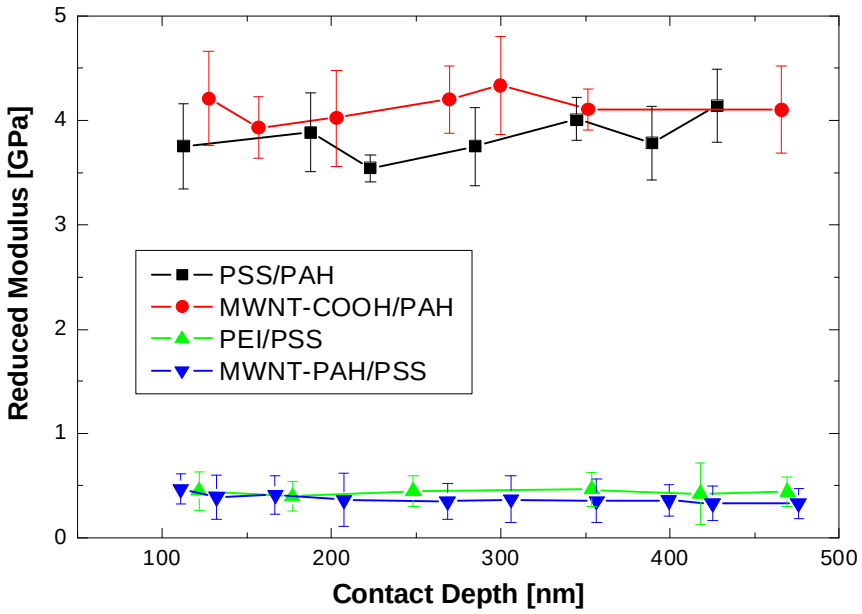

Figure 4.26 Reduced modulus as a function of contact depth. Data obtained for different LBL heterostructures using a Berkovich tip at a load/unload rate of 40 μN/s and 20 s hold time.

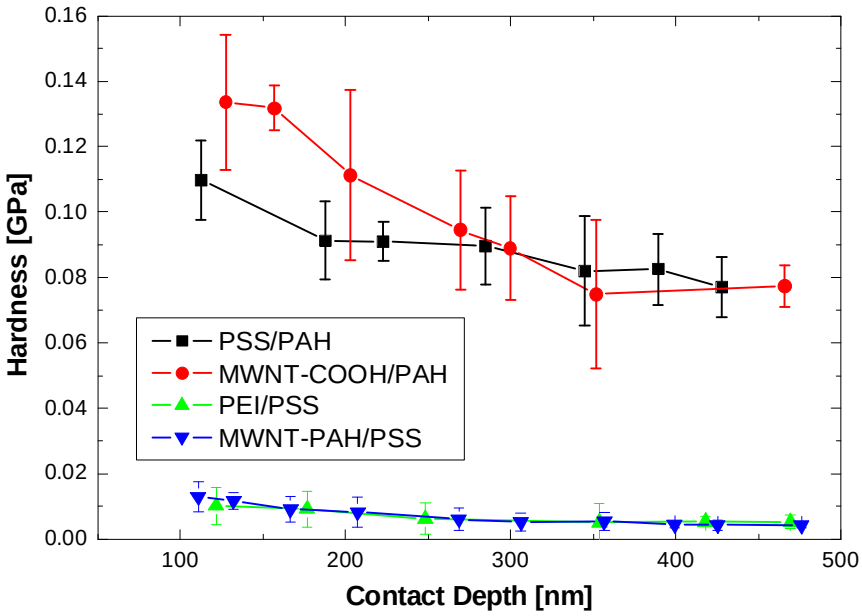

Figure 4.27 Hardness as a function of contact depth. Data obtained for different LBL heterostructures using a Berkovich tip at a load/unload rate of 40 μN/s and 20 s hold time.

As expected, the behavior of H and E_r as a function of the contact depth is consistent with previous observations (Figure 4.21). Briefly: the elastic modulus is relatively independent of the contact depth, and hardness initially reveals a decreasing a trend for small loads and then smoothly attains a plateau (at a contact depth of around 250 nm).

The reduced modulus of PSS/PAH and MWNT-COOH/PAH films (3.8 ± 0.2 GPa and 4.12 ± 0.13 GPa, respectively) is shown to be around 10 times greater than that obtained for PEI/PSS or MWNT-PAH/PSS composites (0.44 ± 0.02 GPa and 0.37 ± 0.04 GPa, respectively). The same situation refers to the hardness: H=0.09 ± 0.01 GPa of PSS/PAH; H=0.11 ± 0.03 GPa of MWNT-COOH/PAH; H=0.007 ± 0.002 GPa of PEI/PSS; and H=0.007 ± 0.003 GPa of MWNT-PAH/PSS. Such a variation of results corresponding to different LBL structures reveals a significant influence of the sample's structure (e.g. different polymers) on the mechanical properties.

The investigated materials were composed of diverse polymers and nanotubes, different deposition cycles and multilayer combinations were also utilized. It is known that LBL assemblies form very intricate systems. Thus, it is barely possible to compare the mechanical performance of different LBL assemblies due to their structural complexity. Nevertheless, it can be observed that the presence of MWNT fillers within the LBL polymeric structure does not lead to important changes in the mechanical properties (in terms of through thickness - perpendicular to the surface properties) of the composites that would differ significantly from the properties of the polymeric LBL systems. Even a high concentration (~50 wt%) and a homogenous distribution of CNTs within a polymer matrix, as well as strong adhesion between the structural components, are insufficient to ensure a significant improvement of H and E_r. It is suggested, that the flexibility of carbon nanotubes and their curvy morphology reduce the reinforcement action. The carbon nanotubes can easily be displaced or deflected by the indenter. As a result, the indenter may essentially only "feel" the resistance of the surrounding matrix. Therefore, the mechanical response of the composite is close to that of the local polymer matrix.

These results are consistent with the study of Pavoor et al. [209]. It was shown that LBL composites of MWNT/PAH exhibit inferior mechanical performance in comparison to LBL films consisting of polyelectrolytes (PAH/PAA) only. Heterostructures were significantly softer than the corresponding polymeric matrices. Lu et al. [210] have investigated SWNT-based LBL composites. They showed an increase of the elastic modulus (by a factor of 2.5) of MWNT/PAA/PDDA composites in comparison to a LBL film composed of only polyelectrolytes (PAA/PDDA). But again, the validity of such a quantitative com-

parison may be questioned since different deposition cycles and compositions of polymers and nanotubes were used. It is shown in Figures 4.26 and 4.27 that the mechanical responses of LBL composites can significantly differ for various LBL assemblies, not only due to the presence of CNT filler in the host material, but mainly because of the differences in the structure of the LBL films (various polymers, functionalized nanotubes, morphologies etc.).

In this paragraph, the hardness and elastic modulus of the different MWNT/polymer composites have been shown. In general, any significant improvement of the mechanical properties (from indentation tests) of the polymeric matrix with CNT filler was observed in comparison to the neat polymer. This is in contrast to the stretching experiments (see 4.2) that have displayed a significant increase of the tensile strength and the tensile elastic modulus of the MWNT-based heterostructures. CNTs have extraordinary axial mechanical properties that play an important role in the reinforcement of the tensile properties of the materials; but due to their curvy morphology and flexibility, CNTs have a modest impact on the hardness and Young's modulus (through thickness) of the polymeric matrices.

To verify our supposition, silica reinforced multiwall carbon nanotubes have been used to fabricate nanocomposites with PMMA. As shown in Figures 4.28 and 4.29, the MWNT@SiO_2/PMMA heterostructures exhibit much higher values of hardness and elastic modulus than neat PMMA (the error bars are not shown for reasons of clarity). Both these quantities increase with an increasing concentration of the MWNT@SiO_2 in the host material. The results demonstrate the great influence of the silica shell of MWNTs on the mechanical response of the composites. This indicates that silica coating of MWNTs changes their bending properties; such nanotubes are more rigid and thus more resistant to the diamond tip during nanoindentation experiments.

The average standard deviations of the data points of the Young's modulus (Figure 4.28) are: 0.27, 1.06, 1.14, and 1.56 GPa for 1, 2, 3, and 4 wt% of the silica coated MWNT in PMMA, respectively. The average standard deviations of the hardness (Figure 4.29) are: 0.006, 0.02, 0.03, and 0.02 GPa for 1, 2, 3 and 4 wt% of MWNT@SiO_2 in the polymer, respectively. These relatively large data errors (comparing to the MWNT/PMMA films) are caused by roughness and the presence of inhomogeneities in the composites. The fabrication method of MWNT@SiO_2/PMMA systems does not ensure a uniform distribution of silica coated CNTs within the film, especially at higher concentrations, due to the poor solubility of CNT@SiO_2 in chloroform. Thus, agglomerations of

nanotubes and possible phase segregation can be observed in nanocomposites with higher CNTs content.

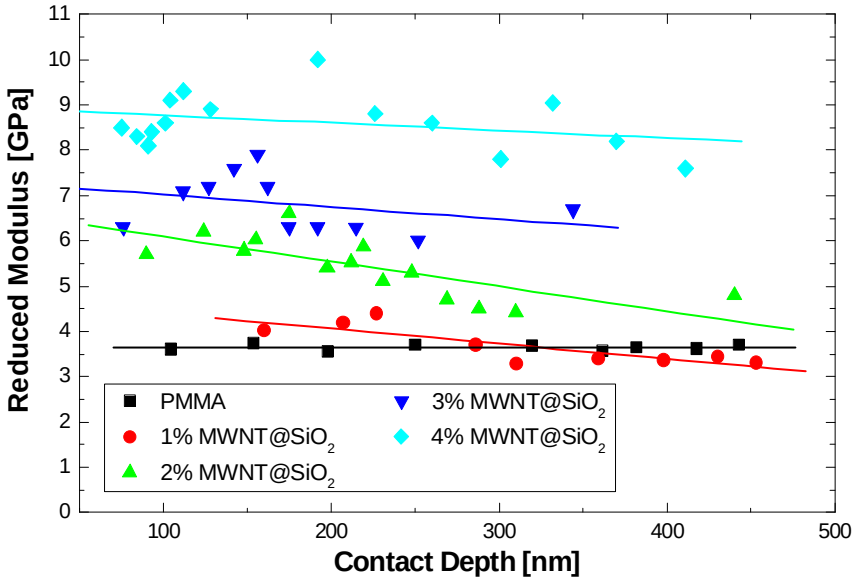

Figure 4.28 Reduced modulus as a function of contact depth. Data obtained for heterostructures of MWNT@SiO_2/PMMA with different nanotubes' concentrations using a Berkovich tip at a load/unload rate of 40 μN/s and 20 s hold time. Standard deviations of the data points are not shown for clarity and are presented in the text. The solid lines are just to guide the eye.

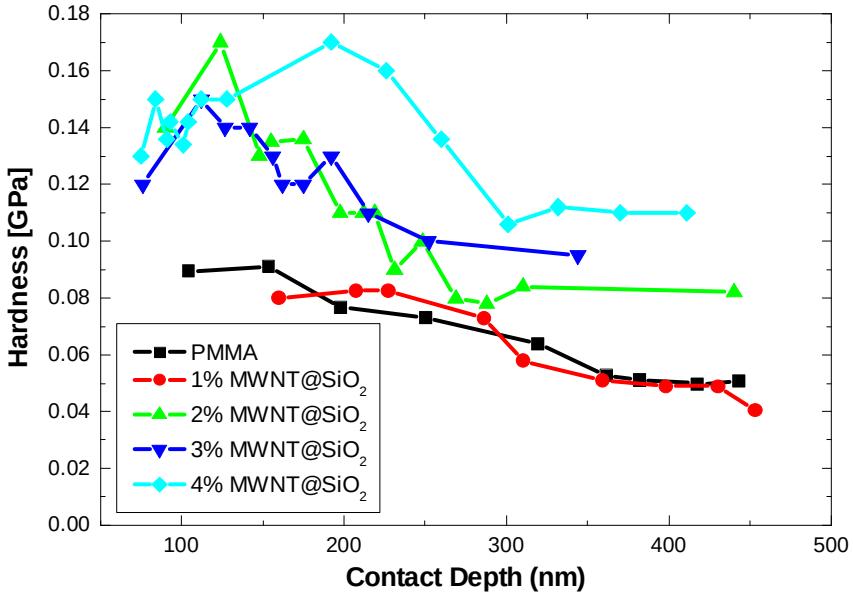

Figure 4.29 Hardness as a function of contact depth. Data obtained for MWNT@SiO_2/PMMA heterostructures with different nanotube concentrations using a Berkovich tip at a load/unload rate of 40 μN/s and 20 s hold time. Standard deviations of the data points are not shown for reasons of clarity and are presented in the text.

MWNT@SiO_2/PMMA composites with 5 wt% nanotubes' load have also been investigated. The reduced modulus for this specimen varies from 5 to 20 GPa and the hardness from 0.08 to 0.22 GPa resulting in unreasonable data deviation. As a consequence, these results are not considered in Figures 4.28 and 4.29. Large systematic errors are also produced by the fairly substantial roughness of the MWNT@SiO_2/PMMA films' surfaces. The influence of the roughness on the H and E_r is more emphatic at low applied loads [203]. It was observed that roughness increases with increasing the MWNT@SiO_2 concentration in the composite: *Ra* was found ranging from 10 nm even up to 100 nm for composites with 1 wt% and 5 wt% of MWNT@SiO_2, respectively. It is assumed that the effect of the surface roughness is neglected when *Ra* is less than 1/10 of the maximum penetration depth. This eliminates the results of a 5 wt% sample, because indents depths in the range of 100 – 500 nm do not satisfy this assumption. The significant influence of the roughness on the nanoindentation results has been a subject of several studies [203,211].

The differences in the mechanical response of the different samples are depicted in Figure 4.30, where load-displacement curves of PMMA, MWNT/PMMA (3 wt%), and MWNT@SiO_2/PMMA (3 wt%) are shown.

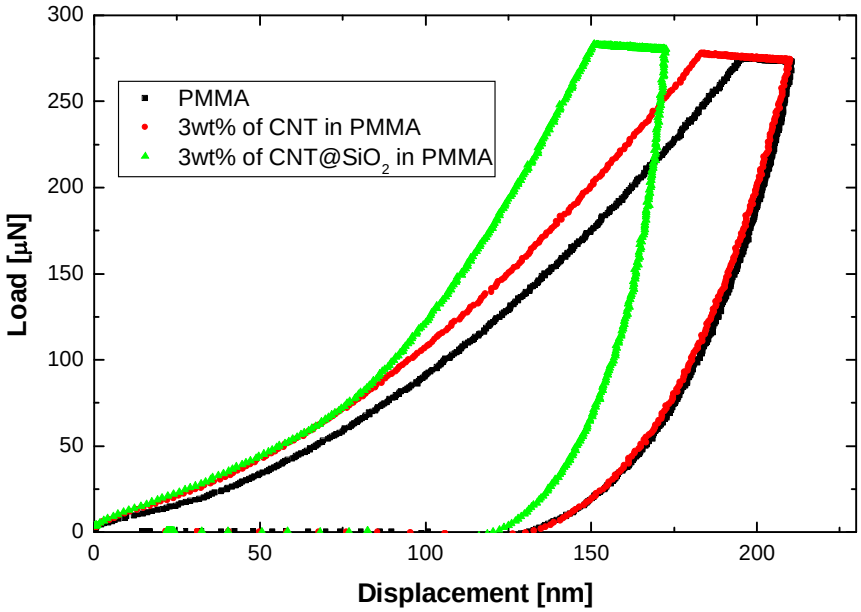

Figure 4.30 Load-displacement curves of different samples. Hardness and reduced modulus were calculated from those plots, resulting in: PMMA H=0.09 GPa and E_r=4 GPa; MWNT/PMMA H=0.09 GPa and E_r=4.1 GPa; MWNT@SiO_2/PMMA H=0.13 GPa and E_r=8 GPa.

PMMA and MWNT/PMMA structures exhibit a softer nature than a composite of MWNT@SiO_2/PMMA: at the same maximum indentation load (300 μN) the indenter performs deeper penetration, resulting in displacements of 210 nm; for MWNT@SiO_2/PMMA the indenter reaches a depth of 160 nm, which indicates a greater hardness of this sample. Corresponding values of hardness and reduced modulus confirm those observations: H=0.09 GPa and E_r=4 GPa, for PMMA, H=0.09 GPa and E_r=4.1 GPa for MWNT/PMMA composite, H=0.13 GPa and E_r=8 GPa for MWNT@SiO_2/PMMA. The absence of steps and discontinuities on the curves indicates that no cracks and fractures occurred in the specimen during the indentation.

LBL composites with silica coated multiwall carbon nanotubes were also fabricated in order to investigate their properties, but due to the large roughness (Ra > 100 nm) of these hybrid materials it was impossible to obtain reasonable results in nanoindentation tests.

Nanoindentation experiments carried out on the different composition of polymers and carbon nanotubes reveal that the presence of MWNTs within the polymeric matrices does not significantly affect the mechanical response of the composites. In general, hardness and elastic modulus have been found to reflect the mechanical properties of the surrounding matrix, emphasizing a modest influence of nanotube filler on the mechanical performance of the heterostructures (even at high concentrations of CNTs in LBL assemblies). This is explained by the flexibility of MWNTs and their curvy morphology. This supposition was confirmed while MWNT@SiO_2 were employed as a reinforcement filler. The average Young's modulus for the 4 wt% samples was found to be approximately three times as high as that for PMMA. For the same CNT concentration, the average hardness increases about two times in comparison to the neat polymer. A silica shell changes the bending performance of the CNTs and hence the indentation properties of composites.

Silica coating of MWNTs opens up possibilities for the production of new, advanced, reinforced materials for a variety of applications.

4.4 Rheology

Rheological investigations of CNT-based composites, as a complement of tensile and nanoindentation tests, give a better understanding of the impact of the carbon nanotube fillers on the mechanical properties of polymeric composites. Dynamic oscillatory rheometry was employed to characterize viscoelastic properties and the rheological percolation threshold of these heterostructures. There are many studies focused on rheometric experiments of CNT/polymer structures [28,38,92,168,169,171,172,210,212-217]. In general, it was found that the viscosity increases with an increasing concentration of carbon nanotubes in the composites. Moreover, liquid-like to solid-like transitions have been observed, which indicate the formation of a percolating network of the filler. Table 4.1 shows values of rheological percolation thresholds obtained in various studies. It is known that the percolation threshold varies significantly with particles size and shape [218]. Fillers with a large aspect ratio form percolating networks at lower weight fractions. This favors carbon nanotubes (as fiber with large aspect ratio) as ideal candidates for the fabrication of composites with improved properties or even with new performance.

Table 4.1 The rheological percolation threshold of different CNT-based polymer composites obtained in various studies. PMMA - poly(methyl methacrylate), PET - poly(ethylene terephthalate), UMWPE - ultrahigh molecular weight polyethylene, PC - polycarbonate, PP - polypropylene, HDPE - high density polyethylene, PEO - poly(ethylene oxide).

Composite	**Preparation Method**	**Rheological Percolation Threshold**	**Ref.**
SWNT/PMMA	Solution mixing	0.12 wt%	[172]
MWNT/PET	Solution mixing	0.6 wt%	[92]
SWNT/UMWPE	Solution mixing	0.6 wt%	[170]
MWNT/PC	Melt mixing	0.5 wt%	[212]
MWNT/PP	Melt mixing	2 wt%	[217]
MWNT/PC	Melt extrusion	2 wt%	[168]
MWNT/PC	Melt extrusion	0.5 wt % at 280 °C , 5 wt% at 170 °C	[169]
SWNT/HDPE	Melt extrusion	1.5 wt %	[38]
SWNT/PEO	Solution mixing	0.09 wt%	[171]

The complex viscosity (η^*), storage (elastic) modulus (G'), and loss modulus (G'') were obtained in dynamic oscillatory experiments. In a controlled strain tests, the strain γ is assigned with an amplitude γ_0, and an angular velocity ω as:

$$\gamma = \gamma_0 \cdot \sin(\omega t) \tag{4.9}$$

where ω is linked to the frequency of the oscillation ($\omega=2\pi f$). The resulting stress is then calculated as:

$$\tau = \tau_0 \sin(\omega t + \delta) \tag{4.10}$$

where τ_0 is the stress amplitude, and δ is the phase angle. The complex modulus G^* is defined:

$$G^* = G' + iG'' \tag{4.11}$$

with the elastic (storage) modulus given by: $G'=G^*\cos\delta=(\tau_0/\gamma_0)\cdot\cos\delta$, and the loss modulus $G''=G^*\sin\delta=(\tau_0/\gamma_0)\cdot\sin\delta$. The complex viscosity η^* is evaluated from:

$$\eta^* = \eta' + i\eta'' = \frac{G^*}{i\omega} \tag{4.12}$$

where $\eta'=G''/\omega=[\tau_0/(\gamma_0\cdot\omega)]\cdot\sin\delta$ is the real part and $\eta''=G'/\omega=[\tau_0/(\gamma_0\cdot\omega)]\cdot\cos\delta$ is the imaginary part of the complex viscosity.

The rheological properties of MWNT/PEI composites (in melts) were investigated in this study. The complex viscosity as a function of the shear frequency is shown in Figure 4.31. Apparently, MWNTs have a crucial effect on the rheological behavior of the composites, even at low loadings. The complex viscosity increases with increasing CNT content in the entire frequency range, but is more pronounced at low frequencies. At high frequencies the impact of the carbon nanotubes on the rheological properties is definitely weaker, which suggests that the nanotubes do not significantly influence the short-range dynamics of the polymer chains. Generally, CNTs do affect polymer chain relaxation but with little effect on the local motion at short ranges [172]. The changes in the complex viscosity of MWNT/PEI composites are caused by similar changes in storage and loss modulus. The values of both G' and G'' at any particular frequency systematically increase with increasing carbon nanotube loads in the polymer matrices (Figures 4.32 and 4.33).

But again, these changes are more pronounced at low frequencies. In general, *G'* was found to be more sensitive to the structural changes than *G''*.

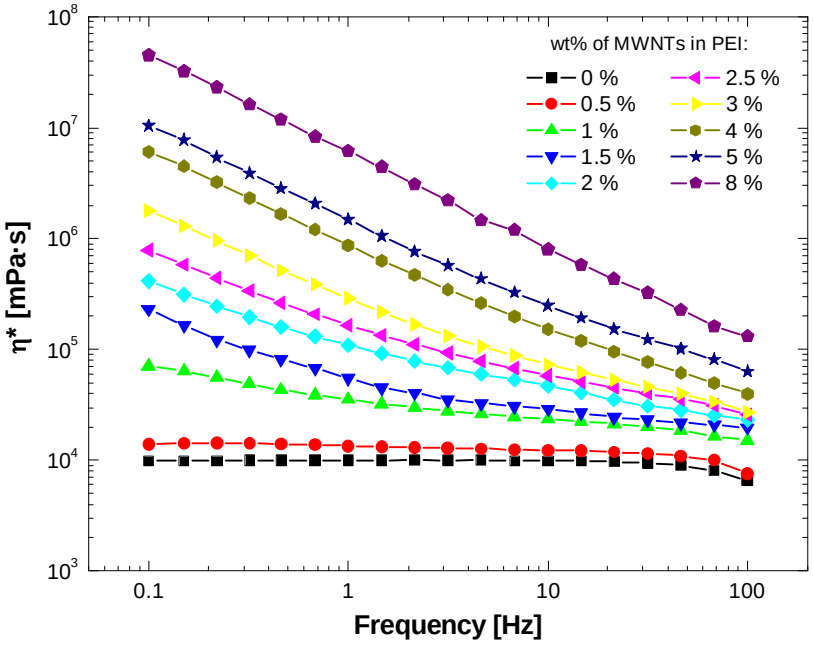

Figure 4.31 Complex viscosity (η^*) of MWNT/PEI composites versus frequency.

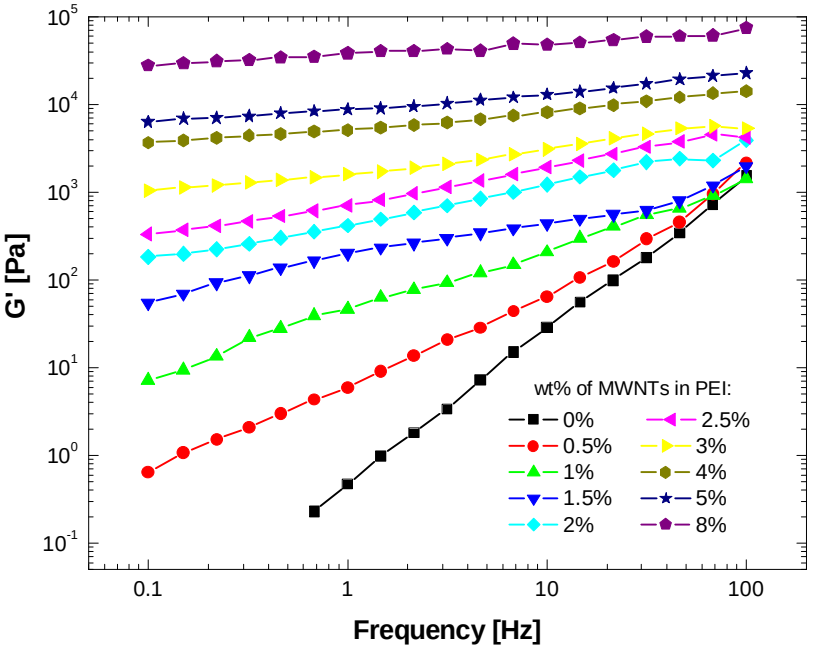

Figure 4.32 Storage modulus (*G'*) of MWNT/PEI composites versus shear frequency.

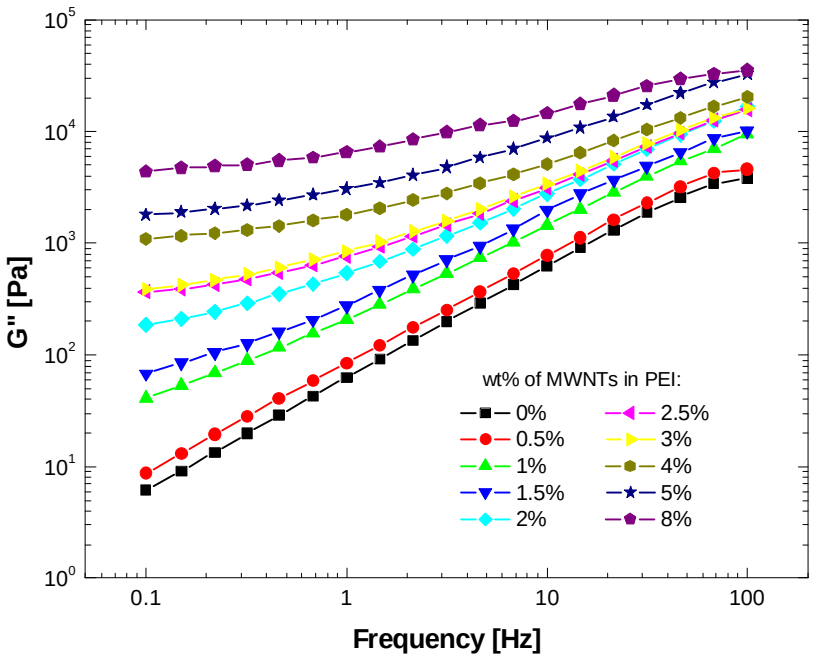

Figure 4.33 Loss modulus (*G''*) of MWNT/PEI composites versus frequency.

The neat PEI polymer (in a melt) behaves like a Newtonian liquid with the viscoelastic properties exhibiting liquid-like characteristics, described by the following functions: $G' \propto \omega^2$, $G'' \propto \omega^1$, and $\eta^* \propto \omega^0$ [168,169]. Similar behavior is observed for the low concentrations of nanotubes (e.g. 0.5 wt %), which is depicted in Figures 4.31, 4.32, and 4.33. Incorporation of MWNTs into the polymer results not only in an increase of the values of *G'*, *G''*, and η^* in the entire frequency range, but also leads to the structural transition in the composite material. The samples with higher nanotube loads exhibit a solid-like behavior, where η^*, *G'*, and *G''* satisfy the following relations: $\eta^* \propto \omega^{-1}$, $G' \propto \omega^0$, and $G'' \propto \omega^0$. Table 4.2 depicts the fitting exponents of the power law equations of $\eta^* \propto \omega^{-\beta}$, $G' \propto \omega^{\beta}$, and $G'' \propto \omega^{\gamma}$ for composites with a different weight fractions of MWNTs. The dependence of these fitting parameters on the concentration of carbon nanotubes indicates the structural changes in MWNT/polymer composites.

As mentioned above, the behavior of composites with low CNT loads corresponds to the behavior of a neat polymer (with liquid-like characteristics): the viscosity is nearly independent of the shear rate (β=0.06 for *m*=0.5 wt%) (Figure 4.31), *G'* and *G''* exhibit practically linear dependence on the frequency (α=1.1 and γ=0.93) (Figures 4.32 and 4.33). For

higher concentrations of MWNTs, η^* shows a shear thinning behavior, where the complex viscosity decreases with increasing the shear frequency (β=0.85 for m=8 wt%). The evident changes are also observed in the behavior of storage and loss moduli. While increasing MWNT loads, G' and G'' show weaker dependence on the frequency, until they become nearly independent on the shear rate at high nanotube concentrations. Again, these changes are more exposed in the low frequency region, due to the critical effect of nanotubes on a long-range polymer relaxation. Such changes in the behavior of the viscosity, storage and loss moduli are related to the structural transition of composites with MWNT inclusions, from liquid- to solid-like systems.

These results indicate that a large scale polymer relaxation in the composites is efficiently restrained by the presence of the carbon nanotubes. At low concentrations, MWNTs act as isolated objects and the viscosity and modulus are dominated by the matrix. Near and above the percolation threshold, the MWNTs form a percolated network which gives rise to a solid-like behavior of the samples – the filler determines the visco-elastic properties of the composites.

Figure 4.34 displays fitting exponents β and α as a function of the weight fraction of MWNTs. The transition point (rheological percolation threshold) can be estimated to lie in the concentration range between 0.5 to 2 wt%. Especially α (G') as a function of wt% of MWNTs demonstrates a sharp decrease at around 0.5-1 wt% MWNTs, which indicates the percolation threshold.

Table 4.2 Rheological parameters for composites with different wt% of MWNTs obtained by fitting the power law dependence to curves of Figures 4.31, 4.32, and 4.33; respectively.

	wt% of MWNTs in PEI									
	0 %	**0.5 %**	**1 %**	**1.5%**	**2 %**	**2.5%**	**3 %**	**4 %**	**5 %**	**8 %**
η^* power law dependence ($\eta^* \propto \omega^{-\beta}$) value of β	0.02	0.06	0.20	0.32	0.41	0.47	0.59	0.73	0.74	0.85
G' power law dependence ($G' \propto \omega^{\alpha}$) value of α	1.74	1.1	0.74	0.44	0.44	0.4	0.26	0.19	0.18	0.12
G'' power law dependence ($G'' \propto \omega^{\alpha}$) value of γ	0.97	0.93	0.8	0.76	0.67	0.57	0.56	0.43	0.43	0.32

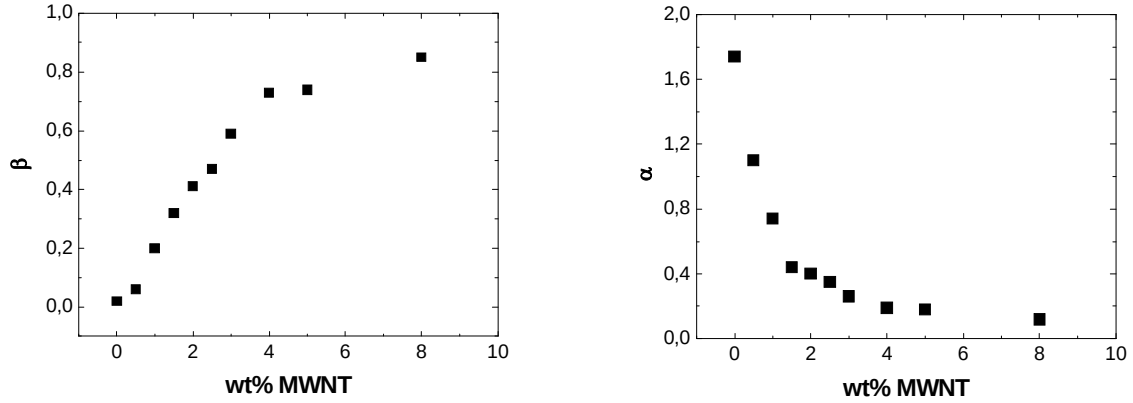

Figure 4.34 Power law exponents β and α ($\eta^* \propto \omega^{-\beta}$ and $G' \propto \omega^{\alpha}$) as a function of MWNT contents.

The rheological percolation threshold can also be roughly estimated from Figures 4.31 and 4.32. Considering the low frequency region only, drastic changes in the behavior of complex viscosity are observed between samples with 0.5 and 1 wt% of CNT loads. The same relates to *G'*.

However, to be more accurate, the power law equations (2.13) and (2.14) were used to determine the value of the rheological percolation threshold. The functions were fitted to the experimental data points of *G'* at 0.1 Hz and 1 Hz, and η^* at 0.1 Hz for $m>m_c$ (concentrations above percolation threshold). Figures 4.35 and 4.36 show the storage modulus and complex viscosity as a function of MWNT content at 1 Hz, respectively. The inset plots of Figures 4.35 and 4.36 present the log-log dependence of the η^* and *G'*, as a function of the reduced mass fraction (m-m_c), respectively.

The scaling parameters were found by incrementally varying m_c until the best linear fit to the data points was obtained (with the best achieved, optimal value of correlation coefficient *R*). The red lines represent the best fitting of the power law equations to the *G'* and η^* versus MWNT concentrations at 1Hz. The overall fitting results are presented in Table 4.3. The rheological percolation threshold (m_c) was found to be at the MWNT concentrations of 0.5 – 0.7 wt%. Scaling exponents a=2.8 and t=2.7, differ from the theoretical value of the percolating systems in three dimensions ($a=t\cong 2.0$). The rheological percolation threshold does not refer to the geometrical one (see 2.3.2.3), where the filler forms interconnected paths along the entire composite, which is considered in theoretical studies.

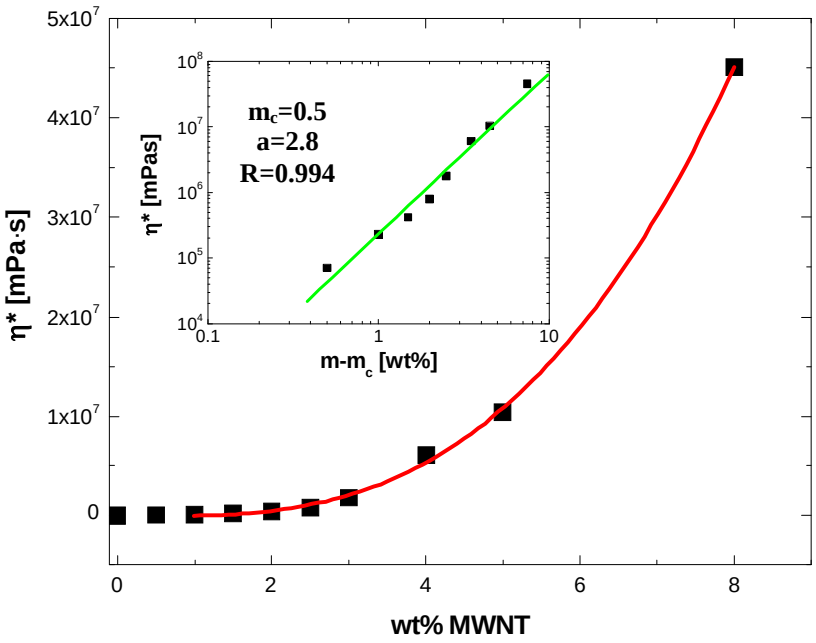

Figure 4.35 Complex viscosity as a function of MWNT contents at 0.1 Hz. Rheological percolation threshold (m_c) is obtained from fitting equation (2.13) for $m>m_c$ (red line). Inset: log-log plot of η^* as a function of the reduced mass fraction.

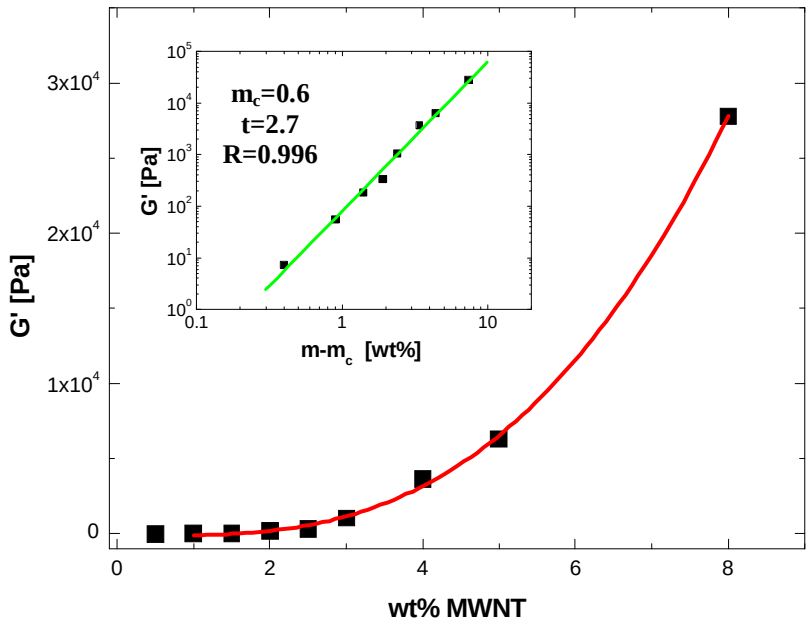

Figure 4.36 Storage modulus as a function of MWNTs content at 0.1 Hz. Rheological percolation threshold (m_c) is obtained from fitting the equation (2.14) $m>m_c$ (red line). Inset: log-log plot of G' as a function of the reduced mass fraction.

Table 4.3 Fitting results from the power law relations of viscosity and storage modulus versus MWNT loadings.

Power law relation	Percolation threshold m_c (%)	Scaling exponent
$\eta^* \propto (m\text{-}m_c)^q$ at 0.1 Hz	0.5	2.8
$G' \propto (m\text{-}m_c)^t$ at 0.1 Hz	0.6	2.7
$G' \propto (m\text{-}m_c)^t$ at 1Hz	0.7	2.9

The low rheological percolation threshold obtained in this study is attributed not only to the high aspect ratio of the CNT filler, but also to the good and homogenous dispersion of MWNTs within PEI. It confirms that our strategy for the functionalization of MWNTs results in a good exfoliation of nanotubes in a solvent and consequently in a polymer.

There are many factors that may affect the visco-elastic response of the samples, including the molecular weight of polymers, their morphology, degree of dispersion of nanotubes in the matrix, aspect ratio of the filler, alignment of CNTs (which diminishes formation of the percolated network), and temperature [169,172]. On this basis it is difficult to compare the percolation threshold found in this study (0.5 wt%) to earlier reported values of diverse materials ranging from 0.1 – 5 wt% (Table 4.1). Nevertheless, a percolation threshold at 0.5 wt% is fairly low, and opens up possibilities for the formation of a new class of polymeric composites with advanced mechanical properties at a low weight fraction of nanotubes. Further improvement of the composite fabrication techniques, together with high aspect ratio of nanotubes can permit the formation of percolated structures even at a lower load of the filler. This is a simple guideline for the modification of the polymeric structures with a modest amount of CNTs but resulting in significant changes of the properties.

4.5 Dielectric spectroscopy

Dynamic dielectric measurements can be used to characterize the electrical properties of CNT-based composites. The addition of carbon nanotubes as a conductive filler to a dielectric host (e.g. polymer) has attracted much interest due to the excellent electrical properties of CNTs and their very large aspect ratio (>1000). The use of carbon nanotubes as

filler in a polymer host opens up possibilities for the fabrication of a new class of reinforced antistatic films, electromagnetic shielding materials, and conductive polymers at very low filler content. It was reported that the effective conductivity of such composites drastically increases with increasing concentration of the carbon nanotubes [49-51,92,94,152,161,162,165,167,168,172-174,219]. The electrical percolation threshold (insulator – conductor transition) was found at very low CNT loads in the host materials. Table 4.4 shows values of electrical percolation thresholds and scaling exponents obtained by fitting the experimental data to the power law equation (2.8), presented in various studies.

Table 4.4 Electrical percolation threshold and scaling exponent of different CNT-based polymer composites obtained in various studies. PVDF - poly(vinylidene fluoride), PVA - polyvinylalcohol, PC - polycarbonate, PET - poly(ethylene terephthalate), P3OT - poly(2-othylthiophene), PMMA - poly(methyl methacrylate).

Composite	**Preparation Method**	**Electrical Percolation Threshold**	**Scaling Exponent (t)**	**Ref.**
MWNT/PVDF	Solution mixing	1.61 vol%	0.85	[50]
SWNT/epoxy	*In-situ* polymerization	0.3 wt%	1.4 - 1.8	[94]
MWNT/PVA	Solution mixing	0.055 wt%	1.36	[167]
MWNT/PC	Solution mixing	1.44 wt%	2.1	[165]
SWNT/epoxy	*In-situ* polymerization	0.074 wt%	1.3	[152]
MWNT/PET	Solution mixing	0.9 wt%	2.2	[92]
SWNT/P3OT	Solution mixing	4 wt %	2.0	[173]
SWNT/PMMA	Solution mixing	0.39 wt %	2.3	[172]
SWNT/PMMA	Solution mixing	0.17 wt%	2.2	[219]

The spectra of the complex conductivity $\sigma^*(\omega)$ and dielectric permittivity $\varepsilon^*(\omega)$ are obtained by a dielectric spectrometer which measures the impedance spectrum $Z^*(\omega)$ of a sample placed between two electrodes. The impedance is obtained from phase and amplitude sensitive measurements of current I^* and voltage U^* on the electrodes and is given by:

$$Z^* = \frac{U^*}{I^*} \tag{4.13}$$

The intrinsic electric properties are evaluated from $Z^*(\omega)$ in a given frequency range. The complex dielectric permittivity is calculated from [194]:

$$\varepsilon^* = \frac{1}{i\omega Z^*(\omega) C_0} \tag{4.14}$$

where, ε^* indicates the experimentally obtained permittivity, ω is the angular frequency, and i the imaginary unit. $C_0 \approx \varepsilon_0 A/d$ is the vacuum capacitance of the experimental setup, where A is the area of the electrode plates, d is the distance between the electrodes, and ε_0=8.85x10^{-12} As/Vm is the permittivity in vacuum. The complex conductivity is related to the complex dielectric permittivity by:

$$\sigma^* = i\omega\varepsilon_0\varepsilon^* \tag{4.15}$$

where, σ^* denotes the complex conductivity.

In this study, dynamic dielectric measurements have been performed in a frequency range of 1 MHz – 1.8 GHz. Figure 4.37 shows the real part of the dielectric permittivity as a function of frequency for MWNT/PDDA composites with different carbon nanotube contents. In general, ε' increases with an increase of MWNT loads in the entire frequency range. However, this increase is more pronounced at lower frequencies. The real part of the dielectric permittivity of the 8 wt% composite is two orders of magnitude higher than that of neat polymer at 1 MHz; and ε' changes by a factor of 10 at 1 GHz . The increase of ε' is related to the formation of mini-capacitors in composites, which gives rise to polarization.

Neat polymers display behavior of ε' being nearly independent of frequency (which relates to the behavior of dielectric materials). A similar trend is observed for samples with low MWNT concentrations (e.g. 0.5 wt%). When the MWNT content increases the behavior of ε' changes following the frequency dependent relation $\varepsilon' \propto \omega^{-u}$ (where u is a fitting parameter), which denotes the decreasing trend of ε' as the frequency increases. Table 4.5 shows the values of the scaling exponent u. The imaginary dielectric permittivity ε'' as a function of frequency (Figure 4.38), exhibits similar dependence on the concentration of CNTs in the nanocomposite. However, above a concentration of 2 wt%, ε'' shows a much higher increase of the values than the real permittivity ε'. At 1 MHz the imaginary permit-

tivity is four orders of magnitude higher as the nanotube concentration increases from 0 to 8 wt%; at 1.8 GHz it changes by a factor of 100. In general, the dielectric constant has been reported to dramatically increase with higher loading of CNTs above the percolation threshold, but at the expense of rapidly increasing dielectric loss (ε'') [161,162,165]. The large increase of dielectric loss above the percolation threshold is directly related to the DC conductivity $\sigma_{DC}=\omega\varepsilon''$ that appears in the percolated network at frequencies below the critical point at which the conductivity changes its behavior from frequency dependent to independent (where σ^* comes into a plateau region - Figure 4.39). Therefore, above the percolation threshold, when conductive paths are formed, ε'' increases rapidly, because the DC conductivity becomes dominant in electrical response of the samples.

These results emphasize one important issue: the fabrication of composites with a high dielectric constant but with low losses can be achieved by efficient separation of the individual conductive particles in a polymer matrix. Thus, DC conductivity can be preserved, which diminishes its contribution to the increase of the imaginary part of the dielectric constant. Well separated conductive inclusions act as capacitors, giving rise to higher values of ε'.

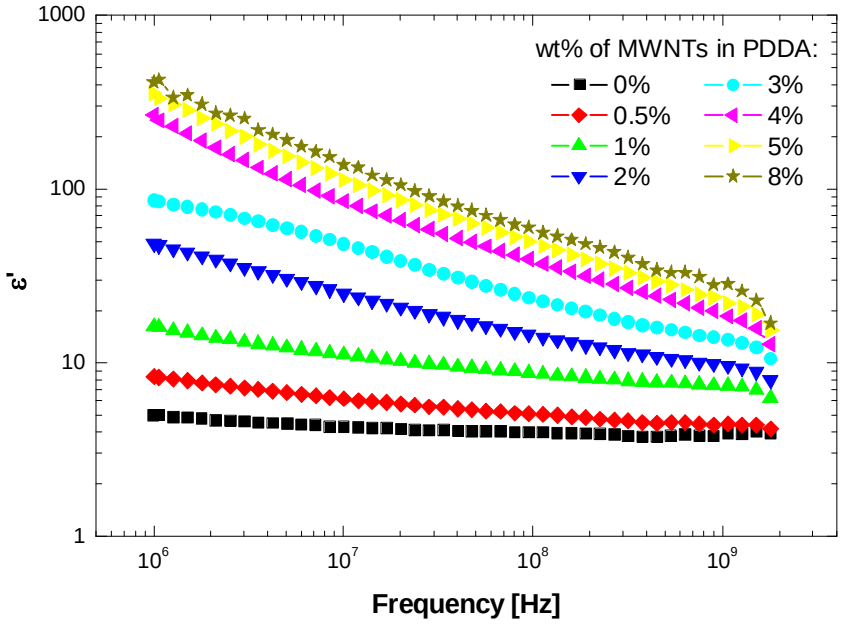

Figure 4.37 Real permittivity (ε') of MWNT/PDDA composites versus frequency.

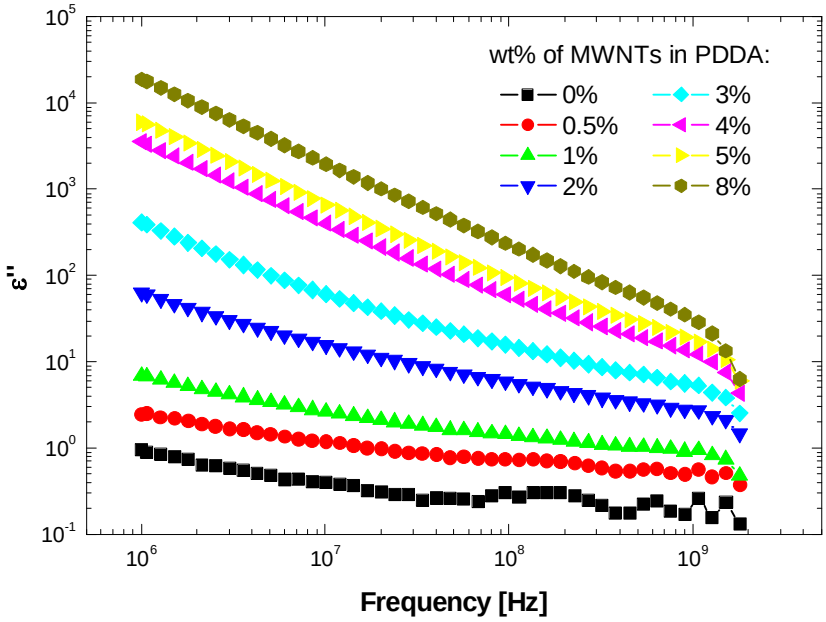

Figure 4.38 Imaginary permittivity (*ε''*) of MWNT/PDDA composites versus frequency.

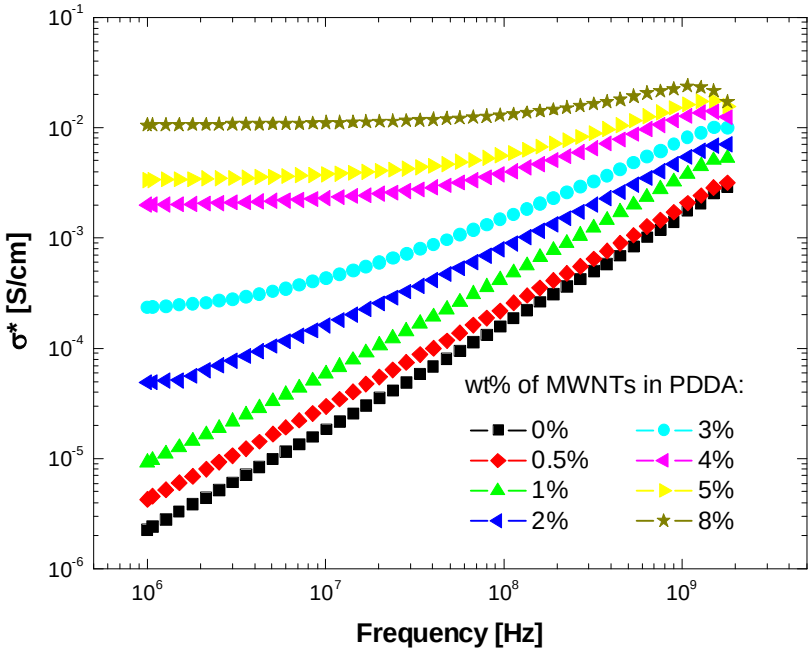

Figure 4.39 Complex conductivity (*σ**) of MWNT/PDDA composites versus frequency.

Table 4.5 Fitting parameters *s* and *u* for composites with different wt% of MWNTs.

	wt% of MWNTs in PDDA					
	0 %	**1 %**	**2 %**	**3 %**	**4 %**	**5 %**
σ^* power law dependence ($\sigma^* \propto \omega^s$) value of *s*	0.95	0.86	0.73	0.64	0.54	0.48
ε' power law dependence ($\varepsilon' \propto \omega^{-u}$) value of *u*	0.03	0.15	0.28	0.31	0.47	0.50

Figure 4.40 shows dielectric measurements of MWNT@SiO_2/PMMA-f (see 3.1.2.2). Upper and lower curves correspond to the real and imaginary parts of the dielectric constant, respectively. The red line is obtained using equation (2.7) with the following parameters: γ/ω_p=0.5, x_{min}=2x$10^{-7}\omega_p^2$, x_{max}=0.1ω_p^2, p=0.01.

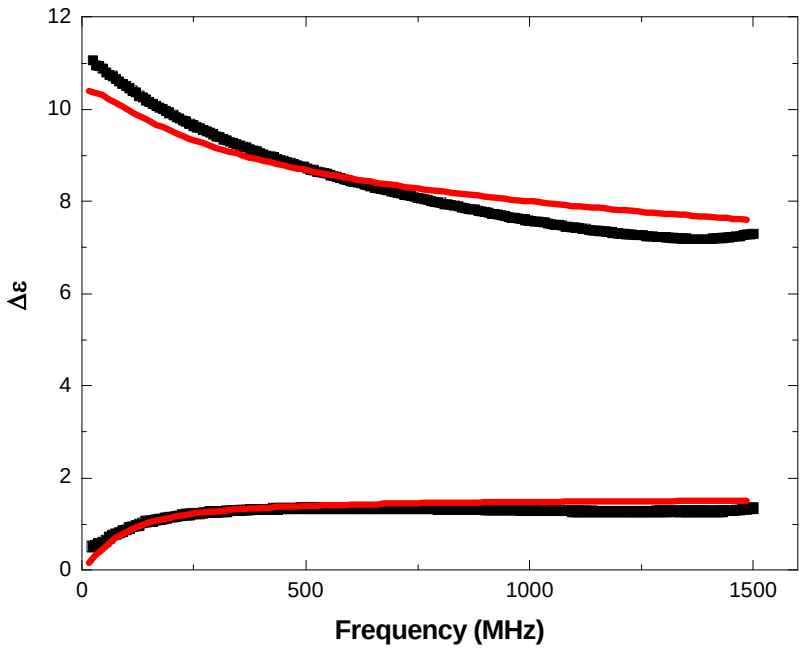

Figure 4.40 The frequency dependence of complex permittivity is shown. Theory (red lines) and dielectric experimental data (black lines) of MWNT@SiO_2/PMMA-f composite. Upper and lower curves correspond to the real and imaginary permittivity, respectively.

The silica shell on the surface of MWNTs efficiently prevents charge transport between nanotubes leading to an enhancement of the dielectric function due to the increase of polarization (ε'). It is difficult to compare these results with that of MWNT/PDDA due to the diverse morphologies, different polymers, and preparation methods employed for fabrication of these composites. But one important difference in the behavior of the imaginary permittivity is found (compare with Figure 4.38): ε'' increases with decreasing the frequency in MWNT/PDDA composites (Figure 4.38), in MWNT@SiO_2/PMMA-f sample ε'' decreases with decreasing frequency and converges to zero (Figure 4.40). Theory [163] predicts such behavior of dielectric composites only for well separated (e.g. electrically isolated) metallic inclusions. Figure 4.40 shows a good fit of the theoretical and experimental data points.

The behavior of ε'' of the MWNT/PDDA composites follows the experimental results shown by Grimmes et al. [161,162] which were well fitted to the theoretical functions proposed by Lagarkov et al. [155,160]. The differences in the behavior of ε'' are explained by the charge flow (DC conductivity) between adjacent nanotubes. Carbon nanotubes in polymers form some bundles or interconnected structures even at low concentrations which give rise to electron flow between them, and therefore, to high values of ε'' (dielectric loss), especially at low frequencies. In the case of MWNT@SiO_2, the silica shell efficiently prevents charge transfer between nanotubes, which diminishes the dielectric loss and enhances the polarization of capacitor inclusions. Hence, at frequencies converging to zero, the dielectric loss is predicted to approach zero, too.

Figure 4.39 shows the frequency dependence of the complex conductivity of PDDA composites with different MWNT contents. For lower concentrations (<1 wt%) the conductivity is frequency dependent: it increases linearly with increasing frequency which corresponds to the behavior of the neat polymer. The curves present typical $\sigma^* \propto \omega^s$ dependence with a scaling exponent approaching 1 (Table 4.5), which is the expected behavior for insulating materials. In the vicinity and above the percolation threshold the conductivity becomes frequency independent but only below a critical frequency. The frequency independent region of the curve (plateau) is characteristic for conductive materials where σ* relates to the DC conductivity. Such a phenomenon confirms the insulator-conductor transition at the critical concentration of conductive filler – the electrical percolation threshold. Above the percolation threshold the electrical properties of composites are dominated by the percolating paths of the conductive MWNTs. Table 4.5 shows the values of scaling exponents obtained using the frequency relation of σ* and ε' ($\sigma^* \propto \omega^s$ and $\varepsilon' \propto \omega^{-u}$). Critical

exponents should satisfy the relation $s+u=1$ [50,157,174]. This condition is fullfilled in this study (Table 4.5). Figure 4.39 shows that the conductivity increases significantly with increasing MWNT contents in composites. In particular at low frequency, the conductivity of a 8 wt% composite increased by 4 orders of magnitude in relation to the neat PDDA.

In order to get a more accurate estimation of the electrical percolation threshold, the power law equation (2.12) was fitted to experimental data points (Figure 4.41). The percolation power law refers to the low frequency AC conductivity (where $\omega \rightarrow 0$) at concentrations above the percolation threshold. This conductivity was extrapolated from the frequency independent region (plateau) of $\sigma^*(\omega)$ (Figure 4.39). As mentioned before, these values relate to the DC conductivity.

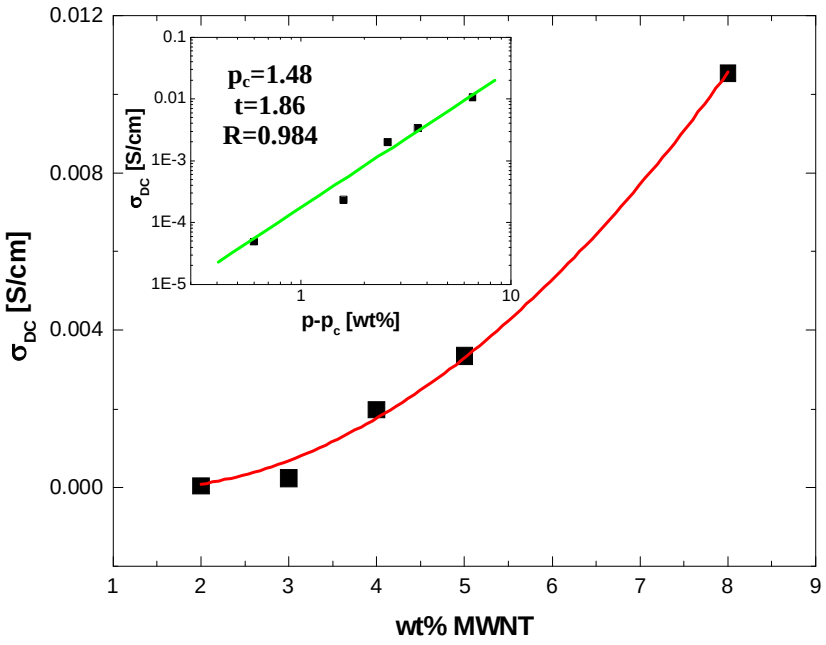

Figure 4.41 Direct current conductivity (σ_{DC}) as a function of MWNT content. Electrical percolation threshold (p_c) is obtained from fitting the equation (2.12) for $p>p_c$ (red line). Inset: log-log plot of σ_{DC} as a function of the reduced mass fraction.

The value of the fitting exponent t (equation (2.12)) was estimated from the slope of the linear relation of σ_{DC} and p-p_c on the log-log scale (inset of Figure 4.41). The scaling parameters were found by incrementally varying p_c until the best linear fit to the data points was obtained (with the optimal value for the correlation coefficient R). The fitting line is plotted as a red solid line. The electrical percolation threshold occurs at 1.48 wt%

MWNTs with a scaling exponent of t=1.86 which is close to the theoretical prediction of this value in 3D percolated system ($t \cong 2$). Theoretical predictions of the scaling exponents refer to these systems, where particles of the filler are in physical contact and form geometrical percolated networks. In insulator-conductor composites clusters of CNTs are separated from each other by thin layers of insulating polymers (electrons transport along the conductive paths occurs through tunneling) [157,165,167]. Therefore, the estimated values of t may significantly differ from the theoretical ones. Similar observations were reported in previous studies (Table 4.4).

According to the percolation theory, σ_0 (equation (2.12)) should approach the conductivity of the filler (in this case MWNTs) above the percolation threshold. Here σ_0 was found to be 3.9 mS/cm which is much lower than the corresponding conductivity of MWNTs (~100 S/cm). This difference is caused by the contact resistance between MWNTs or clusters of MWNTs in the composite, which decreases the effective conductivity between MWNTs. As mentioned, carbon nanotubes or their bundles are coated with an insulating polymer layer which results in poor electrical contact between the conductive species. The conduction of electrons in MWNT/PDDA composites is explained by quantum tunneling in which the barrier height decreases with temperature (equation (2.9)) [49].

The relatively low value of the electrical percolation threshold (p_c=1.48 wt%) is attributed to the high aspect ratio of MWNTs and the uniform distribution of well exfoliated nanotubes within the PDDA matrix. The experimental values of the electrical percolation threshold have been shown by different groups to vary between 0.05 – 4 wt% (Table 4.4). These fairly large differences relate to the degree of CNTs' dispersions in polymer, aspect ratio of the filler, polymer properties [29], and temperature [94].

It was found that the rheological percolation threshold m_c=0.6 wt% is significantly lower than the electrical percolation threshold p_c=1.48 wt%. This is consistent with earlier mentioned expectations (see 2.3.2.3). Briefly: to reach the electrical percolation threshold and therefore be electrically conductive, nanocomposites need filler particles to be in close vicinity of each other (up to 5 nm), so that the charge flow is possible (e.g. by tunneling). The rheological percolation refers to systems of interconnected polymer chains and carbon nanotubes. Therefore, nanotubes can just be linked by random coils of polymer chains (with distances between CNTs even more than 10 nm) to form the rheological percolating network (Figure 2.3). Thus, the CNT-CNT distance required for the rheological percolation

threshold is longer than that for the electrical percolation threshold. Namely, a lower weight fraction of nanotubes can already restrict the polymer motion in contrast to the higher weight fraction that is required to form a conductive network throughout the matrix. In general, polymer chain immobility and the distance between neighboring nanotubes determine the rheological and electrical percolation threshold, respectively.

In this study, different samples were used for dielectric and rheometric measurements, due to the experimental apparatus limitations, CNT-COOH/PDDA and CNT-COOH/PEI, respectively. This is an additional factor that may affect the final values of percolation thresholds and makes comparisons difficult. Nevertheless, the theoretically predicted trend of $m_c<p_c$ is satisfied here.

The results of this study confirm that the percolation theory well describes the electrical response of the nanocomposites. The critical concentration of the metallic filler at which the conductive path is formed in the polymer, causing the insulator-conductor transition, is shown to be at 1.48 wt%. This indicates a broad range of possible applications of polymeric composites with low loads of nanotubes as antistatic coatings, EMI shields, and conductive structures.

The fabrication of composites with a high dielectric constant but with low losses can be achieved by efficient separation of the individual conductive particles in a polymer matrix. This is shown by efficient coating of the conductive carbon nanotubes with insulating silica shell, which prevents the charge flow (DC conductivity) between filler particles within the polymer matrices.

4.6 Optical properties of the CNT/QD composites

The formation of CNT/nanoparticle heterostructures is of both fundamental and technological interest. Combining the unique properties of CNTs and nanoparticles a new class of the nanocomposites can be made meeting a broad range of advanced applications. In this study, a novel approach for fabrication of the heterostructures of carbon nanotubes and semi-conductive nanocrystals has been shown. In particular, optical properties of systems composed of MWNTs and quantum dots have been determined.

A novel class of MWNT/QDs and MWNT@SiO_2/QDs heterostructures (see 3.1.2.3 and 4.1.4) has been characterized in terms of their optical properties using UV-vis and PL spectroscopy. Figure 4.42 illustrates the UV-vis absorption of MWNTs, and

MWNT@SiO_2 before and after coupling reaction with CdSe-CdS quantum dots. The absorption spectrum of the CdSe-CdS quantum dots is also shown for reference. As expected, the MWNTs and MWNT@SiO_2 give featureless absorption spectra, with a higher degree of scattering in the MWNT@SiO_2 sample arising from the silica shell. Due to the light scattering of MWNTs and silica, and the low concentration of NCs, the characteristic UV-vis signal of the QDs cannot fully be resolved. Even so, the spectra of MWNT@SiO_2/QD and MWNT/QD do exhibit weak features directly corresponding to the absorption edge of CdSe-CdS QDs at around 600 nm. This is consistent with other reports, in which is shown that UV-vis spectra of CNT/QD systems do not display any extra features that would arise from charge diffusion or electronic interaction between the CNTs and QDs in their ground state [131,132,142]. Only selected results obtained from nanocomposites containing CdSe-CdS quantum dots are shown in Figure 4.42. In spite of this, consistent results were achieved for all CNT/QD heterostructures fabricated in this study (specifically MWNTs and MWNT@SiO_2 with ZnO, CdSe, CdSe-ZnS).

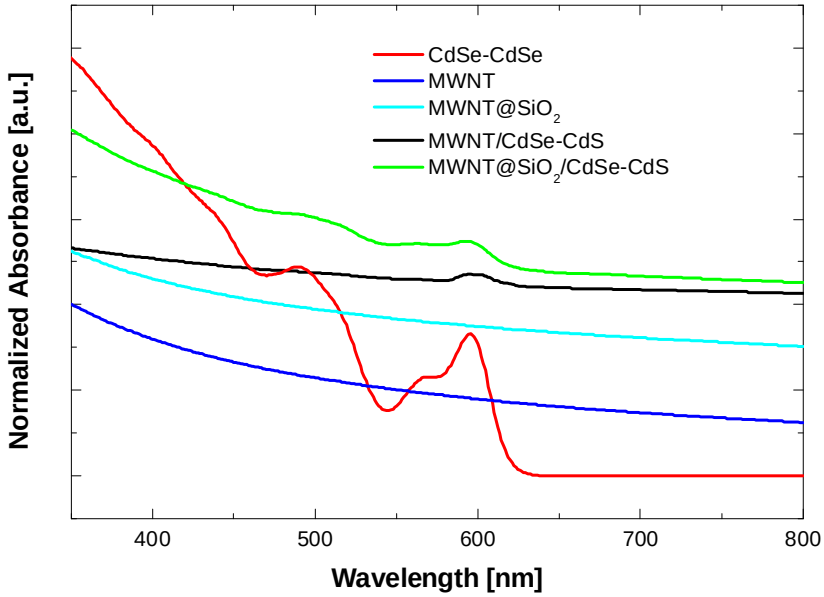

Figure 4.42 UV-Vis absorption spectrum of CdSe-CdS, MWNT, MWNT@SiO_2, MWNT/CdSe-CdS, and MWNT@SiO_2/CdS-CdSe.

Recently, it has been reported, that carbon nanotubes can act as electron-acceptors in their photo-excited state, wherein charge and energy transfer between conjugated species and CNTs may occur [135,220-223]. Given the work function of MWNTs is estimated to

be in the range of 4.4 - 5.1 eV [224,225] and the Fermi level lies in the HOMO-LUMO gap of the CdSe nanoparticles, MWNTs are capable of efficient electron scavenging (Figure 4.43). Figure 4.44 represents PL spectra of CdSe (red line), MWNT/CdSe (blue line), MWNTs (green line), and MWNT@SiO_2/CdSe (black line). The characteristic luminescence peak for CdSe particles with an average size of 4.2 nm is located at 591 nm. It is observed that the PL band from the QDs disappears after conjugation to MWNTs. There are two possible explanations for this quenching: charge transfer or non-radiative energy transfer from the photo-excited semiconducting particles to the carbon nanotubes.

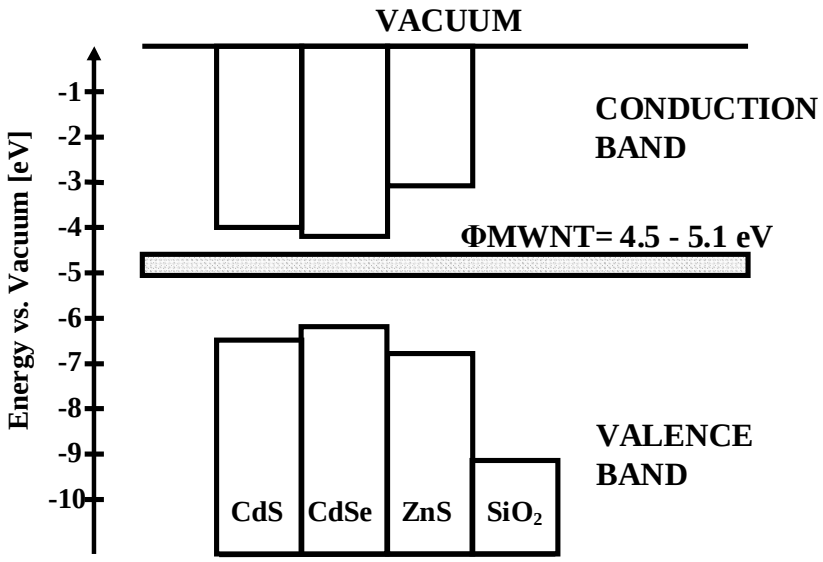

Figure 4.43 Schematic energetic band positions for MWNTs, SiO_2, CdSe, CdS, and ZnS [226,227].

In contrast, the PL spectrum of MWNT@SiO_2/CdSe nanocomposites still displays the QD emission peak at 591 nm. As we used similar concentrations of MWNTs and MWNT@SiO_2 with the same amount of CdSe nanocrystals in each sample, the results shown in Figure 4.44 clearly demonstrate that the quenching of the QDs emission is suppressed by the presence of the insulating silica shell on MWNTs. The large band gap and thickness of the SiO_2 layer rule out both charge transfer and electron tunneling as possible quenching mechanisms, further supporting our supposition that quenching may be a result of electron injection into the MWNTs. Moreover, the observed quenching does not relate to interactions of QDs with ligand functionalities that covalently link the QDs to the

MWNTs as amine functional groups were used as the coupling agent in both cases. Secondly, amine ligands are commonly used for passivation of surface-defects (electron traps) of CdSe nanocrystals and do not introduce trapping energy levels into the band gap of these quantum dots [180].

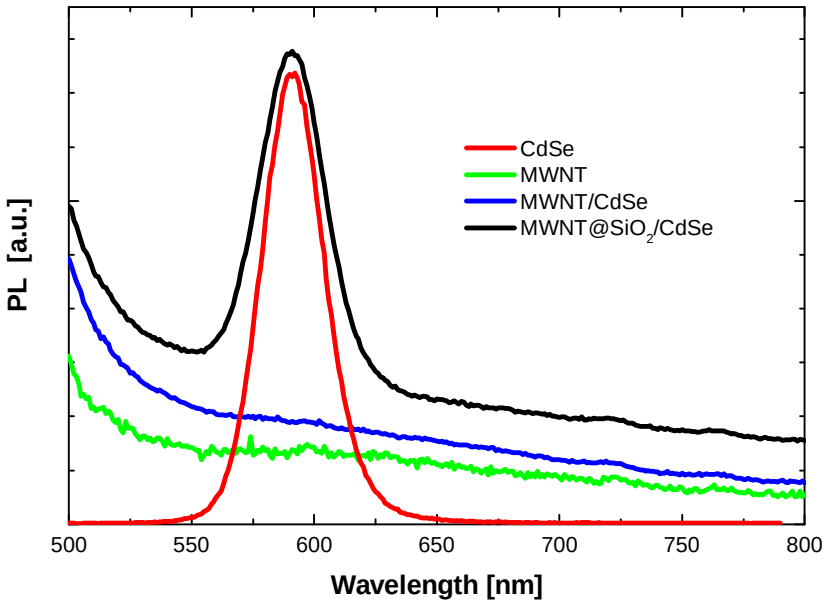

Figure 4.44 PL spectra of CNT/QD and CNT@SiO_2/QD heterostructures at λ_{ex}=440 nm: CdSe (red line), MWNT (green line), MWNT/CdSe (blue line), and MWNT@SiO_2/CdSe (black line).

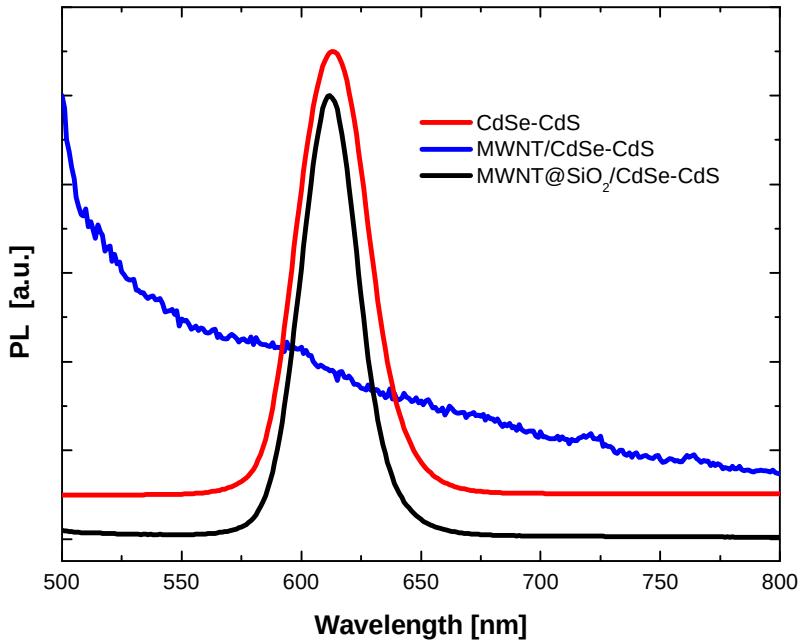

Figure 4.45 PL spectra of CNT/QD and CNT@SiO_2/QD heterostructures at λ_{ex}=440 nm: CdSe-CdS (red line), MWNT/CdSe-CdS (blue line) and MWNT@SiO_2/CdSe-CdS (black line).

In principle, the overcoating of one semiconductor with another of a wider band gap should completely confine the charge carriers to the core. Interestingly, luminescence quenching is also observed from the CdS overcoated particles (Figure 4.45). However, the conduction band offsets between CdSe and CdS are small (~ 0.32 eV), and as such the lighter, the more mobile electron may tunnel through the shell [228]. Given that MWNTs are appropriate acceptors, the electron may be scavenged by the MWNTs resulting in non-radiative decay or even permanent oxidation. Furthermore, the lattice mismatch between CdSe and CdS, although relatively small (~3.9 %), will inevitably result in dislocations and other defects, which will aid carrier diffusion from the core to the surface of the QDs [229]. Therefore, charge carriers are not fully confined in the core of core-shell particles, due to the relatively small band gap offset and lattice mismatch of the crystals. This enables electrons to be trapped by the carbon nanotubes. Overcoating the MWNTs with silica is again seen to prevent quenching.

The above suppositions were additionally confirmed by further observations of MWNT/QDs heterostructures. It turned out that after long light exposition of the composites, the size of the nanoparticles tends to decrease (some blue-shift of PL peak appeared, which refers to the size decrease). This is explained by a photo-catalytic redox reaction. Interactions between MWNTs and QDs involve charge transfer of photo-excited electrons from the conductive band of the donor (QDs) to the empty electronic states of the acceptor (MWNTs) resulting in non-radiative decay of the QD excited state. This phenomenon supports further oxidation and consequently decomposition of the nanocrystals. Earlier investigations on semiconductor-metal composites have revealed that interactions between these components enhance the efficiency of photo-catalytic redox process [230,231]. Electron transfer between photo-excited semiconductor and metal was shown to play an important role in photo-catalysis. In the case of MWNT@SiO_2/QD system, some very slow changes (decomposition) were also observed but at the same level as for neat QDs.

All of this supports the supposition that quenching most likely occurs by an electron transfer between QDs and MWNTs. A similar effect has been reported recently: complete quenching of QDs' emission has been shown for CNT/QD hybrids, where carbon nanotubes acted as an electron acceptor of excited semiconductors [119,232].

Figure 4.43 shows the work function of MWNTs (4.5 – 5.0 eV) that lies in the HOMO-LUMO gap of semiconductor nanocrystals. Charge transfer from the QD conduction band to MWNT conduction band is therefore energetically favorable.

In summary, a new approach for the preparation of MWNT/NCs heterostructures with a highly defined morphology is shown. QDs on bare MWNT were found to exhibit no luminescence, while the MWNT@SiO_2QD composites retained their luminescence. The ability to allow or prevent charge transfer from photo-excited QDs to CNT opens up promising possibilities for applications in photoelectric and optical devices, biological sensors, and catalytic materials.

CHAPTER V

SUMMARY

In the frame of this thesis, insights into the fundamental problems in the fabrication of CNT-based composites are presented. We have introduced novel approaches and solutions for effective exfoliation and uniform dispersion of carbon nanotubes in solvents and polymers, which are crucial for a further commercial exploitation of these unique materials. It is shown that carbon nanotubes as components of nanocomposites have a significant effect on the mechanical, electrical, and optical properties of these hybrid materials. The results presented here indicate the potential of utilizing CNT-based nanocomposites for mechanical, electrical, sensing, optical, and actuating applications.

The effective utilization of CNTs in composite applications strongly depends on the ability to homogeneously disperse them throughout the matrix. Therefore, various surface functionalization strategies were employed in order to overcome the poor solubility of CNTs in solvents and polymers.

Different polyelectrolytes (in particular poly(allylamine hydrochloride)) were non-covalently adsorbed on the MWNTs' surface in this study. In a fairly simple process high stability, good exfoliation, and dispersion of CNT in both organic and aqueous solvents were achieved. This is advantageous over other reported methods [16], which mainly require complex chemical treatment, resulting in dispersion in only organic or aqueous solvent.

Multiwall carbon nanotubes were covalently functionalized by commonly used oxidation methods and further modification of oxidized nanotubes. These strategies resulted in a good dispersion of the nanotubes in various solvents.

Furthermore, a novel and simple strategy for a covalent silica coating of carbon nanotubes was introduced. Structural investigations revealed that every individual carbon nanotube has been uniformly coated with an insulating layer of silicon dioxide. This efficient technique is adaptable to a large-scale production of MWNT@SiO_2 hybrid structures. Fur-

ther functionalization of silica coated nanotubes with 3APTMS and PhTMS resulted in good and stable dispersions in aqueous and organic solvents, respectively.

It could be shown that non-covalent functionalization techniques, in contrast to covalent ones, are non-invasive and do not introduce additional defects to the structure of the nanotubes.

In order to satisfy the technological demand for lightweight, reinforced, and conductive polymers, CNTs were employed as a filling component of composites produced by different approaches.

For the first time, we report the fabrication of high strength, lightweight composites with multiwall carbon nanotubes by means of the layer-by-layer assembly technique. The films consist of subsequent layers of polyelectrolytes and carbon nanotubes with a strong interfacial bonding between the structural components, mediated by electrostatic attraction, van der Waals adhesion, mechanical interlocking, and chemical bonding. This method assures high concentrations and uniform distributions of nanotubes within a polymer matrix. Moreover, an alternating adsorption of monolayers of components reduces the phase segregation and makes these composites highly homogeneous, with the nanotubes and polymers being well interwoven and interpenetrated. Various polyelectrolytes and MWNT morphologies were used in the fabrication of LBL films.

A solution-mixing procedure was also used to form diverse MWNT/polymer and MWNT@SiO_2/polymer nanocomposites with concentrations of nanotubes ranging from 0 to 8 wt%. Structural investigations revealed a high homogeneity of these composite materials.

Combining the unique properties of both CNTs and nanoparticles enables a new class of nanocomposites to be developed, meeting the requirements for a broad range of advanced applications. In this context, we have developed a novel strategy for the fabrication of MWNT/nanocrystal and MWNT@SiO_2/nanocrystal heterostructures with a highly defined morphology. In a fairly simple process, straight coupling of nanocrystals to both silica coated and PAH-functionalized nanotubes was performed in organic and aqueous solvents. As a result, every individual nanotube was uniformly coated with nanocrystals, independent of size, charge, or surface properties (e.g. hydrophilic or hydrophobic); this is advantageous over other reported techniques for decoration of nanotubes with nanocrystals [123,142,186,187]. The formation of CNT/NC composites occurred through the covalent

attachment of nanocrystals to amine functionalities of PAH modified carbon nanotubes. Our step-by-step process offers the flexibility to tailor the nanocrystals prior to the conjugation.

The mechanical properties of the LBL assembled nanocomposites with “hollow” and “bamboo” MWNTs were investigated in tensile tests. Experimental data show that these composites are strong hybrid films with mechanical properties significantly exceeding many carbon nanotube composites made by solution-mixing, melt-mixing, or in-situ polymerization. LBL films with “bamboo” type carbon nanotubes display an ultimate tensile strength of 160 ± 35 MPa (which is 20 times more than LBL of only polymers) and a Young’s modulus of 5.5 ± 0.8 GPa as compared to 110 ± 30 MPa and 2.7 ± 0.7 GPa of films made from common “hollow” MWNTs. This is greater than the tensile strength and Young’s modulus of strong industrial plastics, which are 5 - 60 MPa and below 2 GPa, respectively. Our results indicate that the morphology of the nanotubes can substantially improve interfacial bonds between components, improving the ultimate strength of the composites. The “bamboo” morphology provides structural anchors; this enhances the mechanical bonds between the MWNTs and the polymer and reduces the pull-out of the nanotubes from the polymer matrix.

The stretching results of LBL multilayer films with oxidized “hollow” MWNTs show a drastic decrease in the strength of the composites. The tensile strength and Young’s modulus are 40 ± 15 MPa and 1.1 ± 0.3 GPa, respectively. This indicates that oxidation and any further covalent functionalization of carbon nanotubes apparently reduces their mechanical performance due to the disruption of some aromatic bonds of the CNTs in the oxidation process.

Nanoindentation experiments were carried out on different MWNT/polymer nanocomposites, including LBL assemblies and solution-mixed structures. The data reveal that the presence of MWNTs within the polymeric systems does not significantly affect the mechanical response of the composites, even at high concentrations of the MWNTs in LBL assemblies. In general, hardnesses and elastic moduli were found to reflect the mechanical properties of the surrounding matrix, emphasizing a modest influence of the nanotube filler on the mechanical performance of the hybrid materials, due to the flexibility and curvy morphology of the MWNTs. This supposition was confirmed when MWNT@SiO_2 were employed as reinforcement fillers. The average Young’s modulus for 4 wt% samples was

found to be approximately three times as high as that for the neat polymer. For the same CNT concentration, the average hardness increased about two times in comparison to the neat polymer. A silica shell on the surface of the MWNTs changes their bending performance, consequently affecting the mechanical properties of their composites.

CNTs have an extraordinary axial strength that plays an important role in the tensile reinforcement action of the composites; however due to their curvy morphology and flexibility, carbon nanotubes have a modest impact on the hardness of the polymeric systems. A silica coating of the MWNTs offers new possibilities for the formation of reinforced heterostructures with high strength and hardness.

The visco-elastic properties of MWNT/polyethylenimine composites with MWNT concentrations ranging from 0 to 8 wt%, were examined by means of the shear oscillatory tests. The complex viscosity increased as the concentration of the nanotubes increased, which was, in turn, accompanied by an increase in elastic properties, represented by the storage modulus *G'*. This indicates that the polymer mobility is restrained by the presence of carbon nanotubes in polymeric matrices.

Systems composed of two different components experience property transitions above a certain weight fraction of the filler known as the percolation threshold. With the increase of the MWNT load in the composites, the complex viscosity becomes frequency dependent and the dynamic moduli curves approach a plateau (which is more pronounced at low frequencies). These changes are related to the structural transition (from liquid-like to solid-like behaviour) of polymeric melts, indicating the formation of a percolated network of the filler within the nanocomposites. A rheological percolation threshold m_c at 0.5 wt% of MWNT contents were obtained. This low value of m_c relates to a high aspect ratio of the nanotubes and a homogeneous dispersion of the MWNTs within the polymer matrix.

Our results imply a simple guideline for the modification of the polymeric structures with a modest amount of CNTs, but resulting in significant changes of the visco-elastic properties.

The addition of carbon nanotubes as a conductive filler to a dielectric host (e.g. polymer) has attracted much interest due to the excellent electrical properties of CNTs and their very large aspect ratio (>1000). This opens up possibilities for the fabrication of a new class of reinforced antistatic films, electromagnetic shielding materials, and conductive polymers at very low filler contents. In this context, the dependence of the dielectric prop-

erties of MWNT/PDDA composites on frequency and different volume fraction of the MWNTs were studied. The presence of MWNTs in the polymer significantly affects the permittivity and conductivity spectra; a great increase of the complex conductivity and dielectric constant as the MWNTs' concentration increased is shown. The complex conductivity at 10^{-2} S/cm of composites with 8 wt% MWNTs content was found to be approximately four orders of magnitude higher than that for the neat polymer (the electrical conductivities of the intrinsically conducting-polymer systems can reach values up to 10^4 S/cm, however in many cases the application of these polymers is limited due to the poor chemical stability, sensitivity to corrosive media, and conductivity variations. Conductivity of composites composed of polymers and other metallic inclusions (carbon black, metal powder) can reach high values; however, at high concentrations causing the mechanical properties of such heterostructures to degrade [233-235]).

The critical concentration of the metallic filler at which the conductive path is formed in the polymer, causing the insulator-conductor transition, was estimated to be at 1.48 wt%. This is significantly higher than the rheological percolation threshold of 0.5 wt%. To reach the electrical percolation thresholds and therefore be electrically conductive, nanocomposites need filler particles to be in close vicinity of each other, so that a charge flow is possible (e.g. by tunneling, hopping). The rheological percolation network refers to systems of interconnected polymer chains and carbon nanotubes, where nanotubes are linked by random coils of polymer chains. The CNT-CNT distance required for the rheological percolation threshold is therefore longer than that for the electrical percolation threshold. Thus, a lower weight fraction of nanotubes can already restrict the polymer motion in contrast to the higher weight fraction that is required to form a conductive network throughout the matrix.

Results of this work indicate possible applications of polymeric composites with low loads of conductive nanotubes as antistatic coatings, EMI shields, and conductive polymeric systems.

The fabrication of composites with a high dielectric constant but with low losses can be achieved by efficient separation of the individual conductive particles in a host material. Silica coating of the CNTs forms insulating shells that prevent the charge flow between filler particles in the polymers. It is shown that a super-dielectric can be made in this way, which can have a very large, low frequency dielectric constant, and low dielectric loss.

Finally, we presented a new approach for the preparation of MWNT/QDs heterostructures with highly defined morphologies. The structural and optical properties of these composites were characterized by electron microscopy and photoluminescence spectroscopy. A complete quenching of PL bands in both, QD core and core/shell heterostructures was observed after adsorption to the CNTs, presumably through an electron transfer between QDs and MWNTs. The deposition of a silica shell (with thicknesses >20nm) around the CNTs preserves the fluorescence properties by insulating the QD from the surface of the CNT.

Our results provide evidence that the MWNTs can be efficiently applied for the fabrication of reinforced and conductive polymer composites for biomedical, space, and structural units as well as for electronic components with high strength requirements. Moreover, the ability to allow or prevent a charge transfer from photo-excited QDs to CNTs opens up promising possibilities for applications in photoelectric and optical devices, biological sensors and catalytic materials.

The acquired knowledge can be useful for a further optimization of the CNT nanocomposite materials and towards their practical applications. Outstanding steps in the development of this research should entail comprehensive studies on dispersion techniques of CNTs with different morphologies, optimized large-scale production of CNT/polymer composites and process automatization. In order to achieve a better understanding as well as better characteristics of different nanocomposites with MWNTs and MWNT@SiO_2 components, further mechanical, electrical, and optical measurements are required.

REFERENCES

[1] Ajayan, P. M.; Braun, P. V.; Schadler, L. S.; "Nanocomposite science and technology"; Wiley-VCH: Weinheim, **(2003)**.

[2] Glushanin, S.; Topolov, V. Y.; Krivoruchko, A. V.; "Features of piezoelectric properties of 0-3 PbTiO3-type ceramic/polymer composites", *Materials Chemistry and Physics* 97 (2-3), 357-364, **(2006)**.

[3] Hine, P.; Broome, V.; Ward, I.; "The incorporation of carbon nanofibres to enhance the properties of self reinforced, single polymer composites", *Polymer* 46 (24), 10936-10944, **(2005)**.

[4] Cioffi, N.; Torsi, L.; Ditaranto, N.; Tantillo, G.; Ghibelli, L.; Sabbatini, L.; Bleve-Zacheo, T.; D'Alessio, M.; Zambonin, P. G.; Traversa, E.; "Copper nanoparticle/polymer composites with antifungal and bacteriostatic properties", *Chemistry of Materials* 17 (21), 5255-5262, **(2005)**.

[5] Pelaiz-Barranco, A.; Marin-Franch, P.; "Piezo-, pyro-, ferro-, and dielectric properties of ceramic/polymer composites obtained from two modifications of lead titanate", *Journal of Applied Physics* 97 (3) **(2005)**.

[6] Huang, Z. M.; Zhang, Y. Z.; Kotaki, M.; Ramakrishna, S.; "A review on polymer nanofibers by electrospinning and their applications in nanocomposites", *Composites Science and Technology* 63 (15), 2223-2253, **(2003)**.

[7] Jordan, J.; Jacob, K. I.; Tannenbaum, R.; Sharaf, M. A.; Jasiuk, I.; "Experimental trends in polymer nanocomposites - a review", *Materials Science and Engineering A-Structural Materials Properties Microstructure and Processing* 393 (1-2), 1-11, **(2005)**.

[8] Gerard, J. F.; "Fillers and filled polymers"; Wiley-VCH: Weinheim, **(2001)**.

[9] An, L. N.; Xu, W. X.; Rajagopalan, S.; Wang, C. M.; Wang, H.; Fan, Y.; Zhang, L. G.; Jiang, D. P.; Kapat, J.; Chow, L.; Guo, B. H.; Liang, J.; Vaidyanathan, R.; "Carbon-nanotube-reinforced polymer-derived ceramic composites", *Advanced Materials* 16 (22), 2036-2040, **(2004)**.

[10] Meyyappan, M.; "Carbon nanotubes science and applications"; CRC Press: Boca Raton, FL, **(2005)**.

[11] Ajayan, P. M.; Stephan, O.; Colliex, C.; Trauth, D.; "Aligned Carbon Nanotube Arrays Formed by Cutting A Polymer Resin-Nanotube Composite", *Science* 265 (5176), 1212-1214, **(1994)**.

[12] Harris, P. J. F.; "Carbon nanotubes and related structures new materials for the twenty-first century"; Cambridge University Press: Cambridge, **(2001)**.

[13] O'Connell, M. J.; "Carbon nanotubes properties and applications"; CRC Taylor & Francis: Boca Raton, **(2006)**.

[14] Moniruzzaman, M.; Winey, K. I.; "Polymer nanocomposites containing carbon nanotubes", *Macromolecules* 39 (16), 5194-5205, **(2006)**.

[15] Sennett, M.; Welsh, E.; Wright, J. B.; Li, W. Z.; Wen, J. G.; Ren, Z. F.; "Dispersion and alignment of carbon nanotubes in polycarbonate", *Applied Physics A-Materials Science & Processing* 76 (1), 111-113, **(2003)**.

[16] Hirsch, A.; Vostrowsky, O.; "Functionalization of carbon nanotubes", *Functional Molecular Nanostructures* 245, 193-237, **(2005)**.

[17] Zhang, H. T.; Wu, G.; Chen, X. H.; Qiu, X. G.; "Synthesis and magnetic properties of nickel nanocrystals", *Materials Research Bulletin* 41 (3), 495-501, **(2006)**.

[18] LizMarzan, L. M.; Giersig, M.; Mulvaney, P.; "Synthesis of nanosized gold-silica core-shell particles", *Langmuir* 12 (18), 4329-4335, **(1996)**.

[19] Alivisatos, A. P.; "Semiconductor clusters, nanocrystals, and quantum dots", *Science* 271 (5251), 933-937, **(1996)**.

[20] Endo, M.; PhD thesis, Nagoya University, Japan, **(1978)**.

[21] Iijima, S.; "Helical Microtubules of Graphitic Carbon", *Nature* 354 (6348), 56-58, **(1991)**.

[22] Kataura, H.; Kumazawa, Y.; Maniwa, Y.; Umezu, I.; Suzuki, S.; Ohtsuka, Y.; Achiba, Y.; "Optical properties of single-wall carbon nanotubes", *Synthetic Metals* 103 (1-3), 2555-2558, **(1999)**.

[23] Wu, H. L.; Ma, C. C. M.; Yang, Y. T.; Kuan, H. C.; Yang, C. C.; Chiang, C. L.; "Morphology, electrical resistance, electromagnetic interference shielding and mechanical properties of functionalized MWNT and poly(urea urethane) nanocomposites", *Journal of Polymer Science Part B-Polymer Physics* 44 (7), 1096-1105, **(2006)**.

[24] Andrews, R.; Jacques, D.; Qian, D. L.; Rantell, T.; "Multiwall carbon nanotubes: Synthesis and application", *Accounts of Chemical Research* 35 (12), 1008-1017, **(2002)**.

[25] Kumar, S.; Dang, T. D.; Arnold, F. E.; Bhattacharyya, A. R.; Min, B. G.; Zhang, X. F.; Vaia, R. A.; Park, C.; Adams, W. W.; Hauge, R. H.; Smalley, R. E.; Ramesh, S.; Willis, P. A.; "Synthesis, structure, and properties of PBO/SWNT composites", *Macromolecules* 35 (24), 9039-9043, **(2002)**.

[26] Coleman, J. N.; Khan, U.; Blau, W. J.; Gun'ko, Y. K.; "Small but strong: A review of the mechanical properties of carbon nanotube-polymer composites", *Carbon* 44 (9), 1624-1652, **(2006)**.

[27] Chen, W.; Tao, X. M.; Xue, P.; Cheng, X. Y.; "Enhanced mechanical properties and morphological characterizations of poly(vinyl alcohol)-carbon nanotube composite films", *Applied Surface Science* 252 (5), 1404-1409, **(2005)**.

[28] Sandler, J. K. W.; Kirk, J. E.; Kinloch, I. A.; Shaffer, M. S. P.; Windle, A. H.; "Ultra-low electrical percolation threshold in carbon-nanotube-epoxy composites", *Polymer* 44 (19), 5893-5899, **(2003)**.

[29] Shaffer, M. S. P.; Windle, A. H.; "Fabrication and characterization of carbon nanotube/poly(vinyl alcohol) composites", *Advanced Materials* 11 (11), 937-942, **(1999)**.

[30] Weisenberger, M. C.; Grulke, E. A.; Jacques, D.; Rantell, T.; Andrews, R.; "Enhanced mechanical properties of polyacrylonitrile/multiwall carbon nanotube composite fibers", *Journal of Nanoscience and Nanotechnology* 3 (6), 535-539, **(2003)**.

[31] Zhang, X. F.; Liu, T.; Sreekumar, T. V.; Kumar, S.; Moore, V. C.; Hauge, R. H.; Smalley, R. E.; "Poly(vinyl alcohol)/SWNT composite film", *Nano Letters* 3 (9), 1285-1288, **(2003)**.

[32] Zhang, X. F.; Liu, T.; Sreekumar, T. V.; Kumar, S.; Hu, X. D.; Smith, K.; "Gel spinning of PVA/SWNT composite fiber", *Polymer* 45 (26), 8801-8807, **(2004)**.

[33] Baskaran, D.; Mays, J. W.; Bratcher, M. S.; "Noncovalent and nonspecific molecular interactions of polymers with multiwalled carbon nanotubes", *Chemistry of Materials* 17 (13), 3389-3397, **(2005)**.

[34] Chen, J.; Liu, H. Y.; Weimer, W. A.; Halls, M. D.; Waldeck, D. H.; Walker, G. C.; "Noncovalent engineering of carbon nanotube surfaces by rigid, functional conjugated polymers", *Journal of the American Chemical Society* 124 (31), 9034-9035, **(2002)**.

[35] Xu, H. M.; Li, D.; Liang, J.; "Study on electrical and thermal properties of PMMA/aligned carbon nanotubes composites", *Chinese Journal of Inorganic Chemistry* 21 (9), 1353-1356, **(2005)**.

[36] Mylvaganam, K.; Zhang, L. C.; "Chemical bonding in polyethylene-nanotube composites: A quantum mechanics prediction", *Journal of Physical Chemistry B* 108 (17), 5217-5220, **(2004)**.

[37] Shofner, M. L.; Khabashesku, V. N.; Barrera, E. V.; "Processing and mechanical properties of fluorinated single-wall carbon nanotube-polyethylene composites", *Chemistry of Materials* 18 (4), 906-913, **(2006)**.

[38] Zhang, Q. H.; Rastogi, S.; Chen, D. J.; Lippits, D.; Lemstra, P. J.; "Low percolation threshold in single-walled carbon nanotube/high density polyethylene composites prepared by melt processing technique", *Carbon* 44 (4), 778-785, **(2006)**.

[39] Kim, B.; Park, H.; Sigmund, W. M.; "Rheological behavior of multiwall carbon nanotubes with polyelectrolyte dispersants", *Colloids and Surfaces A-Physicochemical and Engineering Aspects* 256 (2-3), 123-127, **(2005)**.

[40] Paloniemi, H.; Lukkarinen, M.; Aaritalo, T.; Areva, S.; Leiro, J.; Heinonen, M.; Haapakka, K.; Lukkari, J.; "Layer-by-layer electrostatic self-assembly of single-wall carbon nanotube polyelectrolytes", *Langmuir* 22 (1), 74-83, **(2006)**.

[41] Xu, G. Y.; Wu, W. T.; Wang, Y. S.; Pang, W. M.; Wang, P. H.; Zhu, G. R.; Lu, F.; "Synthesis and characterization of water-soluble multiwalled carbon nanotubes grafted by a thermoresponsive polymer", *Nanotechnology* 17 (10), 2458-2465, **(2006)**.

[42] Wang, S. R.; Liang, Z. Y.; Liu, T.; Wang, B.; Zhang, C.; "Effective amino-functionalization of carbon nanotubes for reinforcing epoxy polymer composites", *Nanotechnology* 17 (6), 1551-1557, **(2006)**.

[43] An, L. N.; Xu, W. X.; Rajagopalan, S.; Wang, C. M.; Wang, H.; Fan, Y.; Zhang, L. G.; Jiang, D. P.; Kapat, J.; Chow, L.; Guo, B. H.; Liang, J.; Vaidyanathan, R.; "Carbon-nanotube-reinforeed polymer-derived ceramic composites", *Advanced Materials* 16 (22), 2036-+, **(2004)**.

[44] Poyato, R.; Vasiliev, A. L.; Padture, N. P.; Tanaka, H.; Nishimura, T.; "Aqueous colloidal processing of single-wall carbon nanotubes and their composites with ceramics", *Nanotechnology* 17 (6), 1770-1777, **(2006)**.

[45] Hjortstam, O.; Isberg, P.; Soderholm, S.; Dai, H.; "Can we achieve ultra-low resistivity in carbon nanotube-based metal composites?", *Applied Physics A-Materials Science & Processing* 78 (8), 1175-1179, **(2004)**.

[46] Zhan, G. D.; Kuntz, J. D.; Wan, J. L.; Mukherjee, A. K.; "Single-wall carbon nanotubes as attractive toughening agents in alumina-based nanocomposites", *Nature Materials* 2 (1), 38-42, **(2003)**.

[47] Allaoui, A.; Bai, S.; Cheng, H. M.; Bai, J. B.; "Mechanical and electrical properties of a MWNT/epoxy composite", *Composites Science and Technology* 62 (15), 1993-1998, **(2002)**.

[48] Safadi, B.; Andrews, R.; Grulke, E. A.; "Multiwalled carbon nanotube polymer composites: Synthesis and characterization of thin films", *Journal of Applied Polymer Science* 84 (14), 2660-2669, **(2002)**.
[49] Kim, Y. J.; Shin, T. S.; Choi, H. D.; Kwon, J. H.; Chung, Y. C.; Yoon, H. G.; "Electrical conductivity of chemically modified multiwalled carbon nanotube/epoxy composites", *Carbon* 43 (1), 23-30, **(2005)**.
[50] Wang, L.; Dang, Z. M.; "Carbon nanotube composites with high dielectric constant at low percolation threshold", *Applied Physics Letters* 87 (4) **(2005)**.
[51] Moisala, A.; Li, Q.; Kinloch, I. A.; Windle, A. H.; "Thermal and electrical conductivity of single- and multi-walled carbon nanotube-epoxy composites", *Composites Science and Technology* 66 (10), 1285-1288, **(2006)**.
[52] Yu, A. P.; Hui, H.; Bekyarova, E.; Itkis, M. E.; Gao, J.; Zhao, B.; Haddon, R. C.; "Incorporation of highly dispersed single-walled carbon nanotubes in a polyimide matrix", *Composites Science and Technology* 66 (9), 1190-1197, **(2006)**.
[53] Park, C.; Wilkinson, J.; Banda, S.; Ounaies, Z.; Wise, K. E.; Sauti, G.; Lillehei, P. T.; Harrison, J. S.; "Aligned single-wall carbon nanotube polymer composites using an electric field", *Journal of Polymer Science Part B-Polymer Physics* 44 (12), 1751-1762, **(2006)**.
[54] Rozhin, A. G.; Sakakibara, Y.; Kataura, H.; Matsuzaki, S.; Ishida, K.; Achiba, Y.; Tokumoto, M.; "Anisotropic saturable absorption of single-wall carbon nanotubes aligned in polyvinyl alcohol", *Chemical Physics Letters* 405 (4-6), 288-293, **(2005)**.
[55] Huang, Z. P.; Carnahan, D. L.; Rybczynski, J.; Giersig, M.; Sennett, M.; Wang, D. Z.; Wen, J. G.; Kempa, K.; Ren, Z. F.; "Growth of large periodic arrays of carbon nanotubes", *Applied Physics Letters* 82 (3), 460-462, **(2003)**.
[56] Zhou, W.; Ooi, Y. H.; Russo, R.; Papanek, P.; Luzzi, D. E.; Fischer, J. E.; Bronikowski, M. J.; Willis, P. A.; Smalley, R. E.; "Structural characterization and diameter-dependent oxidative stability of single wall carbon nanotubes synthesized by the catalytic decomposition of CO", *Chemical Physics Letters* 350 (1-2), 6-14, **(2001)**.
[57] Journet, C.; Bernier, P.; "Production of carbon nanotubes", *Applied Physics A-Materials Science & Processing* 67 (1), 1-9, **(1998)**.
[58] Journet, C.; Maser, W. K.; Bernier, P.; Loiseau, A.; delaChapelle, M. L.; Lefrant, S.; Deniard, P.; Lee, R.; Fischer, J. E.; "Large-scale production of single-walled carbon nanotubes by the electric-arc technique", *Nature* 388 (6644), 756-758, **(1997)**.
[59] Kokai, F.; Koshio, A.; Shiraishi, M.; Matsuta, T.; Shimoda, S.; Ishihara, M.; Koga, Y.; Deno, H.; "Modification of carbon nanotubes by laser ablation", *Diamond and Related Materials* 14 (3-7), 724-728, **(2005)**.
[60] Thostenson, E. T.; Ren, Z. F.; Chou, T. W.; "Advances in the science and technology of carbon nanotubes and their composites: a review", *Composites Science and Technology* 61 (13), 1899-1912, **(2001)**.
[61] Wong, E. W.; Sheehan, P. E.; Lieber, C. M.; "Nanobeam mechanics: Elasticity, strength, and toughness of nanorods and nanotubes", *Science* 277 (5334), 1971-1975, **(1997)**.
[62] Lau, K. T.; Hui, D.; "The revolutionary creation of new advanced materials - carbon nanotube composites", *Composites Part B-Engineering* 33 (4), 263-277, **(2002)**.
[63] Li, F.; Cheng, H. M.; Bai, S.; Su, G.; Dresselhaus, M. S.; "Tensile strength of single-walled carbon nanotubes directly measured from their macroscopic ropes", *Applied Physics Letters* 77 (20), 3161-3163, **(2000)**.
[64] Iijima, S.; Brabec, C.; Maiti, A.; Bernholc, J.; "Structural flexibility of carbon nanotubes", *Journal of Chemical Physics* 104 (5), 2089-2092, **(1996)**.
[65] Chae, H. G.; Sreekumar, T. V.; Uchida, T.; Kumar, S.; "A comparison of reinforcement efficiency of various types of carbon nanotubes in poly acrylonitrile fiber", *Polymer* 46 (24), 10925-10935, **(2005)**.
[66] Odom, T. W.; Huang, J. L.; Kim, P.; Lieber, C. M.; "Atomic structure and electronic properties of single-walled carbon nanotubes", *Nature* 391 (6662), 62-64, **(1998)**.
[67] Berger, C.; Poncharal, P.; Yi, Y.; de Heer, W.; "Ballistic conduction in multiwalled carbon nanotubes", *Journal of Nanoscience and Nanotechnology* 3 (1-2), 171-177, **(2003)**.
[68] Urbina, A.; Echeverria, I.; Perez-Garrido, A.; az-Sanchez, A.; Abellan, J.; "Quantum conductance steps in solutions of multiwalled carbon nanotubes", *Physical Review Letters* 90 (10) **(2003)**.
[69] Poncharal, P.; Berger, C.; Yi, Y.; Wang, Z. L.; de Heer, W. A.; "Room temperature ballistic conduction in carbon nanotubes", *Journal of Physical Chemistry B* 106 (47), 12104-12118, **(2002)**.
[70] Schonenberger, C.; Bachtold, A.; Strunk, C.; Salvetat, J. P.; Forro, L.; "Interference and Interaction in multi-wall carbon nanotubes", *Applied Physics A-Materials Science & Processing* 69 (3), 283-295, **(1999)**.

[71] Minami, N.; Kazaoui, S.; Jacquemin, R.; Yamawaki, H.; Aoki, K.; Kataura, H.; Achiba, Y.; "Optical properties of semiconducting and metallic single wall carbon nanotubes: effects of doping and high pressure", *Synthetic Metals* 116 (1-3), 405-409, **(2001)**.

[72] Banerjee, S.; Kahn, M. G. C.; Wong, S. S.; "Rational chemical strategies for carbon nanotube functionalization", *Chemistry-A European Journal* 9 (9), 1899-1908, **(2003)**.

[73] Kim, J. A.; Seong, D. G.; Kang, T. J.; Youn, J. R.; "Effects of surface modification on rheological and mechanical properties of CNT/epoxy composites", *Carbon* 44 (10), 1898-1905, **(2006)**.

[74] Park, H.; Zhao, J. J.; Lu, J. P.; "Effects of sidewall functionalization on conducting properties of single wall carbon nanotubes", *Nano Letters* 6 (5), 916-919, **(2006)**.

[75] Dettlaff-Weglikowska, U.; Skakalova, V.; Graupner, R.; Jhang, S. H.; Kim, B. H.; Lee, H. J.; Ley, L.; Park, Y. W.; Berber, S.; Tomanek, D.; Roth, S.; "Effect of SOCl2 treatment on electrical and mechanical properties of single-wall carbon nanotube networks", *Journal of the American Chemical Society* 127 (14), 5125-5131, **(2005)**.

[76] Jost, O.; Gorbunov, A. A.; Pompe, W.; Pichler, T.; Friedlein, R.; Knupfer, M.; Reibold, M.; Bauer, H. D.; Dunsch, L.; Golden, M. S.; Fink, J.; "Diameter grouping in bulk samples of single-walled carbon nanotubes from optical absorption spectroscopy", *Applied Physics Letters* 75 (15), 2217-2219, **(1999)**.

[77] Hone, J.; Whitney, M.; Piskoti, C.; Zettl, A.; "Thermal conductivity of single-walled carbon nanotubes", *Physical Review B* 59 (4), R2514-R2516, **(1999)**.

[78] Yi, W.; Lu, L.; Zhang, D. L.; Pan, Z. W.; Xie, S. S.; "Linear specific heat of carbon nanotubes", *Physical Review B* 59 (14), R9015-R9018, **(1999)**.

[79] Wong, Y. M.; Kang, W. P.; Davidson, J. L.; Soh, K. L.; Choi, B. K.; Hofmeister, W.; "Carbon nanostructure field emission devices", *Journal of Vacuum Science & Technology B* 24 (2), 1008-1012, **(2006)**.

[80] Nalwa, H. S.; "Handbook of surfaces and interfaces of materials"; Academic Press: San Diego, **(2001)**.

[81] Bechinger, C.; Rudhardt, D.; Leiderer, P.; Roth, R.; Dietrich, S.; "Understanding depletion forces beyond entropy", *Physical Review Letters* 83 (19), 3960-3963, **(1999)**.

[82] Balasubramanian, K.; Burghard, M.; "Chemically functionalized carbon nanotubes", *Small* 1 (2), 180-192, **(2005)**.

[83] Tang, W. Z.; Santare, M. H.; Advani, S. G.; "Melt processing and mechanical property characterization of multi-walled carbon nanotube/high density polyethylene (MWNT/HDPE) composite films", *Carbon* 41 (14), 2779-2785, **(2003)**.

[84] Baskaran, D.; Mays, J. W.; Bratcher, M. S.; "Polymer adsorption in the grafting reactions of hydroxyl terminal polymers with multi-walled carbon nanotubes", *Polymer* 46 (14), 5050-5057, **(2005)**.

[85] Ge, J. J.; Zhang, D.; Li, Q.; Hou, H. Q.; Graham, M. J.; Dai, L. M.; Harris, F. W.; Cheng, S. Z. D.; "Multiwalled carbon nanotubes with chemically grafted polyetherimides", *Journal of the American Chemical Society* 127 (28), 9984-9985, **(2005)**.

[86] Liu, Y.; Wu, D. C.; Zhang, W. D.; Jiang, X.; He, C. B.; Chung, T. S.; Goh, S. H.; Leong, K. W.; "Polyethylenimine-grafted multiwalled carbon nanotubes for secure noncovalent immobilization and efficient delivery of DNA", *Angewandte Chemie-International Edition* 44 (30), 4782-4785, **(2005)**.

[87] O'Connell, M. J.; Boul, P.; Ericson, L. M.; Huffman, C.; Wang, Y. H.; Haroz, E.; Kuper, C.; Tour, J.; Ausman, K. D.; Smalley, R. E.; "Reversible water-solubilization of single-walled carbon nanotubes by polymer wrapping", *Chemical Physics Letters* 342 (3-4), 265-271, **(2001)**.

[88] Star, A.; Stoddart, J. F.; Steuerman, D.; Diehl, M.; Boukai, A.; Wong, E. W.; Yang, X.; Chung, S. W.; Choi, H.; Heath, J. R.; "Preparation and properties of polymer-wrapped single-walled carbon nanotubes", *Angewandte Chemie-International Edition* 40 (9), 1721-1725, **(2001)**.

[89] Lou, X. D.; Daussin, R.; Cuenot, S.; Duwez, A. S.; Pagnoulle, C.; Detrembleur, C.; Bailly, C.; Jerome, R.; "Synthesis of pyrene-containing polymers and noncovalent sidewall functionalization of multiwalled carbon nanotubes", *Chemistry of Materials* 16 (21), 4005-4011, **(2004)**.

[90] Ravindran, S.; Chaudhary, S.; Colburn, B.; Ozkan, M.; Ozkan, C. S.; "Covalent coupling of quantum dots to multiwalled carbon nanotubes for electronic device applications", *Nano Letters* 3 (4), 447-453, **(2003)**.

[91] Dalton, A. B.; Collins, S.; Munoz, E.; Razal, J. M.; Ebron, V. H.; Ferraris, J. P.; Coleman, J. N.; Kim, B. G.; Baughman, R. H.; "Super-tough carbon-nanotube fibres - These extraordinary composite fibres can be woven into electronic textiles", *Nature* 423 (6941), 703, **(2003)**.

[92] Hu, G. J.; Zhao, C. G.; Zhang, S. M.; Yang, M. S.; Wang, Z. G.; "Low percolation thresholds of electrical conductivity and rheology in poly(ethylene terephthalate) through the networks of multi-walled carbon nanotubes", *Polymer* 47 (1), 480-488, **(2006)**.

[93] Bavastrello, V.; Erokhin, V.; Carrara, S.; Sbrana, F.; Ricci, D.; Nicolini, C.; "Morphology and conductivity in poly(ortho-anisidine)/carbon nanotubes nanocomposite films", *Thin Solid Films* 468 (1-2), 17-22, **(2004)**.
[94] Barrau, S.; Demont, P.; Peigney, A.; Laurent, C.; Lacabanne, C.; "DC and AC conductivity of carbon nanotubes-polyepoxy composites", *Macromolecules* 36 (14), 5187-5194, **(2003)**.
[95] Ramasubramaniam, R.; Chen, J.; Liu, H. Y.; "Homogeneous carbon nanotube/polymer composites for electrical applications", *Applied Physics Letters* 83 (14), 2928-2930, **(2003)**.
[96] Song, P. C.; Liu, C. H.; Fan, S. S.; "Improving the thermal conductivity of nanocomposites by increasing the length efficiency of loading carbon nanotubes", *Applied Physics Letters* 88 (15) **(2006)**.
[97] Garmestani, H.; Al-Haik, M. S.; Dahmen, K.; Tannenbaum, R.; Li, D. S.; Sablin, S. S.; Hussaini, M. Y.; "Polymer-mediated alignment of carbon nanotubes under high magnetic fields", *Advanced Materials* 15 (22), 1918-1921, **(2003)**.
[98] Kim, B.; Sigmund, W. M.; "Self-alignment of shortened multiwall carbon nanotubes on polyelectrolyte layers", *Langmuir* 19 (11), 4848-4851, **(2003)**.
[99] Qian, D.; Dickey, E. C.; Andrews, R.; Rantell, T.; "Load transfer and deformation mechanisms in carbon nanotube-polystyrene composites", *Applied Physics Letters* 76 (20), 2868-2870, **(2000)**.
[100] Ruan, S. L.; Gao, P.; Yang, X. G.; Yu, T. X.; "Toughening high performance ultrahigh molecular weight polyethylene using multiwalled carbon nanotubes", *Polymer* 44 (19), 5643-5654, **(2003)**.
[101] Coleman, J. N.; Cadek, M.; Blake, R.; Nicolosi, V.; Ryan, K. P.; Belton, C.; Fonseca, A.; Nagy, J. B.; Gun'ko, Y. K.; Blau, W. J.; "High-performance nanotube-reinforced plastics: Understanding the mechanism of strength increase", *Advanced Functional Materials* 14 (8), 791-798, **(2004)**.
[102] Gorga, R. E.; Cohen, R. E.; "Toughness enhancements in poly(methyl methacrylate) by addition of oriented multiwall carbon nanotubes", *Journal of Polymer Science Part B-Polymer Physics* 42 (14), 2690-2702, **(2004)**.
[103] Meincke, O.; Kaempfer, D.; Weickmann, H.; Friedrich, C.; Vathauer, M.; Warth, H.; "Mechanical properties and electrical conductivity of carbon-nanotube filled polyamide-6 and its blends with acrylonitrile/butadiene/styrene", *Polymer* 45 (3), 739-748, **(2004)**.
[104] Liu, T. X.; Phang, I. Y.; Shen, L.; Chow, S. Y.; Zhang, W. D.; "Morphology and mechanical properties of multiwalled carbon nanotubes reinforced nylon-6 composites", *Macromolecules* 37 (19), 7214-7222, **(2004)**.
[105] Sandler, J. K. W.; Pegel, S.; Cadek, M.; Gojny, F.; van Es, M.; Lohmar, J.; Blau, W. J.; Schulte, K.; Windle, A. H.; Shaffer, M. S. P.; "A comparative study of melt spun polyamide-12 fibres reinforced with carbon nanotubes and nanofibres", *Polymer* 45 (6), 2001-2015, **(2004)**.
[106] Ogasawara, T.; Ishida, Y.; Ishikawa, T.; Yokota, R.; "Characterization of multi-walled carbon nanotube/phenylethynyl terminated polyimide composites", *Composites Part A-Applied Science and Manufacturing* 35 (1), 67-74, **(2004)**.
[107] Liu, L. Q.; Wagner, H. D.; "Rubbery and glassy epoxy resins reinforced with carbon nanotubes", *Composites Science and Technology* 65 (11-12), 1861-1868, **(2005)**.
[108] Kang, M.; Myung, S. J.; Jin, H. J.; "Nylon 610 and carbon nanotube composite by in situ interfacial polymerization", *Polymer* 47 (11), 3961-3966, **(2006)**.
[109] Liu, L. Q.; Barber, A. H.; Nuriel, S.; Wagner, H. D.; "Mechanical properties of functionalized single-walled carbon-nanotube/poly(vinyl alcohol) nanocomposites", *Advanced Functional Materials* 15 (6), 975-980, **(2005)**.
[110] Manchado, M. A. L.; Valentini, L.; Biagiotti, J.; Kenny, J. M.; "Thermal and mechanical properties of single-walled carbon nano tubes-polypropylene composites prepared by melt processing", *Carbon* 43 (7), 1499-1505, **(2005)**.
[111] Kearns, J. C.; Shambaugh, R. L.; "Polypropylene fibers reinforced with carbon nanotubes", *Journal of Applied Polymer Science* 86 (8), 2079-2084, **(2002)**.
[112] Gao, J. B.; Itkis, M. E.; Yu, A. P.; Bekyarova, E.; Zhao, B.; Haddon, R. C.; "Continuous spinning of a single-walled carbon nanotube-nylon composite fiber", *Journal of the American Chemical Society* 127 (11), 3847-3854, **(2005)**.
[113] Mamedov, A. A.; Kotov, N. A.; Prato, M.; Guldi, D. M.; Wicksted, J. P.; Hirsch, A.; "Molecular design of strong single-wall carbon nanotube/polyelectrolyte multilayer composites", *Nature Materials* 1 (3), 190-194, **(2002)**.
[114] Rouse, J. H.; Lillehei, P. T.; "Electrostatic assembly of polymer/single walled carbon nanotube multilayer films", *Nano Letters* 3 (1), 59-62, **(2003)**.
[115] Fornes, T. D.; Baur, J. W.; Sabba, Y.; Thomas, E. L.; "Morphology and properties of melt-spun polycarbonate fibers containing single- and multi-wall carbon nanotubes", *Polymer* 47 (5), 1704-1714, **(2006)**.
[116] He, P. G.; Bayachou, M.; "Layer-by-layer fabrication and characterization of DNA-wrapped single-walled carbon nanotube particles", *Langmuir* 21 (13), 6086-6092, **(2005)**.

[117] Li, C. S.; Tang, Y. P.; Yao, K. F.; Zhou, F.; Ma, Q.; Lin, H.; Tao, M. S.; Liang, J.; "Decoration of multiwall nanotubes with cadmium sulfide nanoparticles", *Carbon* 44 (10), 2021-2026, **(2006)**.
[118] Chen, J. H.; Lu, G. H.; "Controlled decoration of carbon nanotubes with nanoparticles", *Nanotechnology* 17 (12), 2891-2894, **(2006)**.
[119] Grzelczak, M.; Correa-Duarte, M. A.; Salgueirino-Maceira, V.; Giersig, M.; Diaz, R.; Liz-Marzan, L. M.; "Photoluminescence quenching control in quantum dot-carbon nanotube composite colloids using a silica-shell spacer", *Advanced Materials* 18 (4), 415-419, **(2006)**.
[120] Unger, E.; Duesberg, G. S.; Liebau, M.; Graham, A. P.; Seidel, R.; Kreupl, F.; Hoenlein, W.; "Decoration of multi-walled carbon nanotubes with noble- and transition-metal clusters and formation of CNT-CNT networks", *Applied Physics A-Materials Science & Processing* 77 (6), 735-738, **(2003)**.
[121] Oh, S. D.; So, B. K.; Choi, S. H.; Gopalan, A.; Lee, K. P.; Yoon, K. R.; Choi, I. S.; "Dispersing of Ag, Pd, and Pt-Ru alloy nanoparticles on single-walled carbon nanotubes by gamma-irradiation", *Materials Letters* 59 (10), 1121-1124, **(2005)**.
[122] Bottini, M.; Tautz, L.; Huynh, H.; Monosov, E.; Bottini, N.; Dawson, M. I.; Bellucci, S.; Mustelin, T.; "Covalent decoration of multi-walled carbon nanotubes with silica nanoparticles", *Chemical Communications* (6), 758-760, **(2005)**.
[123] Banerjee, S.; Wong, S. S.; "In situ quantum dot growth on multiwalled carbon nanotubes", *Journal of the American Chemical Society* 125 (34), 10342-10350, **(2003)**.
[124] Banerjee, S.; Wong, S. S.; "Formation of CdSe nanocrystals onto oxidized, ozonized single-walled carbon nanotube surfaces", *Chemical Communications* (16), 1866-1867, **(2004)**.
[125] Banerjee, S.; Wong, S. S.; "In-situ growth of "fused", ozonized single-walled carbon nanotube - CdTe quantum dot junctions"", *Advanced Materials* 16 (1), 34-37, **(2004)**.
[126] Du, J. M.; Fu, L.; Liu, Z. M.; Han, B. X.; Li, Z. H.; Liu, Y. Q.; Sun, Z. Y.; Zhu, D. B.; "Facile route to synthesize multiwalled carbon nanotube/zinc sulfide heterostructures: Optical and electrical properties", *Journal of Physical Chemistry B* 109 (26), 12772-12776, **(2005)**.
[127] Jiang, L. Q.; Gao, L.; "Fabrication and characterization of ZnO-coated multi-walled carbon nanotubes with enhanced photocatalytic activity", *Materials Chemistry and Physics* 91 (2-3), 313-316, **(2005)**.
[128] Kim, H.; Sigmund, W.; "Zinc sulfide nanocrystals on carbon nanotubes", *Journal of Crystal Growth* 255 (1-2), 114-118, **(2003)**.
[129] Ravindran, S.; Bozhilov, K. N.; Ozkan, C. S.; "Self assembly of ordered artificial solids of semiconducting ZnS capped CdSe nanoparticles at carbon nanotube ends", *Carbon* 42 (8-9), 1537-1542, **(2004)**.
[130] Sheeney-Haj-Khia, L.; Basnar, B.; Willner, I.; "Efficient generation of photocurrents by using CdS/Carbon nanotube assemblies on electrodes", *Angewandte Chemie-International Edition* 44 (1), 78-83, **(2005)**.
[131] Shi, J. H.; Qin, Y. J.; Wu, W.; Li, X. L.; Guo, Z. X.; Zhu, D. B.; "In situ synthesis of CdS nanoparticles on multi-walled carbon nanotubes", *Carbon* 42 (2), 455-458, **(2004)**.
[132] Zhao, L. P.; Gao, L. A.; "Coating multi-walled carbon nanotubes with zinc sulfide", *Journal of Materials Chemistry* 14 (6), 1001-1004, **(2004)**.
[133] Chen, Y. J.; Zhu, C. L.; Wang, T. H.; "The enhanced ethanol sensing properties of multi-walled carbon nanotubes/SnO2 core/shell nanostructures", *Nanotechnology* 17 (12), 3012-3017, **(2006)**.
[134] Sun, Z. Y.; Yuan, H. Q.; Liu, Z. M.; Han, B. X.; Zhang, X. R.; "A highly efficient chemical sensor material for H2S: alpha-Fe2O3 nanotubes fabricated using carbon nanotube templates", *Advanced Materials* 17 (24), 2993-2997, **(2005)**.
[135] Landi, B. J.; Castro, S. L.; Ruf, H. J.; Evans, C. M.; Bailey, S. G.; Raffaelle, R. P.; "CdSe quantum dot-single wall carbon nanotube complexes for polymeric solar cells", *Solar Energy Materials and Solar Cells* 87 (1-4), 733-746, **(2005)**.
[136] Gaponik, N.; Talapin, D. V.; Rogach, A. L.; Hoppe, K.; Shevchenko, E. V.; Kornowski, A.; Eychmuller, A.; Weller, H.; "Thiol-capping of CdTe nanocrystals: An alternative to organometallic synthetic routes", *Journal of Physical Chemistry B* 106 (29), 7177-7185, **(2002)**.
[137] Hikmet, R. A. M.; Talapin, D. V.; Weller, H.; "Study of conduction mechanism and electroluminescence in CdSe/ZnS quantum dot composites", *Journal of Applied Physics* 93 (6), 3509-3514, **(2003)**.
[138] Talapin, D. V.; Rogach, A. L.; Kornowski, A.; Haase, M.; Weller, H.; "Highly luminescent monodisperse CdSe and CdSe/ZnS nanocrystals synthesized in a hexadecylamine-trioctylphosphine oxide-trioctylphospine mixture", *Nano Letters* 1 (4), 207-211, **(2001)**.
[139] Talapin, D. V.; Haubold, S.; Rogach, A. L.; Kornowski, A.; Haase, M.; Weller, H.; "A novel organometallic synthesis of highly luminescent CdTe nanocrystals", *Journal of Physical Chemistry B* 105 (12), 2260-2263, **(2001)**.

[140] Xie, R. G.; Kolb, U.; Li, J. X.; Basche, T.; Mews, A.; "Synthesis and characterization of highly luminescent CdSe-Core CdS/Zn0.5Cd0.5S/ZnS multishell nanocrystals", *Journal of the American Chemical Society* 127 (20), 7480-7488, **(2005)**.
[141] Banerjee, S.; Wong, S. S.; "Synthesis and characterization of carbon nanotube-nanocrystal heterostructures", *Nano Letters* 2 (3), 195-200, **(2002)**.
[142] Haremza, J. M.; Hahn, M. A.; Krauss, T. D.; "Attachment of single CdSe nanocrystals to individual single-walled carbon nanotubes", *Nano Letters* 2 (11), 1253-1258, **(2002)**.
[143] Chaudhary, S.; Kim, J. H.; Singh, K. V.; Ozkan, M.; "Fluorescence microscopy visualization of single-walled carbon nanotubes using semiconductor nanocrystals", *Nano Letters* 4 (12), 2415-2419, **(2004)**.
[144] Kim, H.; Sigmund, W.; "Zinc oxide nanowires on carbon nanotubes", *Applied Physics Letters* 81 (11), 2085-2087, **(2002)**.
[145] Zhang, J. H.; Yang, C. R.; Wang, Y. J.; Feng, T.; Yu, W. D.; Jiang, J.; Wang, X.; Liu, X. H.; "Improvement of the field emission of carbon nanotubes by hafnium coating and annealing", *Nanotechnology* 17 (1), 257-260, **(2006)**.
[146] Wang, G. X.; Ahn, J. H.; Yao, J.; Lindsay, M.; Liu, H. K.; Dou, S. X.; "Preparation and characterization of carbon nanotubes for energy storage", *Journal of Power Sources* 119, 16-23, **(2003)**.
[147] Wang, M.; Zhang, X.; Lu, M. W.; Liu, Y.; "Effect of defects on resonance of carbon nanotubes as mass sensors", *Applied Physics Letters* 88 (11) **(2006)**.
[148] Yang, M. H.; Yang, Y. H.; Liu, Y. L.; Shen, G. L.; Yu, R. Q.; "Platinum nanoparticles-doped sol-gel/carbon nanotubes composite electrochemical sensors and biosensors", *Biosensors & Bioelectronics* 21 (7), 1125-1131, **(2006)**.
[149] Valentini, E.; Orlanducci, S.; Tamburri, E.; Terranova, M. L.; Curulli, A.; Palleschi, G.; "Single-walled carbon nanotubes on tungsten wires: A new class of microelectrochemical sensors", *Electroanalysis* 17 (1), 28-37, **(2005)**.
[150] Bekyarova, E.; Davis, M.; Burch, T.; Itkis, M. E.; Zhao, B.; Sunshine, S.; Haddon, R. C.; "Chemically functionalized single-walled carbon nanotubes as ammonia sensors", *Journal of Physical Chemistry B* 108 (51), 19717-19720, **(2004)**.
[151] Jiang, X. W.; Bin, Y. Z.; Matsuo, M.; "Electrical and mechanical properties of polyimide-carbon nanotubes composites fabricated by in situ polymerization", *Polymer* 46 (18), 7418-7424, **(2005)**.
[152] Kim, B.; Lee, J.; Yu, I. S.; "Electrical properties of single-wall carbon nanotube and epoxy composites", *Journal of Applied Physics* 94 (10), 6724-6728, **(2003)**.
[153] Jou, W. S.; Cheng, H. Z.; Hsu, C. F.; "A carbon nanotube polymer-based composite with high electromagnetic shielding", *Journal of Electronic Materials* 35 (3), 462-470, **(2006)**.
[154] Kymakis, E.; Amaratunga, G. A. J.; "Optical properties of polymer-nanotube composites", *Synthetic Metals* 142 (1-3), 161-167, **(2004)**.
[155] Lagarkov, A. N.; Matytsin, S. M.; Rozanov, K. N.; Sarychev, A. K.; "Dielectric properties of fiber-filled composites", *Journal of Applied Physics* 84 (7), 3806-3814, **(1998)**.
[156] Garcia-Vidal, F. J.; Pitarke, J. M.; Pendry, J. B.; "Effective medium theory of the optical properties of aligned carbon nanotubes", *Physical Review Letters* 78 (22), 4289-4292, **(1997)**.
[157] Dang, Z. M.; Fan, L. Z.; Shen, Y.; Nan, C. W.; "Dielectric behavior of novel three-phase MWNTs/BaTiO3/PVDF composites", *Materials Science and Engineering B-Solid State Materials for Advanced Technology* 103 (2), 140-144, **(2003)**.
[158] Alvarez, J. V.; Angilella, G. G. N.; "A model dielectric response function for metallic nanotube ropes", *Solid State Communications* 132 (10), 683-688, **(2004)**.
[159] Bommeli, F.; Degiorgi, L.; Wachter, P.; Bacsa, W. S.; deHeer, W. A.; Forro, L.; "Evidence of anisotropic metallic behaviour in the optical properties of carbon nanotubes", *Solid State Communications* 99 (7), 513-517, **(1996)**.
[160] Lagarkov, A. N.; Sarychev, A. K.; "Electromagnetic properties of composites containing elongated conducting inclusions", *Physical Review B* 53 (10), 6318-6336, **(1996)**.
[161] Grimes, C. A.; Mungle, C.; Kouzoudis, D.; Fang, S.; Eklund, P. C.; "The 500 MHz to 5.50 GHz complex permittivity spectra of single-wall carbon nanotube-loaded polymer composites", *Chemical Physics Letters* 319 (5-6), 460-464, **(2000)**.
[162] Grimes, C. A.; Dickey, E. C.; Mungle, C.; Ong, K. G.; Qian, D.; "Effect of purification of the electrical conductivity and complex permittivity of multiwall carbon nanotubes", *Journal of Applied Physics* 90 (8), 4134-4137, **(2001)**.
[163] Kempa, T.; Carnahan, D.; Olek, M.; Correa, M.; Giersig, M.; Cross, M.; Benham, G.; Sennett, M.; Ren, Z.; Kempa, K.; "Dielectric media based on isolated metallic nanostructures", *Journal of Applied Physics* 98 (3), 034310-1-034310-4, **(2005)**.

[164] Watts, P. C. P.; Ponnampalam, D. R.; Hsu, W. K.; Barnes, A.; Chambers, B.; "The complex permittivity of multi-walled carbon nanotube-polystyrene composite films in X-band", *Chemical Physics Letters* 378 (5-6), 609-614, **(2003)**.

[165] Potschke, P.; Dudkin, S. M.; Alig, I.; "Dielectric spectroscopy on melt processed polycarbonate - multiwalled carbon nanotube composites", *Polymer* 44 (17), 5023-5030, **(2003)**.

[166] Watts, P. C. P.; Hsu, W. K.; Barnes, A.; Chambers, B.; "High permittivity from defective multiwalled carbon nanotubes in the X-band", *Advanced Materials* 15 (7-8), 600-603, **(2003)**.

[167] Kilbride, B. E.; Coleman, J. N.; Fraysse, J.; Fournet, P.; Cadek, M.; Drury, A.; Hutzler, S.; Roth, S.; Blau, W. J.; "Experimental observation of scaling laws for alternating current and direct current conductivity in polymer-carbon nanotube composite thin films", *Journal of Applied Physics* 92 (7), 4024-4030, **(2002)**.

[168] Potschke, P.; Fornes, T. D.; Paul, D. R.; "Rheological behavior of multiwalled carbon nanotube/polycarbonate composites", *Polymer* 43 (11), 3247-3255, **(2002)**.

[169] Potschke, P.; Abdel-Goad, M.; Alig, I.; Dudkin, S.; Lellinger, D.; "Rheological and dielectrical characterization of melt mixed polycarbonate-multiwalled carbon nanotube composites", *Polymer* 45 (26), 8863-8870, **(2004)**.

[170] Zhang, Q. H.; Lippits, D. R.; Rastogi, S.; "Dispersion and rheological aspects of SWNTs in ultra-high molecular weight polyethylene", *Macromolecules* 39 (2), 658-666, **(2006)**.

[171] Chatterjee, T.; Yurekli, K.; Hadjiev, V. G.; Krishnamoorti, R.; "Single-walled carbon nanotube dispersions in poly(ethylene oxide)", *Advanced Functional Materials* 15 (11), 1832-1838, **(2005)**.

[172] Du, F. M.; Scogna, R. C.; Zhou, W.; Brand, S.; Fischer, J. E.; Winey, K. I.; "Nanotube networks in polymer nanocomposites: Rheology and electrical conductivity", *Macromolecules* 37 (24), 9048-9055, **(2004)**.

[173] Kymakis, E.; Amaratunga, G. A. J.; "Electrical properties of single-wall carbon nanotube-polymer composite films", *Journal of Applied Physics* 99 (8) **(2006)**.

[174] Nogales, A.; Broza, G.; Roslaniec, Z.; Schulte, K.; Sics, I.; Hsiao, B. S.; Sanz, A.; Garcia-Gutierrez, M. C.; Rueda, D. R.; Domingo, C.; Ezquerra, T. A.; "Low percolation threshold in nanocomposites based on oxidized single wall carbon nanotubes and poly(butylene terephthalate)", *Macromolecules* 37 (20), 7669-7672, **(2004)**.

[175] Olek, M.; Ostrander, J.; Jurga, S.; Mohwald, H.; Kotov, N.; Kempa, K.; Giersig, M.; "Layer-by-layer assembled composites from multiwall carbon nanotubes with different morphologies", *Nano Letters* 4 (10), 1889-1895, **(2004)**.

[176] Olek, M.; Kempa, K.; Jurga, S.; Giersig, M.; "Nanomechanical properties of silica-coated multiwall carbon nanotubes-poly(methyl methacrylate) composites", *Langmuir* 21 (7), 3146-3152, **(2005)**.

[177] Olek, M.; Busgen, T.; Hilgendorff, M.; Giersig, M.; "Quantum dot modified multiwall carbon nanotubes", *Journal of Physical Chemistry B* 110 (26), 12901-12904, **(2006)**.

[178] Firkowska, I.; Olek, M.; Pazos-Perez, N.; Rojas-Chapana, J.; Giersig, M.; "Highly ordered MWNT-based matrixes: Topography at the nanoscale conceived for tissue engineering", *Langmuir* 22 (12), 5427-5434, **(2006)**.

[179] Olek, M.; Hilgendorff, M.; Giersig, M.; "A simple route for the attachment of colloidal nanocrystals to noncovalently modified multiwalled carbon nanotubes", *Colloids and Surfaces A: Physicochemical and Engineering Aspects* In Press, Corrected Proof, Available online since 17 May 2006 **(2006)**.

[180] van Embden, J.; Mulvaney, P.; "Nucleation and growth of CdSe nanocrystals in a binary ligand system", *Langmuir* 21 (22), 10226-10233, **(2005)**.

[181] Rau, K.; Singh, R.; Goldberg, E.; "Nanoindentation and nanoscratch measurements on silicone thin films synthesized by pulsed laser ablation deposition (PLAD)", *Materials Research Innovations* 5 (3-4), 151-161, **(2002)**.

[182] Moya, S.; Donath, E.; Sukhorukov, G. B.; Auch, M.; Baumler, H.; Lichtenfeld, H.; Mohwald, H.; "Lipid coating on polyelectrolyte surface modified colloidal particles and polyelectrolyte capsules", *Macromolecules* 33 (12), 4538-4544, **(2000)**.

[183] Fujita, S.; Shiratori, S.; "The initial growth of ultra-thin films fabricated by a weak polyelectrolyte layer-by-layer adsorption process", *Nanotechnology* 16 (9), 1821-1827, **(2005)**.

[184] Losche, M.; Schmitt, J.; Decher, G.; Bouwman, W. G.; Kjaer, K.; "Detailed structure of molecularly thin polyelectrolyte multilayer films on solid substrates as revealed by neutron reflectometry", *Macromolecules* 31 (25), 8893-8906, **(1998)**.

[185] Curran, S. A.; Ellis, A. V.; Vijayaraghavan, A.; Ajayan, P. M.; "Functionalization of carbon nanotubes using phenosafranin", *Journal of Chemical Physics* 120 (10), 4886-4889, **(2004)**.

[186] Han, W. Q.; Zettl, A.; "Coating single-walled carbon nanotubes with tin oxide", *Nano Letters* 3 (5), 681-683, **(2003)**.

[187] Banerjee, S.; Hemraj-Benny, T.; Wong, S. S.; "Covalent surface chemistry of single-walled carbon nanotubes", *Advanced Materials* 17 (1), 17-29, **(2005)**.

[188] Geng, H. Z.; Rosen, R.; Zheng, B.; Shimoda, H.; Fleming, L.; Liu, J.; Zhou, O.; "Fabrication and properties of composites of poly(ethylene oxide) and functionalized carbon nanotubes", *Advanced Materials* 14 (19), 1387-1390, **(2002)**.
[189] Velasco-Santos, C.; Martinez-Hernandez, A. L.; Fisher, F. T.; Ruoff, R.; Castano, V. M.; "Improvement of thermal and mechanical properties of carbon nanotube composites through chemical functionalization", *Chemistry of Materials* 15 (23), 4470-4475, **(2003)**.
[190] Koktysh, D. S.; Liang, X. R.; Yun, B. G.; Pastoriza-Santos, I.; Matts, R. L.; Giersig, M.; Serra-Rodriguez, C.; Liz-Marzan, L. M.; Kotov, N. A.; "Biomaterials by design: Layer-by-layer assembled ion-selective and biocompatible films of TiO2 nanoshells for neurochemical monitoring", *Advanced Functional Materials* 12 (4), 255-265, **(2002)**.
[191] Westenhoff, S.; Kotov, N. A.; "Quantum dot on a rope", *Journal of the American Chemical Society* 124 (11), 2448-2449, **(2002)**.
[192] Wu, A.; Yoo, D.; Lee, J. K.; Rubner, M. F.; "Solid-state light-emitting devices based on the tris-chelated ruthenium(II) complex: 3. High efficiency devices via a layer-by-layer molecular-level blending approach", *Journal of the American Chemical Society* 121 (20), 4883-4891, **(1999)**.
[193] "http://www.cheaptubesinc.com/pricelist.htm"
[194] Feynman, R. P.; Sands, M.; Leighton, R. B.; "The Feynman lectures on physics"; Addison-Wesley: Redwood City, Calif, **(1989)**.
[195] Mawhinney, D. B.; Naumenko, V.; Kuznetsova, A.; Yates, J. T.; Liu, J.; Smalley, R. E.; "Surface defect site density on single walled carbon nanotubes by titration", *Chemical Physics Letters* 324 (1-3), 213-216, **(2000)**.
[196] Pavoor, P. V.; Bellare, A.; Strom, A.; Yang, D. H.; Cohen, R. E.; "Mechanical characterization of polyelectrolyte multilayers using quasi-static nanoindentation", *Macromolecules* 37 (13), 4865-4871, **(2004)**.
[197] Lu, W.; Komvopoulos, K.; "Nanomechanical and nanotribological properties of carbon, chromium, and titanium carbide ultrathin films", *Journal of Tribology-Transactions of the Asme* 123 (4), 717-724, **(2001)**.
[198] Klapperich, C.; Komvopoulos, K.; Pruitt, L.; "Nanomechanical properties of polymers determined from nanoindentation experiments", *Journal of Tribology-Transactions of the Asme* 123 (3), 624-631, **(2001)**.
[199] Du, B. Y.; Tsui, O. K. C.; Zhang, Q. L.; He, T. B.; "Study of elastic modulus and yield strength of polymer thin films using atomic force microscopy", *Langmuir* 17 (11), 3286-3291, **(2001)**.
[200] Briscoe, B. J.; Fiori, L.; Pelillo, E.; "Nano-indentation of polymeric surfaces", *Journal of Physics D-Applied Physics* 31 (19), 2395-2405, **(1998)**.
[201] Olek, M.; Kempa, K.; Giersig, M.; "Multiwall carbon nanotubes-based composites - mechanical characterization using the nanoindentation technique", *International Journal of Materials Research* 97, 1235-1238, **(2006)**.
[202] Oliver, W. C.; Pharr, G. M.; "An Improved Technique for Determining Hardness and Elastic-Modulus Using Load and Displacement Sensing Indentation Experiments", *Journal of Materials Research* 7 (6), 1564-1583, **(1992)**.
[203] Fischer-Cripps, A. C.; "Nanoindentation"; 2nd ed.; Springer: New York, **(2004)**.
[204] Li, X. D.; Gao, H. S.; Scrivens, W. A.; Fei, D. L.; Xu, X. Y.; Sutton, M. A.; Reynolds, A. P.; Myrick, M. L.; "Nanomechanical characterization of single-walled carbon nanotube reinforced epoxy composites", *Nanotechnology* 15 (11), 1416-1423, **(2004)**.
[205] Chudoba, T.; Richter, F.; "Investigation of creep behaviour under load during indentation experiments and its influence on hardness and modulus results", *Surface & Coatings Technology* 148 (2-3), 191-198, **(2001)**.
[206] Dutta, A. K.; Penumadu, D.; Files, B.; "Nanoindentation testing for evaluating modulus and hardness of single-walled carbon nanotube-reinforced epoxy composites", *Journal of Materials Research* 19 (1), 158-164, **(2004)**.
[207] Penumadu, D.; Dutta, A.; Pharr, G. M.; Files, B.; "Mechanical properties of blended single-wall carbon nanotube composites", *Journal of Materials Research* 18 (8), 1849-1853, **(2003)**.
[208] Gregory, J. R.; Spearing, S. M.; "Nanoindentation of neat and in situ polymers in polymer-matrix composites", *Composites Science and Technology* 65 (3-4), 595-607, **(2005)**.
[209] Pavoor, P. V.; Gearing, B. P.; Gorga, R. E.; Bellare, A.; Cohen, R. E.; "Engineering the friction-and-wear behavior of polyelectrolyte multilayer nanoassemblies through block copolymer surface capping, metallic nanoparticles, and multiwall carbon nanotubes", *Journal of Applied Polymer Science* 92 (1), 439-448, **(2004)**.
[210] Lu, H. B.; Huang, G.; Wang, B.; Mamedov, A.; Gupta, S.; "Characterization of the linear viscoelastic behavior of single-wall carbon nanotube/polyelectrolyte multilayer nanocomposite film using nanoindentation", *Thin Solid Films* 500 (1-2), 197-202, **(2006)**.

[211] Bouzakis, K. D.; Michailidis, N.; Hadjiyiannis, S.; Skordaris, G.; Erkens, G.; "The effect of specimen roughness and indenter tip geometry on the determination accuracy of thin hard coatings stress-strain laws by nanoindentation", *Materials Characterization* 49 (2), 149-156, **(2002)**.

[212] Abdel-Goad, M.; Potschke, P.; "Rheological characterization of melt processed polycarbonate-multiwalled carbon nanotube composites", *Journal of Non-Newtonian Fluid Mechanics* 128 (1), 2-6, **(2005)**.

[213] Kinloch, I. A.; Roberts, S. A.; Windle, A. H.; "A rheological study of concentrated aqueous nanotube dispersions", *Polymer* 43 (26), 7483-7491, **(2002)**.

[214] Lozano, K.; Yang, S. Y.; Zeng, Q.; "Rheological analysis of vapor-grown carbon nanofiber-reinforced polyethylene composites", *Journal of Applied Polymer Science* 93 (1), 155-162, **(2004)**.

[215] McNally, T.; Potschke, P.; Halley, P.; Murphy, M.; Martin, D.; Bell, S. E. J.; Brennan, G. P.; Bein, D.; Lemoine, P.; Quinn, J. P.; "Polyethylene multiwalled carbon nanotube composites", *Polymer* 46 (19), 8222-8232, **(2005)**.

[216] Song, Y. S.; Youn, J. R.; "Influence of dispersion states of carbon nanotubes on physical properties of epoxy nanocomposites", *Carbon* 43 (7), 1378-1385, **(2005)**.

[217] Seo, M. K.; Park, S. J.; "Electrical resistivity and rheological behaviors of carbon nanotubes-filled polypropylene composites", *Chemical Physics Letters* 395 (1-3), 44-48, **(2004)**.

[218] Garboczi, E. J.; Snyder, K. A.; Douglas, J. F.; Thorpe, M. F.; "Geometrical Percolation-Threshold of Overlapping Ellipsoids", *Physical Review e* 52 (1), 819-828, **(1995)**.

[219] Skakalova, V.; Dettlaff-Weglikowska, U.; Roth, S.; "Electrical and mechanical properties of nanocomposites of single wall carbon nanotubes with PMMA", *Synthetic Metals* 152 (1-3), 349-352, **(2005)**.

[220] Ago, H.; Shaffer, M. S. P.; Ginger, D. S.; Windle, A. H.; Friend, R. H.; "Electronic interaction between photoexcited poly(p-phenylene vinylene) and carbon nanotubes", *Physical Review B* 61 (3), 2286-2290, **(2000)**.

[221] Cao, L.; Chen, H. Z.; Wang, M.; Sun, J. Z.; Zhang, X. B.; Kong, F. Z.; "Photoconductivity study of modified carbon nanotube/oxotitanium phthalocyanine composites", *Journal of Physical Chemistry B* 106 (35), 8971-8975, **(2002)**.

[222] Cao, L.; Chen, H. Z.; Zhou, H. B.; Zhu, L.; Sun, J. Z.; Zhang, X. B.; Xu, J. M.; Wang, M.; "Carbon-nanotube-templated assembly of rare-earth phthalocyanine nanowires", *Advanced Materials* 15 (11), 909-913, **(2003)**.

[223] Kymakis, E.; Amaratunga, G. A. J.; "Single-wall carbon nanotube/conjugated polymer photovoltaic devices", *Applied Physics Letters* 80 (1), 112-114, **(2002)**.

[224] Ago, H.; Kugler, T.; Cacialli, F.; Salaneck, W. R.; Shaffer, M. S. P.; Windle, A. H.; Friend, R. H.; "Workfunctions and surface functional groups of multiwall carbon nanotubes", *Journal of Physical Chemistry B* 103 (38), 8116-8121, **(1999)**.

[225] Ago, H.; Kugler, T.; Cacialli, F.; Petritsch, K.; Friend, R. H.; Salaneck, W. R.; Ono, Y.; Yamabe, T.; Tanaka, K.; "Workfunction of purified and oxidised carbon nanotubes", *Synthetic Metals* 103 (1-3), 2494-2495, **(1999)**.

[226] Van de Walle, C. G.; Neugebauer, J.; "Universal alignment of hydrogen levels in semiconductors, insulators and solutions", *Nature* 423 (6940), 626-628, **(2003)**.

[227] Bakueva, L.; Musikhin, S.; Sargent, E. H.; Shik, A.; "Influence of nanocrystals on the energy levels and luminescent properties of the polymer matrix in conjugated polymer-dielectric nanocomposites", *Surface Science* 532, 1051-1055, **(2003)**.

[228] Xie, R. G.; Kolb, U.; Li, J. X.; Basche, T.; Mews, A.; "Synthesis and characterization of highly luminescent CdSe-Core CdS/Zn0.5Cd0.5S/ZnS multishell nanocrystals", *Journal of the American Chemical Society* 127 (20), 7480-7488, **(2005)**.

[229] Li, J. B.; Wang, L. W.; "First principle study of core/shell structure quantum dots", *Applied Physics Letters* 84 (18), 3648-3650, **(2004)**.

[230] Ohtani, B.; Ikeda, S.; Nakayama, H.; Nishimoto, S.; "Shape- and size-selective photocatalytic reactions by layered titanic acid powder suspended in deaerated aqueous alcohol solutions", *Physical Chemistry Chemical Physics* 2 (22), 5308-5313, **(2000)**.

[231] Subramanian, V.; Wolf, E. E.; Kamat, P. V.; "Catalysis with TiO2/gold nanocomposites. Effect of metal particle size on the Fermi level equilibration", *Journal of the American Chemical Society* 126 (15), 4943-4950, **(2004)**.

[232] Robel, I.; Bunker, B. A.; Kamat, P. V.; "Single-walled carbon nanotube-CdS nanocomposites as light-harvesting assemblies: Photoinduced charge-transfer interactions", *Advanced Materials* 17 (20), 2458-2463, **(2005)**.

[233] Busmann, H. G.; Gunther, B.; Meyer, U.; "Polymer matrix composites filled with nanoporous metal powders: Preparation and electrical properties", *Nanostructured Materials* 12 (1-4), 531-534, **(1999)**.

[234] Mironi-Harpaz, I.; Narkis, M.; "Electrical behavior and structure of polypropylene/ultrahigh molecular weight polyethylene/carbon black immiscible blends", *Journal of Applied Polymer Science* 81 (1), 104-115, **(2001)**.
[235] Finegan, I. C.; Tibbetts, G. G.; "Electrical conductivity of vapor-grown carbon fiber/thermoplastic composites", *Journal of Materials Research* 16 (6), 1668-1674, **(2001)**.

ACKNOWLEDGMENTS

This thesis would have never been done without the support, help, and advice of diverse group of people. First of all I would like to thank my supervisor Prof. Dr. Michael Giersig for giving me the opportunity to do this study in his group and for always keeping me motivated and supporting me with useful advice. I am particularly grateful to Prof. Dr. Josef Hormes for accepting to be a co-referee of this thesis and for the discussion and helpful suggestions and comments.

I thank Dr. Michael Hilgendorff for sharing his extensive knowledge and offering his guidance, and valuable insight to my study, as well as essential corrections and discussions on this thesis (vielen Dank Micha).

Thanks also go to my office mate, Thomas Büsgen for collaboration, crucial help in chemistry issues, and simply for being a good friend. Also thanks to Dr. Georgios Ctistis for vital information and useful comments on the thesis.

Thanks to caesar's members for their general advice and input on various things related to research, as well as things not related. In particular, to current and former NPA's group lab mates: Dr. Miguel Correa-Duarte, Izabela Firkowska, Dr. Yan Gao, Dr. Suna Giannona, Hanna Glaczynska, Renata Jarzebinska, Witold Kandulski, Dr. Peter Karageorgiev, Adam Kosiorek, Ewa Musielak, Piotr Patoka, Nicolas Pazos Perez, Dr. José Rojas-Chapana, Julia Troszczynska, and all the NPA's visitors; thanks to all of you for the great and friendly atmosphere, good company, help with various things, as well as excellent time and fun during and after working hours. Thanks guys, I really have benefited from your scientific knowledge and philosophy of life. At this point I wish you good luck, nice ideas and stunning data.

I would like to express my appreciation to our team assistant Jolanta Kremer, for her invaluable general support, without her, my stay in Bonn would not have been that easy and smooth as it was (thanks a lot!).

Special thanks go to Dr. Kris Kempa (Boston College, USA) for providing me with carbon nanotubes, and for collaborative work and the stimulating discussions on our experimental results.

I feel privileged to have been able to work as a visiting scientist for Prof. Dr. Nicholas Kotov (University of Michigan, before Oklahoma State University), where I started my big

adventure in nanotechnology. I thank him and members of his group for sharing their knowledge, for fruitful discussions, and the great time we spent together.

I would like to thank Prof. Dr. Stefan Jurga (Adam Mickiewicz University, Poland) for the encouragement to begin my PhD studies and for giving me the opportunity to perform dielectric measurements.

I also appreciate working with Prof. Drs. Helmut Möhwald (MPI, Golm, Germany), Paul Mulvaney (Melbourne University, Australia), and Luis Liz-Marzán (University of Vigo, Spain).

I thank the Rapid Prototyping group in caesar for giving me the possibility to use the rheometer, Joel van Embden (Melbourne University, Australia) for QDs fabrication, and Bakyt Orozbaev (Adam Mickiewicz University, Poland) for dielectric measurements.

Finally I would like to thank my parents Alina and Piotr Olek (dziękuję wam za wszystko); I could not be at the point where I am now without them. Thanks to my wife Bernadeta for her love, support and encouragement she always provides (kocham Cię). And last but not least to my son Adam for spreading around childlike optimism that gives me energy during difficult times.